2018-12-01

Pore Pressure Generation and Shear Modulus Degradation during Laminar Shear Box Testing with Prefabricated Vertical Drains

Landon Scott Kinney
Brigham Young University

Pore Pressure Generation and Shear Modulus Degradation During Laminar Shear Box Testing with Prefabricated Vertical Drains

Landon Scott Kinney

A thesis submitted to the faculty of
Brigham Young University
in partial fulfillment of the requirements for the degree of

Master of Science

Kyle M. Rollins, Chair
Kevin W. Franke
Norman L. Jones

Department of Civil and Environmental Engineering

Brigham Young University

ABSTRACT

Pore Pressure Generation and Shear Modulus Degradation
During Laminar Shear Box Testing with
Prefabricated Vertical Drains

Landon Scott Kinney
Department of Civil and Environmental Engineering, BYU
Master of Science

Liquefaction is a costly phenomenon where soil shear modulus degrades as the generation of excess pore pressures begins. One of the methods to mitigate liquefaction, is the use of prefabricated vertical drains. Prefabricated vertical drains provide a drainage path to effectively mitigate the generation of pore pressures and aid in shear modulus recovery.

The aims of this study were to define shear modulus degradation vs. shear strain as a function of excess pore pressure ratio; define the effects of prefabricated vertical drains on the behavior of pore pressure generation vs. shear strain; and to define volumetric strain as a function of shear strain and excess pore pressure ratios.

A large-scale laminar shear box test was conducted and measured on clean sands with prefabricated vertical drains spaced at 3-feet and 4-feet. The resulting test data was analyzed and compared to data without vertical drains.

The results show the effect of increasing excess pore pressure ratios on shear modulus and curves where developed to encompass these effects in design with computer programing like SHAKE or DEEPSOIL. The data also suggests that prefabricated vertical drains effectively mitigate excess pore pressure build-up, thus increased the shear strain resistance before pore pressures were generated. Regarding volumetric strain, the results suggests that the primary factor governing the measured settlement is the excess pore pressure ratio. This indicates that if the drains can reduce the excess pore pressure ratio, then the resulting settlement can successfully be reduced during a shaking event.

The curves for shear modulus vs. cyclic shear strain as function of pore pressure ratio were developed using data with high strain and small strain which leaves a gap of data in the cyclic shear strain range of 0.0001 to 0.01. Further large-scale testing with appropriate sensitivity is needed to observe the effect excess pore pressure generation on intermediate levels of cyclic shear strain.

Keywords: Landon S. Kinney, Kyle M. Rollins, shear modulus, pore pressure ratio, prefabricated vertical drains, volumetric strain, cyclic shear strain

ACKNOWLEDGEMENTS

This study and its parent study were funded by the National Science Foundation, Grant No. CMMI 1052645, and by FHWA pooled fund study TPF-5(244) supported by Departments of Transportation from the states of Alaska, California, New York, and Utah. This support is gratefully acknowledged. However, the conclusions and recommendations are those of the author and do not necessarily represent those of the sponsors.

I want to thank Dr. Rollins for his effort throughout the thesis process, and the faculty at Brigham Young University Department of Civil and Environmental Engineering for their guidance in and out of the classroom. I am grateful for the sustained love and support from my wife, Miranda, and from other friends and family.

TABLE OF CONTENTS

LIST OF TABLES

LIST OF FIGURES

1 INTRODUCTION

1.1 General

Liquefaction is a damaging and costly event caused by large ground motions in earthquakes. Liquefaction causes a loss of shear strength in the soil that can lead to landslides, lateral spreading, and loss of bearing support to foundations. Liquefaction also causes significant amounts of settlement to occur in the soil. These conditions heavily affect infrastructure, especially utility lines and other life-lines. Liquefaction events during the 1964 Niigata Japan earthquake caused nearly $1 billion dollars of damage (NRC, 1985) and over $11.8 billion in damage during the 1995 Kobe Japan Earthquake (EQE, 1995)

Liquefaction occurs when ground motions induce shear stresses in the ground that cause excess pore water pressure to generate. If there is not adequate dissipation during shaking, the pore pressures can increase and become equal to the vertical effective stress. At this point the sand tends to behave as a dense liquid in many respects with relatively little strength.

Typical liquefaction mitigation techniques rely on densifying the soil, using vibrocompaction, stone columns, compaction grouting, dynamic compaction, or explosives. Alternatively, liquefaction can be mitigated using methods that cement the sand particles together such as deep soil mixing columns or panels. However, these methods are time-consuming, expensive and require verification of their effectiveness.

More recently, engineers have investigated the possibility of mitigating liquefaction by installing vertical prefabricated drainage pipes in the soil to allow a quicker, easier drainage path to reduce pore pressure generation. This approach is more rapid and more economical than densification or soil mixing strategies and does not require post-treatment in-situ testing to confirm that the improvement has been sufficient to meet specifications. Unfortunately, the effect of vertical drains has not been tested in an earthquake event and large-scale tests have only involved blast-induced liquefaction (Rollins, Joshua, Mccain, & Goughnour, 2003) or vibratory shaking tests with a vibroseis truck (Chang, Rathje, Stokoe, & Cox, 2004). Some researchers argue that drains may reduce the development of excess pore pressures; however, they claim that the resulting settlement will still be the same as that for an equivalent sand profile without drains. Although both field testing and subsequent small-scale centrifuge testing (Rollins, Joshua, Mccain, & Goughnour, 2003) (Howell & et al, 2009b) with vertical drains has demonstrated settlement reductions of 30 to 60% compared to tests without drainage, no cogent theoretical explanation has been advanced to explain this beneficial effect. A deeper understanding of the liquefaction-induced settlement process is needed to understand the basic relationships that are involved.

The opportunity to investigate the basic mechanisms of liquefaction-induced settlement with and without vertical drains is provided by a series of large-scale laminar shear box shaking tests conducted at the NEES Lab at the University at Buffalo (SUNY-Buffalo). Test results without drains were reported by (Dobry & Abdoun, 2015) while tests with drains were reported by (Oakes, 2015). These test results can be used to define the reduction of shear modulus with shear strain as excess pore pressures develop. They can also be used to define fundamental relationships between excess pore pressure and shear strain - with and without drains. Lastly,

they can also be used to define the relationship between volumetric strain and excess pore pressure with various drain spacings. This thesis will present an analysis of these important relationships and describe observations from these analyses based on these large-scale laminar shear box shaking tests on clean saturated sand.

1.2 Research Objectives

The research objectives for this study are listed below:

- Define the shear modulus degradation vs. shear strain relationship as a function of excess pore pressure ratio for clean sands.
- Define pore pressure generation vs. shear strain behavior in the presence of vertical drains and compare them with relationships without drains for clean sands.
- Determine volumetric strain (% settlement) as a function of shear strain and excess pore pressure ratios for clean sands.

1.3 Organization of Thesis

The thesis will be presented as follows:

- A Literature review of liquefaction approaches; previous testing on cyclic shear strain, pore pressures, and shear modulus variations; and liquefaction mitigation.
- The large-scale test discussion including test equipment, sensor layout, characteristics of sand tested, and test procedures.
- Preliminary results from large scale testing on clean sands including peak pore pressure vs. depth and time, and settlement vs. depth and volumetric strain.

- Methods and results of in-depth analysis for clean sands, including shear strain and shear stress, shear modulus, shear modulus variations with cyclic shear strain, supplemental data from blast liquefaction testing, shear modulus variation by varying pore pressure, cyclic shear strain and pore pressure generation, and pore pressure ratio vs. volumetric strain.
- Conclusions from testing and analysis including shear modulus variations, cyclic shear strains, pore pressure generation, and research limitations and future work.

2 LITERATURE REVIEW

2.1 Definition of Liquefaction

Liquefaction is a phenomenon in which earthquake induced shear deformations cause excess pore water pressures to develop in the pores between sand particles. When excess pore pressures become equal to the initial vertical effective stress between soil particles, the soil particles tend to separate and there is little, if any, frictional resistance between them. At this point, the soil loses shear strength and temporarily behaves as a heavy liquid. Liquefaction is defined as a state when effective stress in a soil is equal to zero because of excess pore water pressure generated in the soil. Earthquake seismic forces produce enough shear stress in a relatively short time to generate excess pore pressures that cannot dissipate quickly even in saturated, cohesionless soils.

The discovery and study of liquefaction was fueled by damaging earthquakes. The first reference to liquefaction was by Hazen (Hazen, 1920). Hazen observed liquefaction occurring in the 1918 Calaveras Dam failure in California. Earthquakes that occurred in Niigata, Japan and Alaska, United States in 1964 urged further research of the liquefaction phenomenon.

Liquefaction is organized into two different categories, flow liquefaction and cyclic mobility. Flow failure occurs when the static shear stress of a soil is greater than the shear strength of a liquefied soil. This results in massive displacement of the soil. Cyclic mobility

occurs when the static shear stress of a soil is less than the shear strength of a liquefied soil. During loading, the soil loses enough shear strength and can experience intermittent movement.

2.2 Liquefaction Potential Evaluation Approaches

Many approaches have been developed to evaluate liquefaction potential in soil because of earthquake shaking. These approaches include stress-based, strain-based, and energy-based methods (Dobry R. , Ladd, Yokel, Chung, & Powell, 1982).

2.2.1 Stress-Based Approach

The stress-based approach is founded on the assumption that the generation of pore water pressure is primarily attributed to the number of cycles of applied shear stress and the magnitude of the shear stress. Simply stated, the stress-based approach compares the earthquake induced cyclic shear stress to the shear strength or liquefaction resistance of the soil. When the induced shear stress exceeds the shear strength, liquefaction would be expected to occur. Many factors affect the results of the stress-based approach. Soil stratification, relative density, lateral earth pressure coefficients, and the age of soil layers can all affect the resistance. Previous seismic shaking events and overconsolidation of the soil can also increase the resistance. Liquefaction resistance can be measured by cyclic shear testing in the laboratory, but it is more commonly estimated from triggering curves based on field case histories where liquefaction has or has not occurred. Because of the many variables that effect the shear stress of a soil, the shear stress approach is unreliable for analysis.

2.2.2 Strain-Based Approach

The strain-based approach is based upon the idea that inter-particle instability at a threshold strain level produces pore pressure generation. Soil that experiences strain less than a defined critical threshold cyclic shear strain (≈ 0.02%) will not exhibit liquefaction behaviors. For higher shear strain levels, excess pore pressure generation can be predicted as a function of the induced shear strain. Cyclic shear strain is can be computed using the equation

$$\gamma_c = \tau_c / G \tag{2-1}$$

where τ_c is the induced cyclic shear stress and G is the shear modulus at that strain level. This requires the use of the stiffness of the soil, G_{max}, for analysis which can be determined from the measured shear wave velocity (V_s) in the field using the equation

$$G_{max} = \rho * V_s^2 \tag{2-2}$$

Dobry (Dobry R. , Ladd, Yokel, Chung, & Powell, 1982) argued that the strain-based approach is an effective and more fundamental approach to liquefaction potential analysis than the stress-based approach. This approach avoids effective stress differences and focuses on the stiffness of the soil, or shear modulus. One difficulty of using the strain-based approach is that the shear modulus must be determined, and it is known to be strain dependent. Therefore, the G_{max} value must be reduced to obtain the modulus G for a given strain level using a G/G_{max} vs. shear strain curve.

Dobry conducted cyclic shear tests on silica sand prepared two separate ways; by wet rodding and dry vibration. The stress-based approach showed significantly different liquefaction resistance depending on the sample preparation method, but the strain-based analysis gave the same liquefaction resistance for a given strain level. Therefore, the testing proved the strain-

based approach to be a more fundamentally sound method for predicting pore pressure development.

Silver and Seed (Silver & Seed, 1971) completed thorough strain-based cyclic triaxial testing on sands with varying relative density and overburden pressures. Their findings strongly suggest that cyclic strain, not stress, controls both densification and liquefaction potential in sands. Because of the fundamental relationship between cyclic shear strain and excess pore pressure generation, the strain-based method will be used in this study to compare the effectiveness of PVD drains.

2.2.3 Energy-Based Approach

Alternatively, the energy-based approach focuses on the energy dissipated through the soil correlated to pore pressure generation. Using energy principles, energy dissipation is estimated and can be correlated to liquefaction resistance as shown by Nemat-Nasser and Shokooh (Nemat-Nasser & Shokooh, 1979) or Davis and Berrill (Davis & Berrill, 1982). The generation of excess pore pressures are associated with the amount of energy applied to the soil. The Energy-based approach will not be used in this thesis.

2.3 Cyclic Shear Strain and Pore Pressure Generation

The development of excess pore pressures during earthquake shaking is closely linked to the shear strains that develop in the soil. As noted previously, a critical threshold strain has been observed in cyclic triaxial tests on sands. This critical threshold strain, γ_t, is defined as the shear strain above which excess pore pressures begin to generate. Tests show a relatively consistent value of about 2×10^{-2}% shear strain for the threshold shear strain.

Early investigations reported by Dobry (Dobry R. , Ladd, Yokel, Chung, & Powell, 1982) were performed on specimens of Monterey Sand No. 0 at three different relative densities (D_r = 45, 60 and 85%). Tests were performed using undrained cyclic triaxial shear with a strain-controlled approach. For each test, the sand specimen was subjected to 10 cycles of strain and the excess pore pressure was measured. For a given relative density, tests were performed on virgin specimens, but at progressively higher strain levels. Plots of the measured excess pore pressure ratio, R_u, ($R_u = \Delta u/\sigma'_o$) vs. cyclic shear strain are provided in Figure 2-1. The pore pressure generation increases after reaching the soil threshold strain and the threshold strain occurs at about 2 x 10^{-2} percent shear strain. The threshold shear strain appears to be insensitive to the sand relative density. In addition, the relative density has a relatively small effect on the generation of pore pressure at larger shear strains.

Dobry also reported results of strain-controlled undrained cyclic triaxial shear tests designed to explore the effect of sample preparation techniques. Tests were performed on crystal silica sand and Monterey No. 1 sand. Specimens were prepared using three methods: moist tamping, dry vibration, and wet rodding and at different confining pressures. Plots of excess pore pressure vs. cyclic shear strain are provided in Figure 2.2. The threshold strain is clearly seen at 2 x 10^{-2} percent shear strain despite the variation in specimen preparation procedure and confining pressure. In addition, the relationship between excess pore pressure ratio and shear strain is not significantly affected. For a stress-controlled test, the cyclic stress ratio causing liquefaction would be strongly affected by variations in these properties. These results strongly suggest that shear strain is a fundamental parameter governing the generation of excess pore pressure.

Subsequently, additional testing was completed by Dobry and Ladd (Dobry & Ladd, 1980) using seven different sands with strain-controlled cyclic triaxial tests. The measured excess pore pressure ratio plotted from all these tests are plotted against cyclic shear strain in Figure 2.3. Most of the data points fall within a relatively narrow band once again suggesting that pore pressure generation is largely governed by shear strain while relative density, confining pressure, and sand type are secondary factors. The results in Figure 2.3 show that the threshold strain is consistently about 10^{-2} (%), which is comparable to other testing.

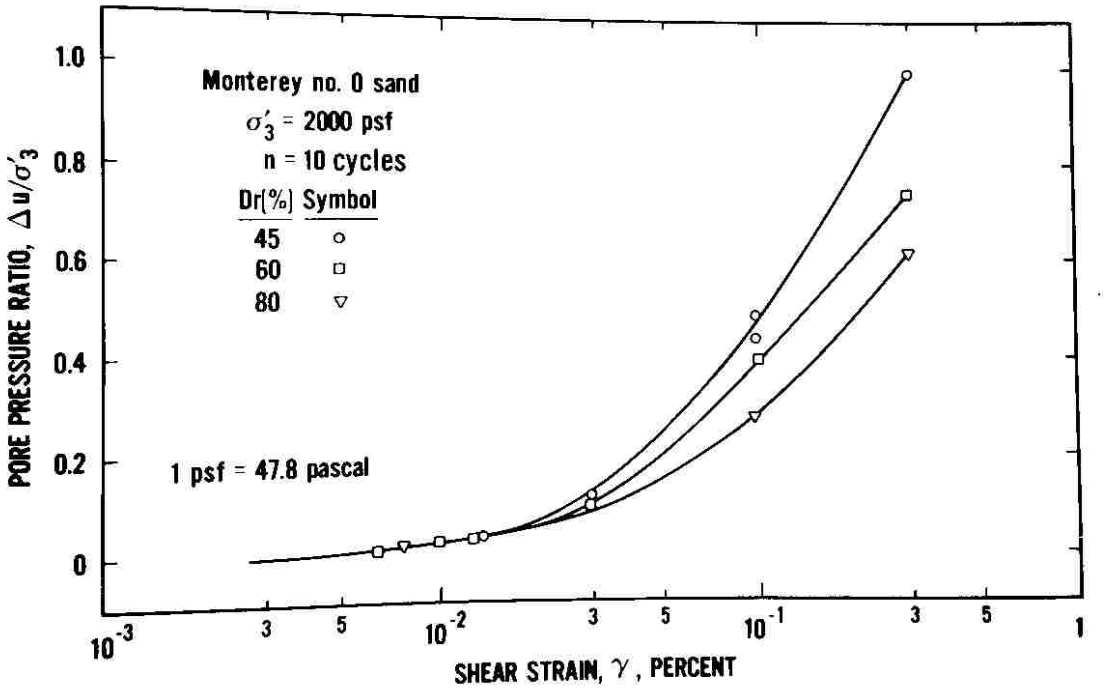

Figure 2-1: Pore Pressure Ratio vs. Shear Strain Curve for Sands with Different Relative Densities from Cyclic Triaxial Shear Tests (Dobry R. , Ladd, Yokel, Chung, & Powell, 1982)

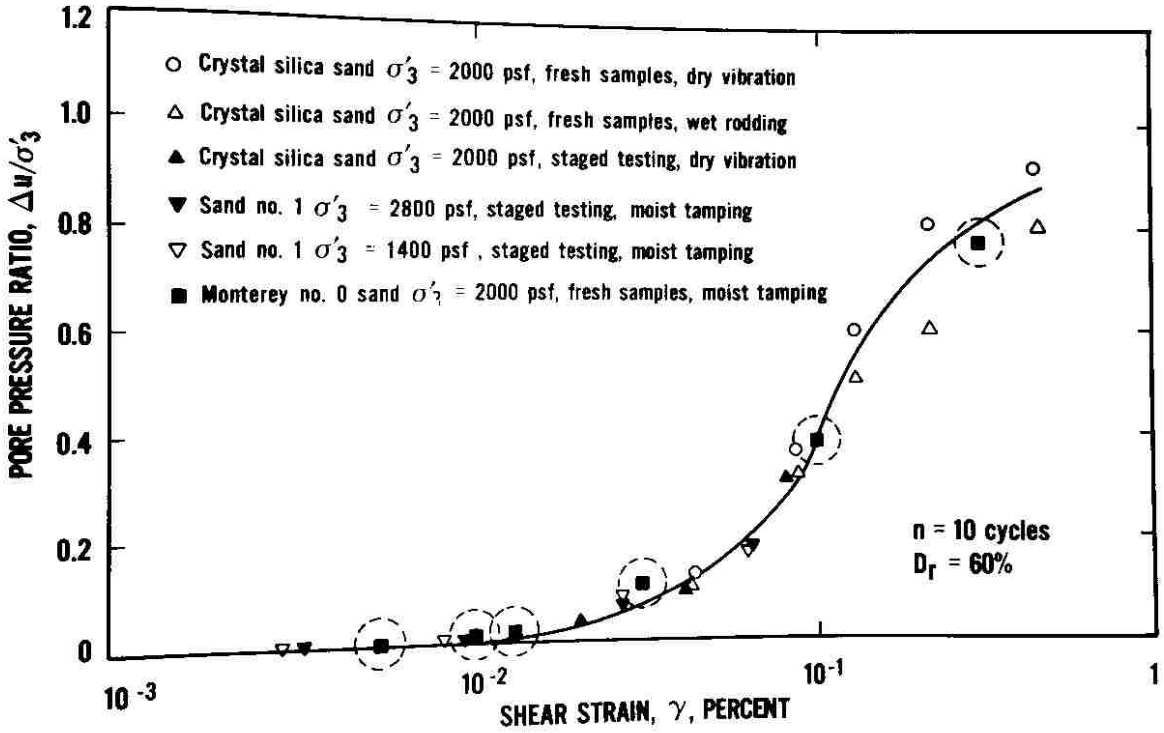

Figure 2-2: Pore Pressure Ratio vs. Shear Strain Curve-Fit for Tests on Two Sands with Different Specimen Preparation Techniques and Confining Pressures from Triaxial Shear Testing ((Dobry R. , Ladd, Yokel, Chung, & Powell, 1982)

Field in-situ testing have produced similar results. Cox, Stokoe, and Rathje (Cox, Stokoe, & Rathje, 2009) performed testing using a large hydraulic shaker or vibroseis on soil with a sensor array. The sensors were successful in measuring soil response during vibroseis. Preliminary results shown similar threshold shear strain. This can be seen in Figure 2.4.

In an article published in 2015, Dobry and Abdoun (Dobry & Abdoun, 2015) investigated the cyclic shear strain needed to trigger liquefaction by testing sands and silty sands in centrifuge tests and large-scale laminar shear box tests. In prior research, the strain-based approach done on

triaxial tests showed a threshold strain, the strain needed to generate pore pressures, in consolidated sands and remained consistent with other laboratory testing and field investigations.

Dobry and Abdoun analyzed eight supplemental centrifuge tests and one large-scale 1-g laminar shear box test on clean and silty sands comparing the pore pressure ratio vs. cyclic strain with previous research using cyclic triaxial shear testing.

The shear strain values were recorded from accelerations at different elevations. As shown in Figure 2.5, the findings noted the threshold cyclic strain needed to produce pore pressures was significantly smaller, from the established $\gamma_{cl} = 0.01$ to 0.03% (Dobry R. , Ladd, Yokel, Chung, & Powell, 1982)to a much smaller $\gamma_{cl} = 0.007\%$. In addition, much higher excess pore pressure ratios developed for a given strain in the large-scale tests than in the triaxial shear tests. Dobry and Abdoun attribute this to:

"1. The greater duration, n=15-23 cycles corresponding to the Mw = 7.5… compared with the 10 cycles used in [previous] tests…

2. The 2D nature of the earthquake horizontal shaking … compared with the 1D cyclic straining for the [previous tests] and

3. The redistribution of excess pore pressures and upward water flow that tends to increase the value of rn in the field at shallower elevations."

Dobry and Abdoun conclude that the "main reason for the much smaller γ_{cl} needed to trigger liquefaction in actual earthquakes is the redistribution of excess pore pressures and upward water flow present in the field."

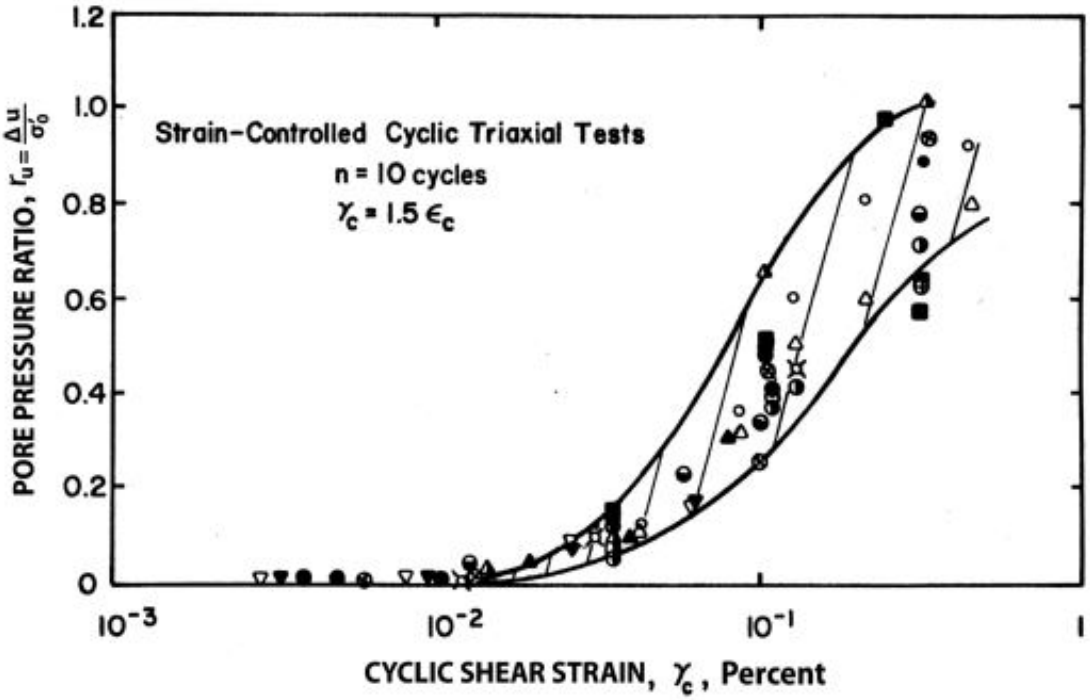

Symbol	Sand	σ'_0 (psf)	D_r (%)	Samples/ Fabric	Measured u Peak (P) or Residual (R)
○	Crystal Silica	2,000	60	Dry Vibration	P
△	" "	2,000	60	Wet Rodding	P
▲	" "	2,000	60	Dry Vibration	P
▼	Sand No. 1	2,800	60	Moist Tamping	P
▽	" "	1,400	60	" "	P
○	Monterey No. 0	2,000	60	" "	P
●	" "	2,000	80	" "	P
□	" "	2,000	45	" "	P
▣	" "	2,000	45	" "	R
■	" "	533	60	" "	P
⊖	" "	4,000	60	" "	P
●	" "	2,000	20	" "	R
●	Banding	2,000	60	" "	R
▲	"	2,000	40	" "	R
●	"	2,000	20	" "	R
●	Heber Road Point Bar	2,000	Dense	Tube Sample	R
○	Heber Road Channel Fill	2,000	Loose	" "	R
⊠	Owi Island	2,000	40	Moist Tamping	R
◯	" "	1,500	40	" "	R
⊖	" "	2,000	Medium Dense	Tube Sample	R
⊖	Mt. St. Helen Debris	2,000-4,000	50	Moist Tamping	R

Figure 2-3: Pore Pressure Ratio Plotted against Shear Strain for Multiple Sands and Densities (Dobry & Ladd, 1980)

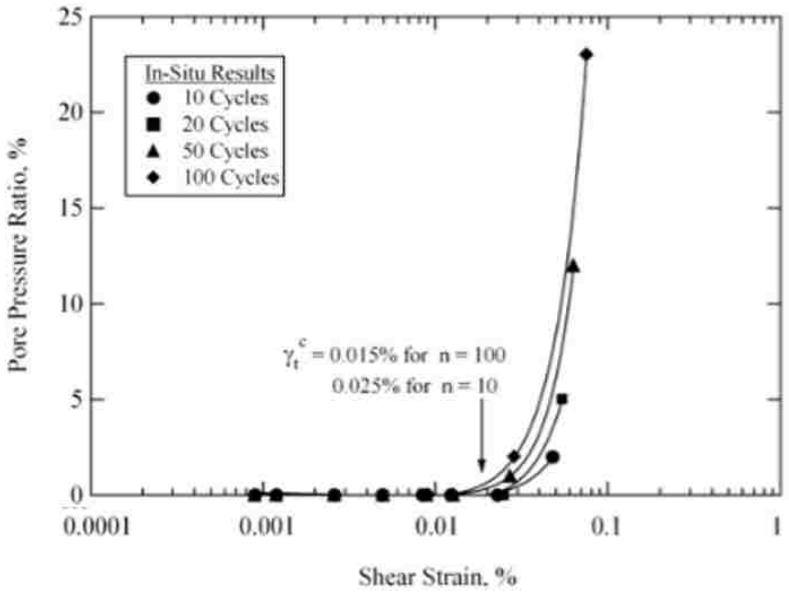

Figure 2-4: Excess Pore Pressure Ratio vs. Shear Strain Obtained from Field Test in Sand Using Vibroseis Truck ((Cox, Stokoe, & Rathje, 2009)

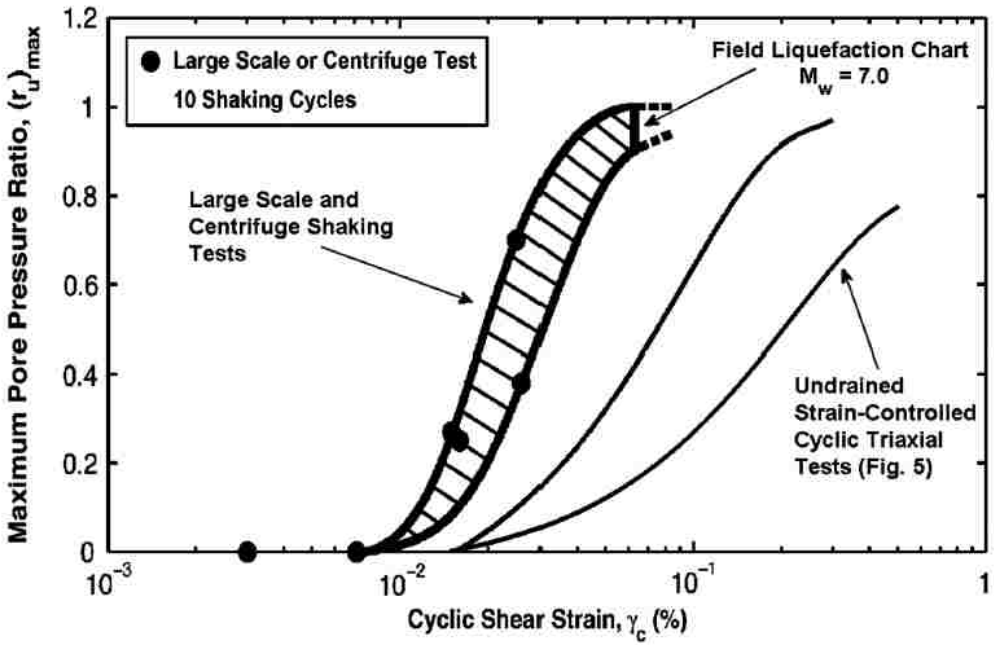

Figure 2-5: Pore Pressure Ratio (Ru)max vs. Cyclic Shear Strain for Large Scale and Centrifuge Tests in Comparison to Strain-Controlled Cyclic Triaxial Tests (Dobry & Abdoun, 2015)

2.4 Shear Modulus Variations

Shear modulus is the relationship between the materials shear stress and shear strain. Shear modulus is defined as the slope secant line of a hysteresis loop formed by plotting the shear stress and shear strain. During cyclic loading, subsequent hysteresis loops are plotted by the increase or decrease of loading on a soil. The changes in the hysteresis loop, and slope of the secant line, signify the changes in the shear modulus. The increased slope of the secant line equates to a higher shear modulus, and lower slope to a lower shear modulus.

2.4.1 Cyclical Triaxial Testing

Seed and Idriss (Seed & Idriss, 1970) characterized soil response under seismic loading by using shear modulus and damping. Seed and Idriss gathered data from various tests, including cyclic triaxial testing, to determine the hysteretic shear stress-shear strain relationships for sand at strain ranges of 10^{-2} to 5%, with careful consideration to primary factors that affect shear moduli such as strain amplitude, void ratio, and number of cycles of loading. The maximum shear modulus (G_{max}) was defined as the value of the shear modulus at essential zero strains or very small strains ($< 10^{-4}$%). Shear moduli at higher cyclic shear strain levels was then normalized by G_{max} and plotted vs. cyclic shear strain. For all data gathered and presented, the range of normalized shear modulus (G/G_{max}) vs. shear strain fell within the relatively narrow band shown in Figure 2-6. In 1986, Seed, Wong, Idriss and Tokimatsu (Seed, Wong, Idriss, & Tokimatsu, 1986) updated this study and found that the range of data for G/G_{max} vs. γ for all available tests on sands was still largely within the range identified previously.

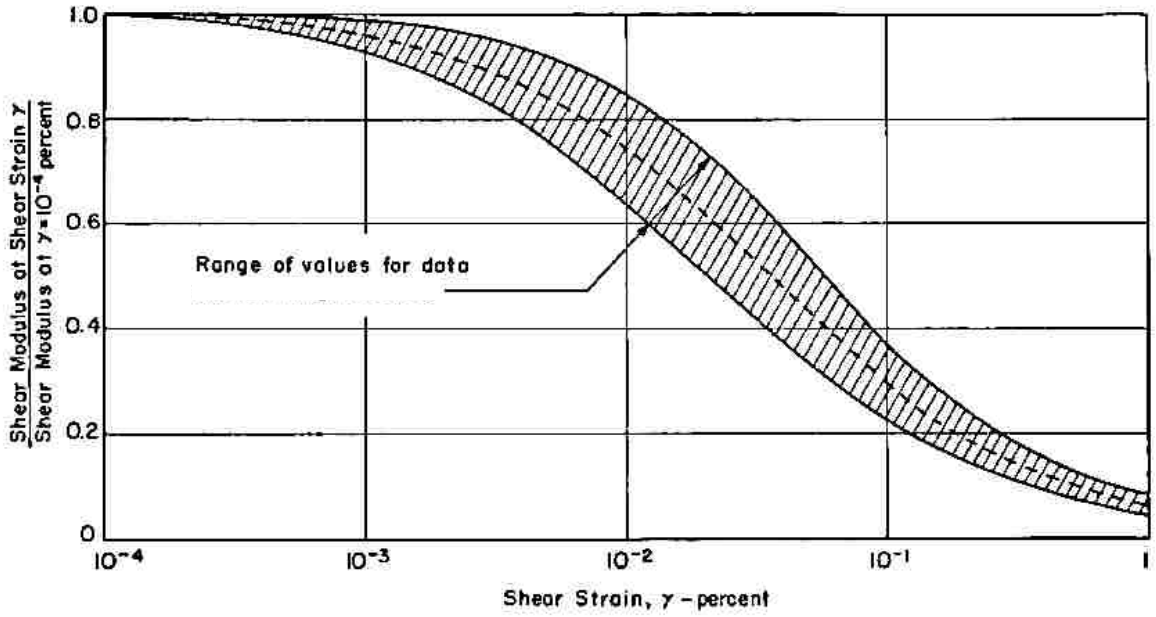

Figure 2-6: Normalized Shear Modulus Reduction Curve (Seed, Wong, Idriss, & Tokimatsu, 1986)

Vucetic and Matasovk (Matasovic & Vucetic, 1993) performed undrained cyclic triaxial shear testing on two sands from Santa Monica Beach to capture the shape of the changing hysteresis loop and shear modulus as a function of shear strain and excess pore pressure ratio. The results are shown in Figure 2-7. The shear stress vs. shear strain curve for each cycle of loading can be observed and can be correlated to the excess pore water pressure ratio (u') at that cycle.

In these tests, the shear modulus reduction is associated with both the cyclic shear strain and the generation of excess pore pressure. This can clearly be seen in Figure 2-8 where the slope of the loop flattens considerably as the excess pore pressure ratio increases. The excess pore water pressure changes the soil particle alignment and the soil loses much of its original shear strength.

Vucetic and Matasovk plotted the results as normalized shear modulus, G/G_o vs. cyclic shear strain as shown in Figure 2-9 where β and s are curve fitting parameters. This resulting G/G_o vs. γ curves fit within the range of data identified by (Seed, Wong, Idriss, & Tokimatsu, 1986) based on previous testing performed on various sands.

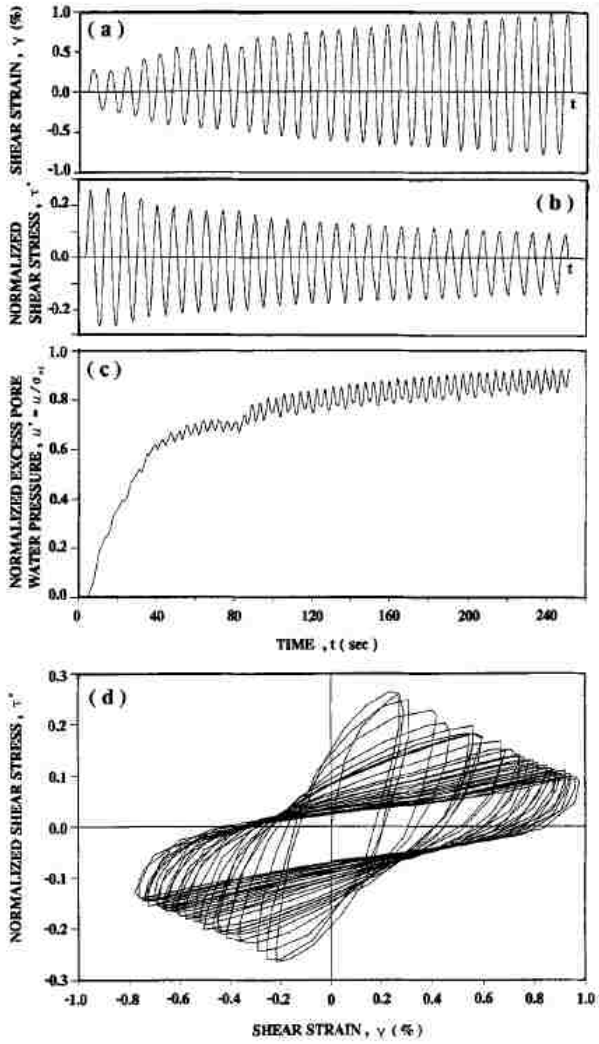

Figure 2-7: Results of Representative Cyclic Test on Santa Monica Beach (SMB) Sand (Matasovic & Vucetic, 1993)

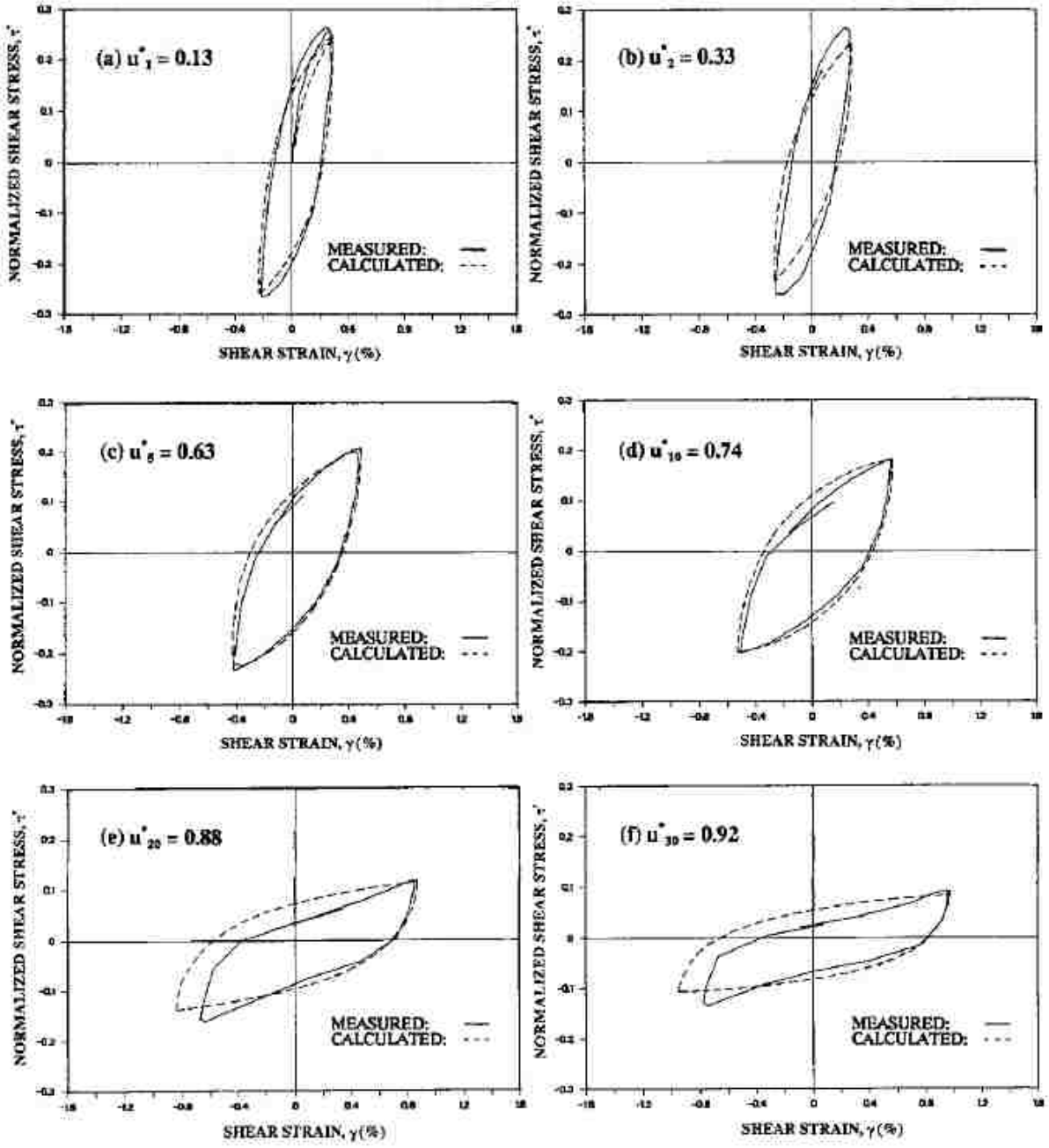

Figure 2-8: Effects of Increased Pore Pressure on Hysteresis Loop (Matasovic & Vucetic, 1993)

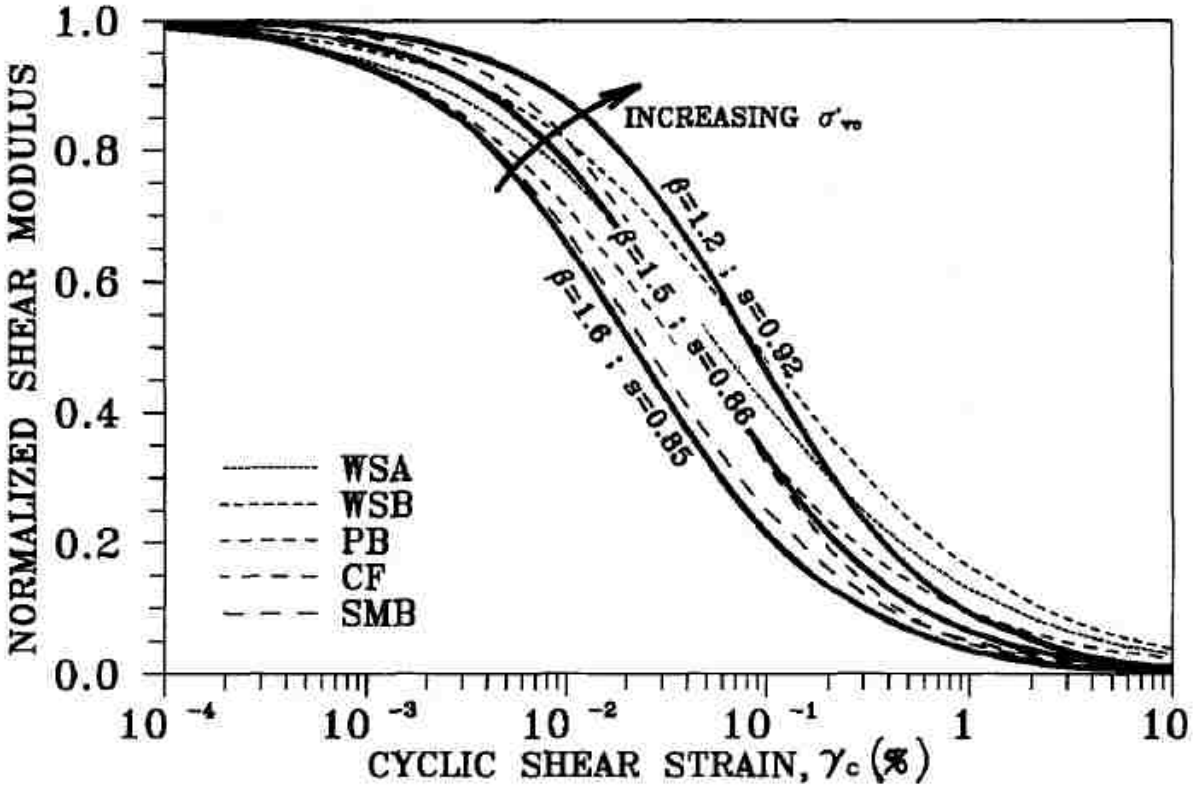

Figure 2-9: Normalized Shear Modulus vs. Cyclic Shear Strain for Santa Monica Beach Sand (Matasovic & Vucetic, 1993)

2.4.2 Shear Modulus Degradation in Gravels from Laboratory Testing

Rollins et al. (Rollins, Evans, Diehl, & Daily, 1998)gathered a decade worth of shear modulus reduction data in gravels and gravely soils based primarily on large cyclic triaxial shear tests. Testing was performed either in drained conditions or with small numbers of cycles so that they were not affected by pore pressure generation. A mean G/G_{max} curve was developed with under and lower standard deviation bounds as shown in Figure 2-10. The range of data was similar but slightly lower than the range of data for identified previously by Seed and Idriss (Seed & Idriss, 1970). By comparing the effect different variables on the normalized curve shape, it was determined that the curve shape was essentially independent of variables such as

fines content, gravel content, and relative density. However, the curve shape was affected by initial confining pressure such that specimens with higher confining pressure experienced progressively less degradation in the shear modulus relative to specimens at lower confining pressures.

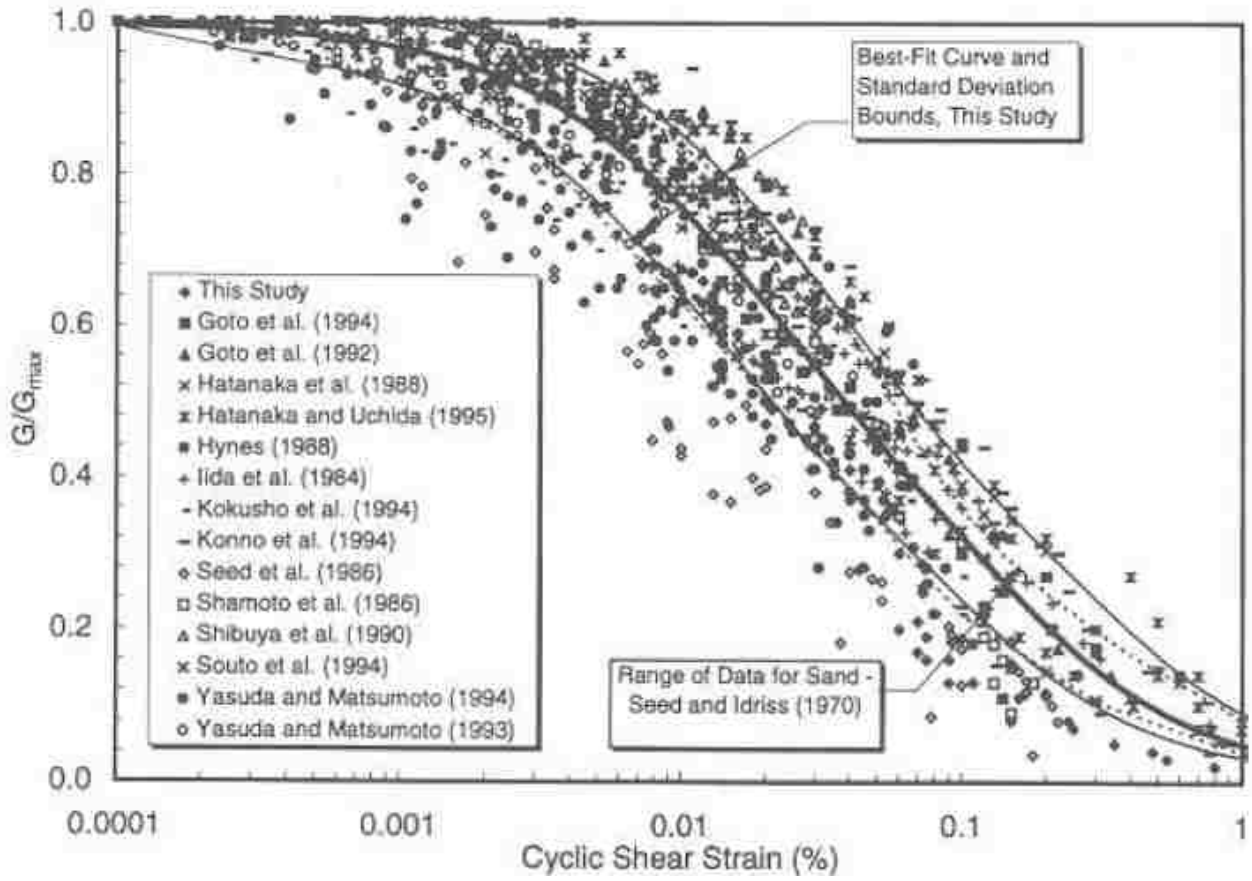

Figure 2-10: Data Defining Best-fit Curve for Shear Modulus Variation in Gravelly Soils (Rollins, Evans, Diehl, & Daily, 1998)

2.4.3 Shear Modulus Degradation in Sands from In-Situ Shear Testing

Field in-situ tests have produced information on the degradation of shear modulus with shear strain and excess pore pressure ratio. Cox, Stokoe, and Rathje (Cox, Stokoe, & Rathje, 2009)

performed cyclic shear testing using a large hydraulic shaker or Vibroseis truck on soil with a sensor array embedded in in a grid pattern in the underlying soil. With repeated cycles of loading at increasing stress levels, the shear modulus decreased as the shear strain increased as presented in Figure 2-11. In addition, pore pressure generation occurred with repeated cyclic loading at a strain of about 0.05%, which is above the threshold strain level ($\gamma \approx 0.02\%$). The increasing pore pressure ratio seems to lead to a decrease in the measured shear modulus as was observed by Vucetic and Matasovk (Matasovic & Vucetic, 1993).

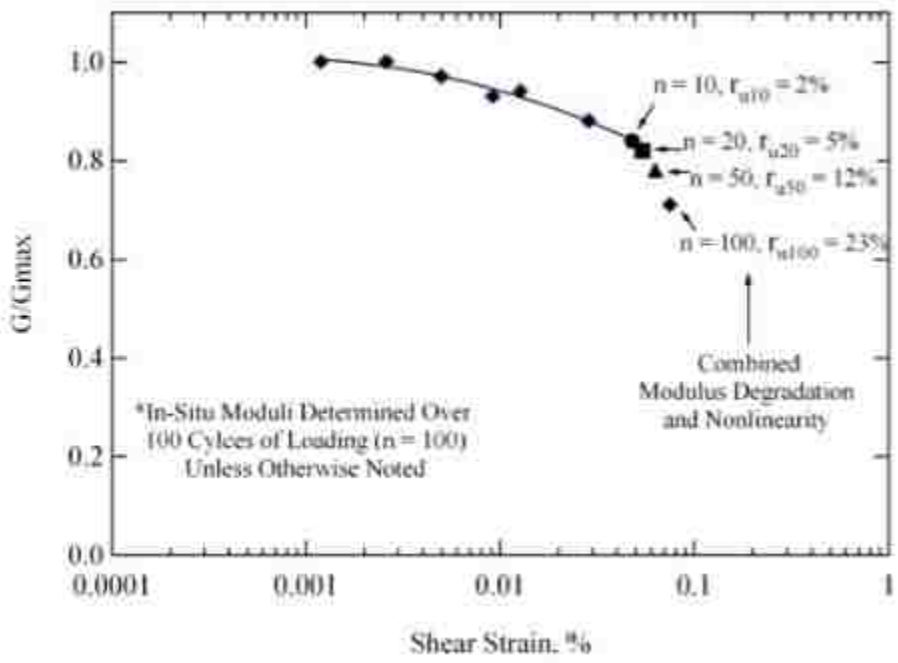

Figure 2-11: Shear Modulus Reduction with Increasing Pore Pressure Ratio (Cox, Stokoe, & Rathje, 2009)

2.4.4 Shear Modulus Degradation from In-Situ Soils During Earthquakes

The variation of shear modulus with shear modulus with shear strain and excess pore pressure was extensively evaluated based on vertical accelerometer array data recorded during

the 1995 Kobe, Japan Earthquake analyzed by Pavlenko and Irikura (Pavlenko & Irikura, 2002). Three vertical accelerometer arrays were installed at sites prior to the earthquake and the soil response was recorded and analyzed. These arrays showed similar shear modulus reduction occurring in-situ with dynamic loading from the earthquake.

The three sites had varying characteristics and properties. The three sites, named Port Island (PI), SGK, and TKS were approximately 2 km, 6 km, and 26 km, respectively, from the epicenter of the Kobe 1995 Earthquake. The Port Island site is of interest because the site experienced liquefaction. The soil profile for PI is shown in Figure 2-12. The site was a reclaimed gravel fill, underlaid by an alluvial clay and an alluvial sand. Interpreted shear stress-strain relationships were obtained between pairs of accelerometers to define the behavior of the soils between the accelerometers. This analysis makes it possible compare the behavior of the different soil types in the profile as shown in Figure 2-12. The shear stress-strain relationships were plotted every 1.5 seconds and plotted to estimate the shear moduli at different depths. A weighted-mean average value of G_{sec} was determined which acts as the average shear modulus within a group of layers and time intervals.

Liquefaction occurred in the upper 0-13 m of soil, and large shear modulus reduction can be viewed in that soil section, see Figure 2-13. The shear modulus was reduced to 80-90% of its initial value within the first 3-5 seconds of intense shaking and continued decreasing during the following 5-7 seconds of shaking. Similar reduction in shear modulus can be viewed in the deeper soil profile that did not experience liquefaction. The non-liquefied soil's shear moduli reduced 50-60% at depths of 27 to 32.5 m.

Immediately after the intense ground shaking, the shear modulus begins to recover, which can be seen in Figure 2-14. The recovery of stiffness is attributed to two processes, pore pressure

dissipation and thixotropic strengthening properties of the soil. In the 0-13 m range, however, the soil did not recover quickly due to its quasi-thixotropic properties after liquefaction.

The effects of liquefaction and pore water pressure have on shear modulus reduction can be seen in the results presented by Pavlenko and Irikura. Both liquefied soils and non-liquefied soils experienced a reduction in shear modulus. The reduction in stiffness can be attributed to shear strains and or pore pressures.

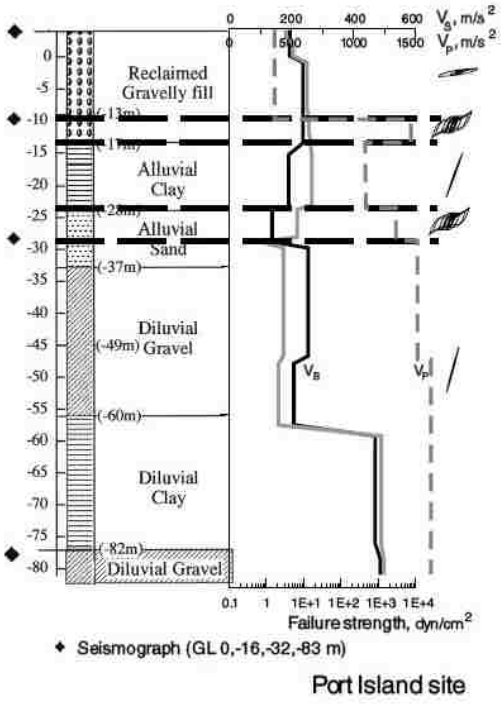

Figure 2-12: Soil Stratification for the Port Island Site (Pavlenko & Irikura, 2002)

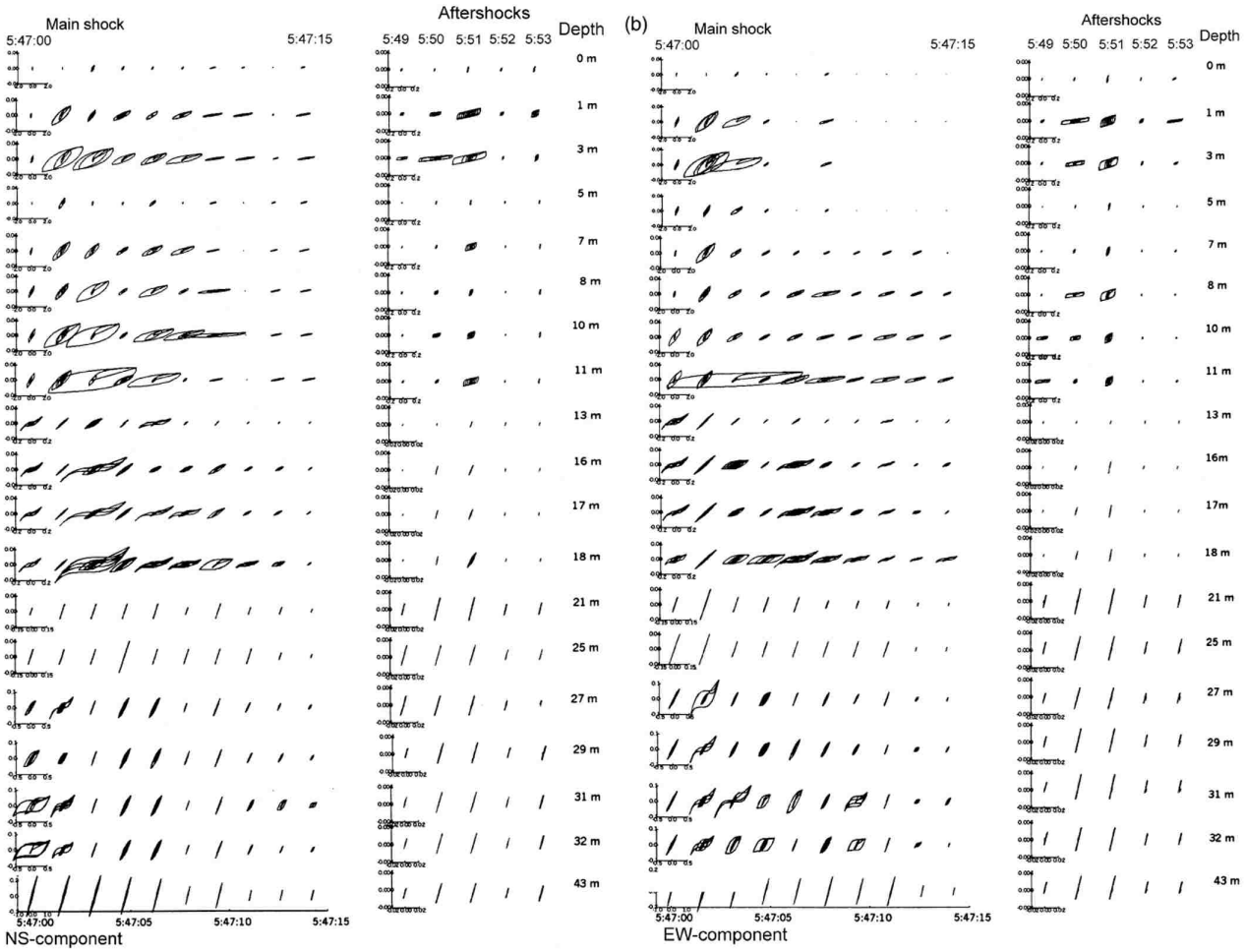

Figure 2-13: Port Island Shear Stress-Strain plots (Pavlenko & Irikura, 2002)

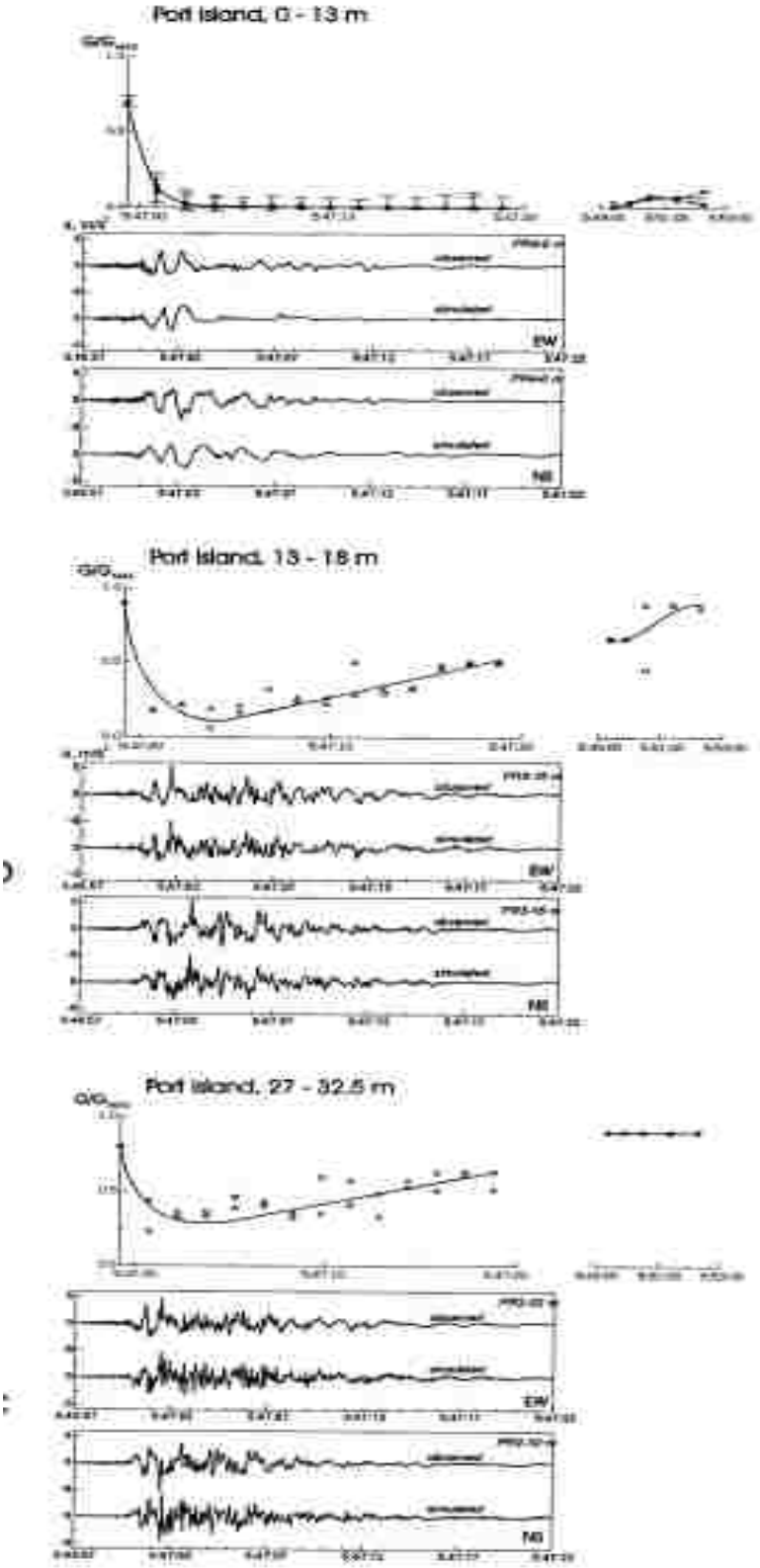

Figure 2-14: Shear Modulus Variation with Time at Port Island (Pavlenko & Irikura, 2002)

Soil response during the 1987 Wildlife Site in Imperial county, California was analyzed by Zeghal and Elgamal (Zeghal & Elgamal, 1994). This site included two earthquakes, the Elmore Ranch (M=6.2) and the Superstition Hill (M=6.6). The Superstition Hill earthquake is of interest due to the increase of pore water pressure experienced. Elmore Ranch did not record an increase in pore pressures.

The site included two accelerometers, one on ground surface and one 7.5 meters (~24.6 feet) below ground surface. The site also deployed six piezometers in the potential liquefiable silty sand layer. The instrumentation can be seen in Figure 2-15

The most intense shaking occurred between seconds 13.7 and 20.6 and pore water pressure increased rapidly. The acceleration continued but decreased with time, at which the pore water pressure continued to increase but at a slower rate, during 20.6 to 96 seconds of time.

The recorded ground motion was presented in shear stress-strain curves created hysteresis loops for the shaking event. The complete hysteresis loops can be seen in Figure 2-16. The pore water pressures or pore pressure ratios were not presented in the research.

During the Superstition Hill earthquake, pore pressures began to increase at 7.5 seconds of shaking, which relates to a shear strain of 0.04%. This relates closely to the threshold strain described by Dobry (Dobry & Ladd, 1980) presented earlier.

The effect of rising pore pressures can be seen in Figure 2-17. As pore water pressure increased through the shaking event, the soil stiffness, or shear modulus, decreased. The soil also exhibited large shear strains with little accompanying shear stresses until a small restorative shear stresses. This behavior is typical of liquefaction.

Figure 2-15 Cross Section and Instrumentation at Wildlife Site (Bennett, McLaughlin, Sarmiento, & Youd, 1984)

Figure 2-16 NS Shear Stress-Strain Histories at 2.9 m Depth for Superstition Hills in 1987 Earthquake ((Zeghal & Elgamal, 1994)

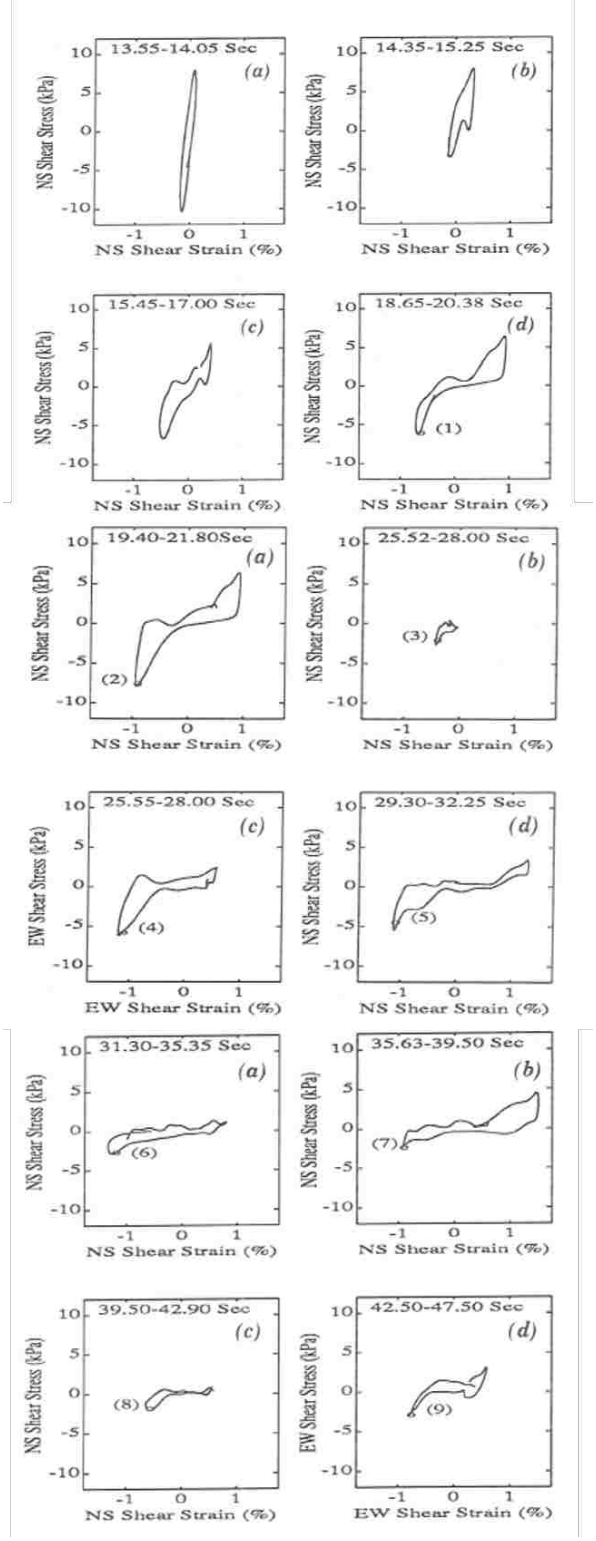

Figure 2-17: Shear Stress-Strain History during Superstition Hill Earthquake (Zeghal & Elgamal, 1994)

2.5 Liquefaction Mitigation Techniques

Techniques for liquefaction mitigation are varied but useful in limiting the damages caused by liquefaction. Techniques include densification, drainage, grouting or solidification, and biological methods.

Densification is defined as the process of air voids being replaced by soils through pressure or force. It is accomplished by dynamic compaction or vibro-compaction. Dynamic compaction method is done by dropping a heavy weight repeatedly on the ground and densifying the soils under impact and the surrounding soils. Vibro-compaction is performed by vibratory hammers and can be used at depth. The vibration causes the sand particles to arrange in a denser array.

Solidification is accomplished by grouting. Grout is injected into the soil, to permeate and fill the voids in the soil. The grout cements the sand particles and increases the shear strength. Jet grouting can also be used to produce a cemented soil. Jet grouting uses jets of water and cement to create a vertical column of soilcrete or a mixture of cemented soil.

Gravel drains, or stone columns, act to densify loose sand as well as providing drainage for soil. This effectively produces drainage paths for the pore water pressure to dissipate. The ability to drain coupled with the increased strength of stone columns can also be useful in reducing the potential for lateral spreading or slope instability. Gravel drains have limited uses in soils with fines. The void spaces in the gravel drain could become contaminated with fines and the effectiveness of the drainage would decrease. In addition, silty sands are more resistant to densification by vibration during stone column installation.

Prefabricated vertical drains allow a cheap and effective way to dissipate pore pressures. A corrugated pipe surrounded with filter fabric allows water to dissipate without fines infiltrating

the drains. They can be constructed and installed relatively cheaply compared to other liquefaction mitigation techniques.

The data analyzed in this thesis was obtained through large scale testing with prefabricated vertical earthquake drains. The results and analysis will show the soil response to cyclic loading, and the potential effects of prefabricated vertical drains.

2.5.1 Liquefaction Mitigation through Vertical Drains

Seed and Booker (Seed & Booker, 1977)pioneered the idea that effective drainage of pore pressures could potentially stabilize soils that are susceptible to liquefaction. Seed and Booker analyzed the drainage that occurs from gravel or rock drains also known as stone columns. Stone columns or gravel columns are a common technique to mitigate earthquake liquefaction but are mainly used for densification and not drainage.

A more modern and economical drainage technique employs prefabricated vertical drains vibrated into the soil. The prefabricated vertical drains (PVD) or "earthquake drains" are slotted drain pipes, typically 75 to 150 mm in diameter. The drains are installed using a vibrating steel mandrel and are typically installed in the ground in a triangular pattern to minimize distance to drainage. The drain is covered with a filter fabric to prevent fines from entering the drain.

There are many benefits to prefabricated vertical drains. The cost of producing and installing PVDs is about 30 to 50% of the cost of densifying the soil with stone columns. Installation is very quick and easy in non-gravelly soils, and PVDs have a higher flow capacity than stone columns. A 100 mm diameter drain can carry very large flow volumes (0.093 $m^{3/}$sec).

This flow volume is more than 10 times greater than that provided by a 1 m diameter stone column (6.51×10^{-3} m^3/sec).

Prefabricated vertical drains have been tested using blast induced liquefaction. Rollins et al (Rollins, Joshua, Mccain, & Goughnour, 2003) installed PVDs at a test site on Treasure Island near San Francisco. The results of the test showed the PVDs, or earthquake drains effectively decreased pore pressure generation at the varying test sites, as seen in Figure 2-18. The reduction of pore pressure is nearly 60% and dissipates in less than 60 secs from blast initiation. The EQ drains, however, did not prevent liquefaction. This is due to the relative quickness of the blast-induced liquefaction.

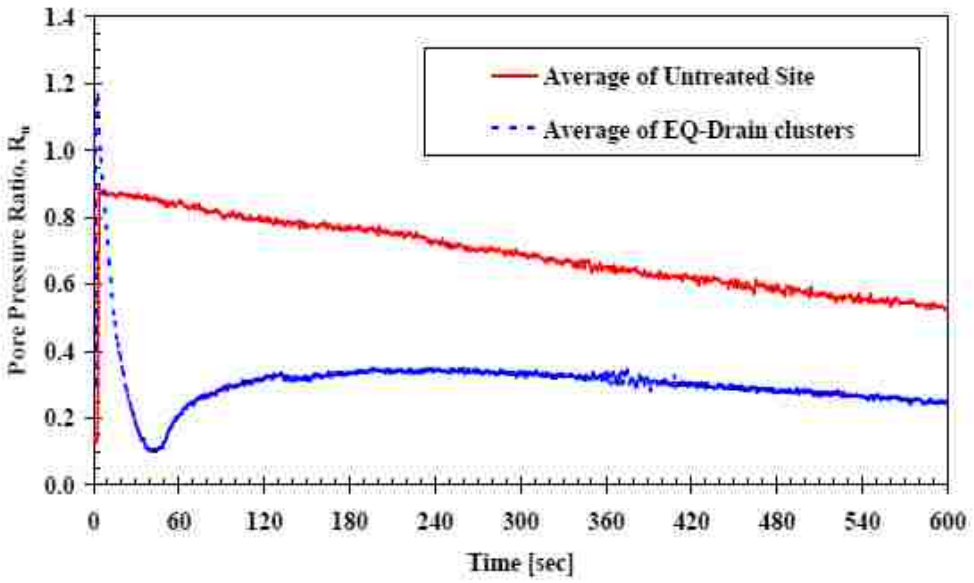

Figure 2-18: Treasure Island Test Results (Rollins, Joshua, Mccain, & Goughnour, 2003)

Howell, Rathje, Kamai, and Boulanger (Howell, Rathje, Kamai, & Boulanger, 2012) performed centrifuge testing with prefabricated vertical drains for liquefaction remediation.

Three dynamic centrifuge tests were performed with both PVD treated and untreated zones on Nevada sand. The centrifuge set-up followed scaling laws for dynamics for comparisons to full-size tests and results. A total of nine shaking events were applied to the model with enough time between each event to allow for complete excess pore water pressure dissipation.

The pore pressure ratio vs. time was plotted for the PVD treated area compared to the untreated area and can be seen Figure 2-19. The areas treated with prefabricated vertical drains showed lower pore pressure ratios. Therefore, the prefabricated vertical drains are effective in mitigating the pore pressure build-up during a shaking event. The drains also increased the rate of dissipation. Treated sands showed lowering pore pressures to 0.2, nine seconds after shaking compared to 0.5 of the untreated sands. This increased pore pressure dissipation had great effect on the amount of deformation observed.

A comparison of results for untreated and treated results can be seen in Figure 2-20. The drains decreased the time the soil experienced pore pressure ratios higher than 0.5. The reduced pore pressure ratio and shorter duration of pore pressures higher than 0.5 lead to less vertical and horizontal displacements.

Sites with earthquake drains installed have yet to experience an actual earthquake ground motions. To avoid blast-induced liquefaction, a large-scale test was completed in 2014 (Oakes, 2015). The results of this test are discussed later in this thesis and a deeper analysis given.

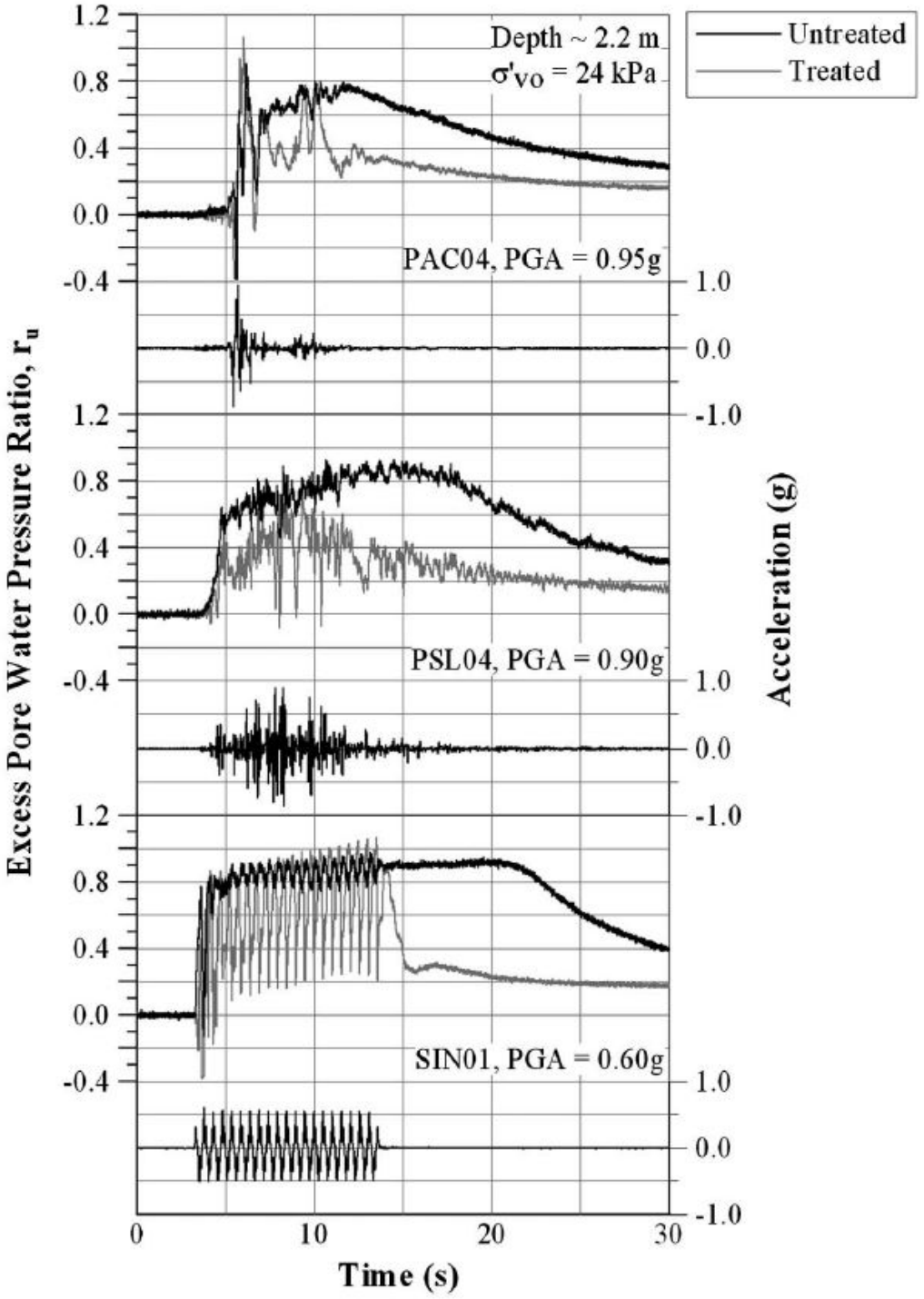

Figure 2-19: Pore Pressure Ratio vs. Time for PVD Treated and Untreated Sand (Howell, Rathje, Kamai, & Boulanger, 2012)

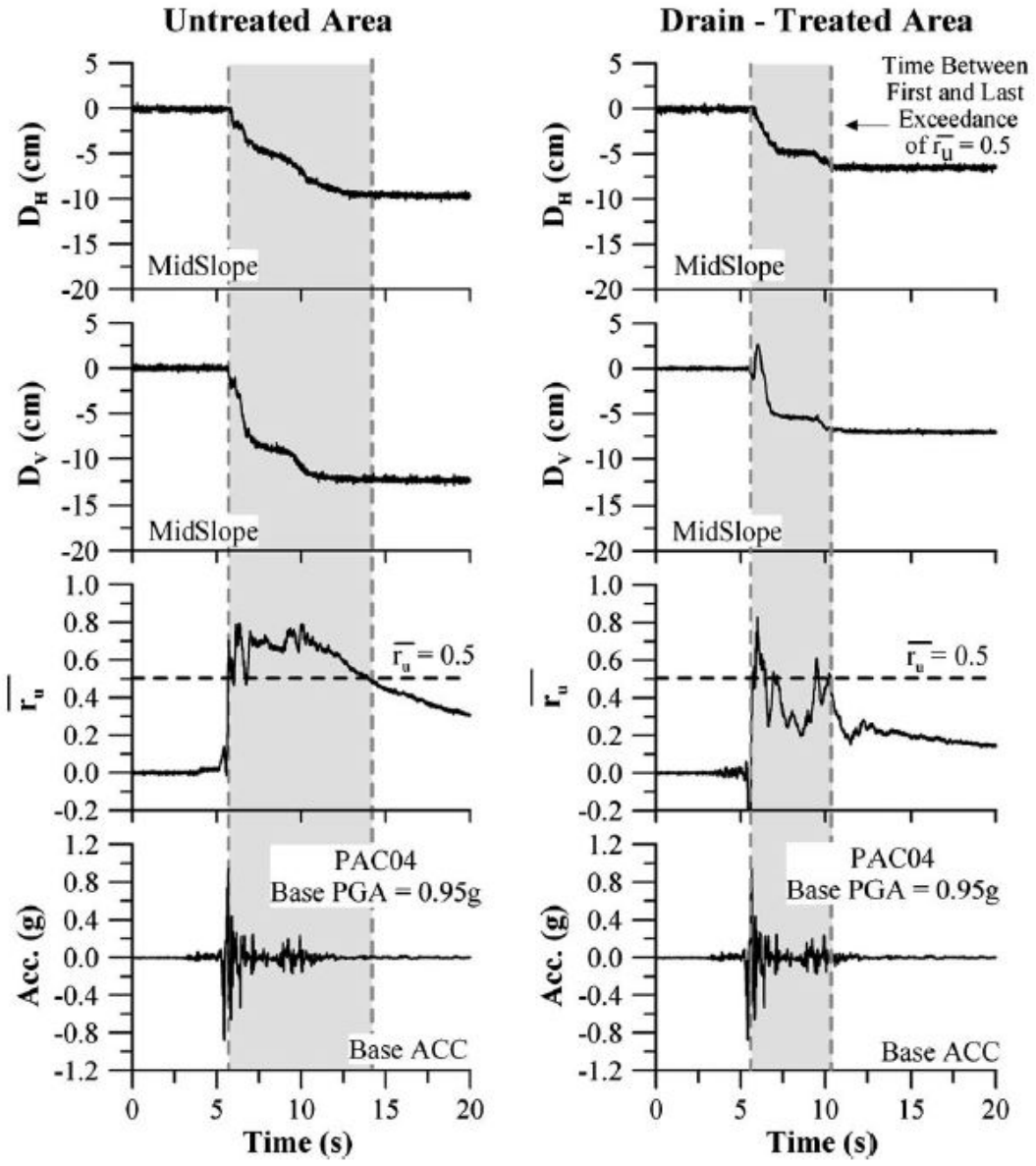

Figure 2-20: Comparisons of PVD Treated and Untreated Results (Howell, Rathje, Kamai, & Boulanger, 2012)

2.6 Literature Review Conclusion

Prefabricated vertical drains (PVDs) have been a recent liquefaction mitigation technique. By relieving pore water pressure buildup, drains could prevent liquefaction from occurring or mitigate pore pressure generation. By mitigating pore pressures, the soil may retain some shear

strength and experience less deformations. Although field liquefaction tests and centrifuge tests have shown the beneficial effects of drainage on pore pressure generation and liquefaction effects, the mechanisms involved in reducing settlement are poorly understood. An assessment of the generation of pore pressure with cyclic shear strain from the laminar shear box testing with and without drains could provide a more fundamental understanding of the mechanisms involved.

The effect of excess pore pressure development on soil shear modulus is difficult to fully understand at presents. Once a soil passes the threshold cyclic shear strain, shear modulus reduction and pore pressure generation occur. Although relatively well-defined relationships have been developed to define shear modulus degradation with shear strain, no well-established relationships are available to include both the effect of shear strain and excess pore pressure ratio. It is common practice to assume that liquefied soil has zero shear strength, but this may vary depending on pore pressure generation. Some residual shear strength may remain and can be correlated with pore pressures, and not purely shear strain. This thesis will help explain the relationship between shear modulus, shear strain, and excess pore pressure ratio by analyzing test data from a large-scale shaking test at UB-SUNY.

3 LARGE-SCALE TESTING

3.1 Introduction

The initial testing performed was a full-scale Earthquake drainage effectiveness testing using stacked laminar shear boxes. The testing was performed at State University of New York-Buffalo. The site is a Network for Earthquake Engineering Simulation (NEES) shared-use facility in the National Science Foundation program.

Two different laminar shear box set ups were used. The first set-up tested was a column of 14.5 feet of pluviated sand with earthquake drains spaced at 4 feet from center. The second test was a 16 feet column of pluviated sand with earthquake drains spaced at 3 feet from center. The list of all tests, with designated titles can be seen in Table 3-1. Both spacing patterns had three rounds of testing, each round having accelerations of 0.05-g, 0.1-g, and 0.2-g applied.

The purpose of this testing was to explore the effects of earthquake drain effectiveness in mitigating liquefaction and settlement with no installation densification or disturbance. To achieve this, each earthquake drain and data-collecting sensor was suspended in place before and during sand placement. The acceleration inputs were performed by hydraulic actuators and inputs were a sinusoidal pattern

The tests were measured with a variety of sensors. These sensors include pore pressure transducers, accelerometers, potentiometers, and string pots. Video cameras, pipes and pumps

were used in collaboration of the sensors. These sensors were provided by University of Buffalo NEES facility, Brigham Young University Civil and Environmental Engineering Department and University at Buffalo Civil Engineering Department.

Table 3-1: Test Reference Titles

Spacing	Round	Acceleration	Reference Title
3 ft.	1	0.05 g	3R1_05g
3 ft.	1	0.1 g	3R1_1g
3 ft.	1	0.2 g	3R1_2g
3 ft.	2	0.05 g	3R2_05g
3 ft.	2	0.1 g	3R2_1g
3 ft.	2	0.2 g	3R2_2g
3 ft.	3	0.05 g	3R3_05g
3 ft.	3	0.1 g	3R3_1g
3 ft.	3	0.2 g	3R3_2g
4 ft.	1	0.05 g	4R1_05g
4 ft.	1	0.1 g	4R1_1g
4 ft.	1	0.2 g	4R1_2g
4 ft.	2	0.05 g	4R2_05g
4 ft.	2	0.1 g	4R2_1g
4 ft.	2	0.2 g	4R2_2g
4 ft.	3	0.05 g	4R3_05g
4 ft.	3	0.1 g	4R3_1g
4 ft.	3	0.2 g	4R3_2g

3.2 Test Equipment

3.2.1 Laminar Shear Box

A large scale laminar shear box was used for this testing, as shown in Figure 3-1. The equipment was designed for liquefaction shakes and soil-foundation-structure interaction tests. The laminar shear box consists of 40 rings vertically stacked. Each ring is rectangular with

dimensions of 16 feet-4$\frac{3}{4}$ inch wide and 9 feet in length and 6 inches in width. The laminate rings varied in mass, from 11.2 KN on the bottom rings to 10.5 KN on the top rings. The laminar boxes totaled 20 inches in height. Each laminar shear box contained a series of roller bearings, allowing the soil to move in any direction.

A stable structural frame was constructed adjacent to the laminar shear box for safety precautions and a measurement reference. Instrumentation was installed to this frame. The laminar box is also surrounded by steel columns and bumpers and bracing constraints to prevent the laminar shear box from exceeding unsafe displacements and avoid overturning.

The testing was accomplished in an undrained state. The laminar shear boxes were lined with two flexible membranes the prevented water seepage through or between the laminar boxes. The membranes were Firestone EPDM. The sand was saturated, and the soil remain in undrained condition during testing.

Figure 3-1: Laminar Shear Box

Figure 3-2: Actuators Placed against the Laminar Shear Boxes

3.2.2 Actuator System

The actuator system is used in moving the laminar shear box in a prescribed input motion. The laminates are stacked on top of a steel plate base. Two 100-kip dynamic actuators are connected to the base and a reaction frame, as shown in Figure 3-2. These actuators are computer controlled and measured. The maximum acceleration the laminar shear box system is 0.3-g.

3.3 Characterization of Sand

The sand used in this tested is a poorly graded Ottawa F55 sand. The grain size distribution curve can be seen in Figure 3-3. The properties of this sand are listed in Table 3-2 below. The Ottawa sand was mixed into a slurry with water, and then diffused evenly in the laminar shear box. The water level was maintained above the soil surface. By deploying these methods, the

relative density was consistent between tests. The relative density was measured by filling buckets during pluviation and weighing the captured sand, see Figure 3-5. The unit weight and relative density were calculated, and below is in Figure 3-4 showing relative density vs. depth.

The sand placement did have some inconsistencies when testing. The 4-foot spacing, round 1 (4R1) testing did not fully excavate the sand, leaving about 2-3 feet of sand. The unexcavated sand experienced a greater shaking effort and densification and led to higher relative densities compared to the other tests. This lead to much higher relative densities compared to the remaining soil. This did affect the soils ability to resist liquefaction and increase the relative shear strength of the soil and will be noted in the results.

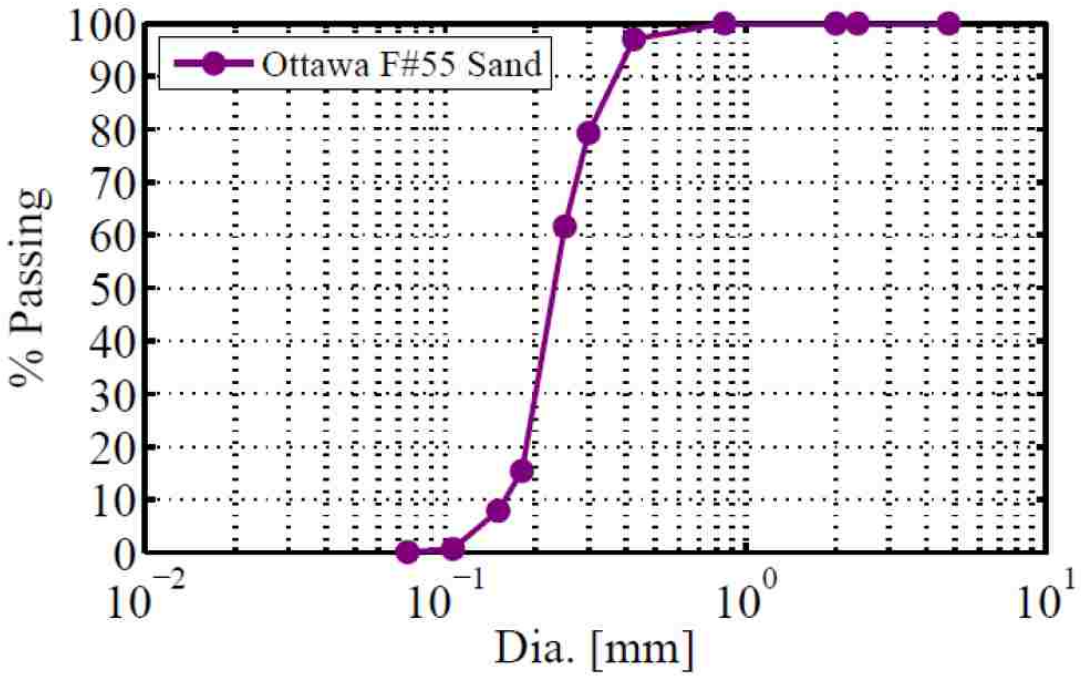

Figure 3-3: Ottawa Grain Size Distribution (Oakes, 2015)

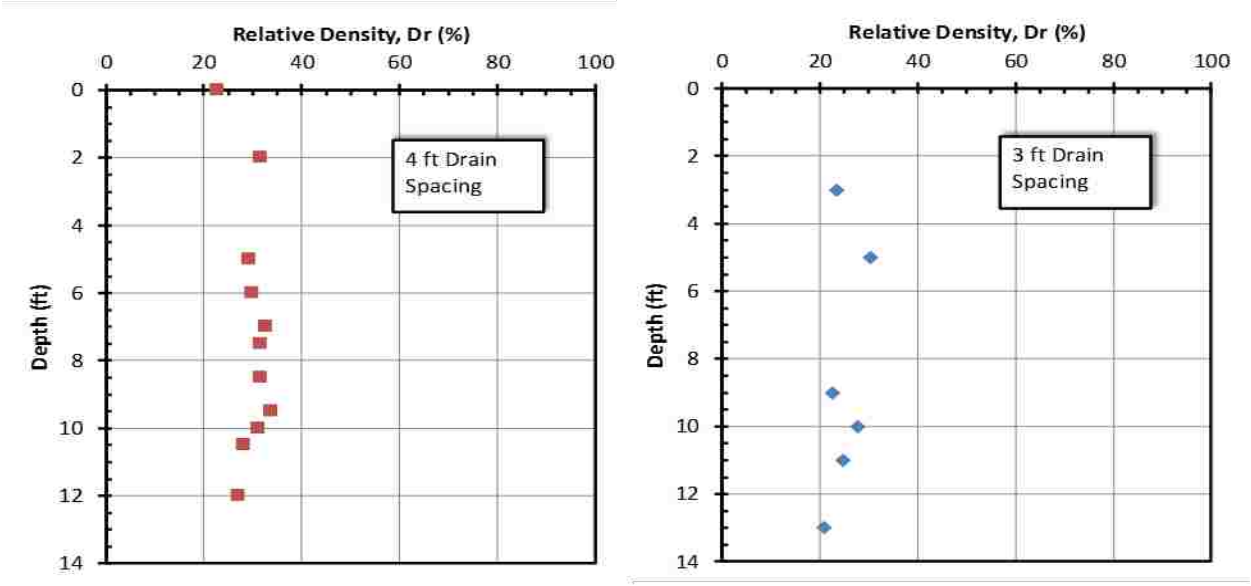

Figure 3-4: Relative Density for 4 Foot and 3 Foot Spaced Tests (Oakes, 2015)

Table 3-2: Properties of Ottawa Sand

Parameters	*Values*
FC (%)	0
e_{max}	0.800
e_{min}	0.608
D_{10} *(mm)*	0.161
D_{30} *(mm)*	0.201
D_{50} *(mm)*	0.230
D_{60} *(mm)*	0.245
C_u	1.522
C_c	1.024

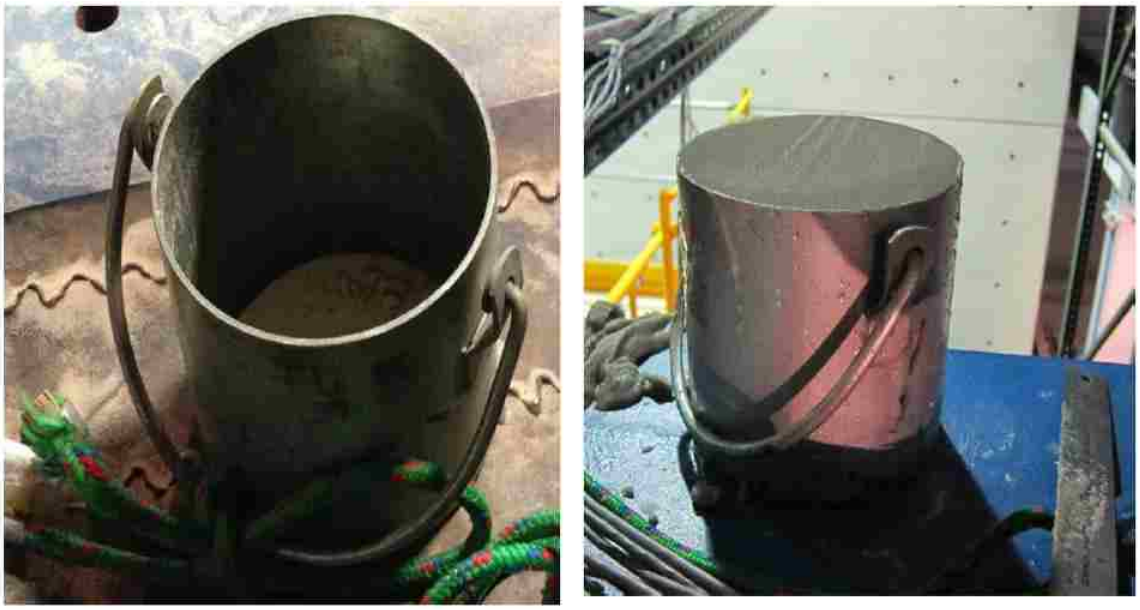

Figure 3-5: Buckets for Density Measurements

3.4 Test Layout

3.4.1 Drain Layout

The testing effort included two different drain spacing. The testing was done with 4-foot spacing and 3-foot spacing. The differing spacing, 3-foot compared to 4-foot, allowed to see how the pore pressure dissipation is affected by spacing of the drains, and was the main reason for the project research.

The schematic of the earthquake drains is shown below in Figure 3-6 and Figure 3-7. The drain layout was spread out in three to four arrays, allowing the drains to be spaced from center to center. The drains were tied to a framework above the laminar shear box to maintain continuity in spacing.

3.4.2 Sensor Layout

Each test had sensor arrays to capture the data during the testing. The sensor array can be seen in Figure 3-8 and Figure 3-9. Table 3-3 shows the number of each type of instrumentation installed for testing. The sensors were evenly spaced within the sample to capture the overall effects during the shaking event. These arrays were tied to a framework above the laminar shear box. Three vertical arrays of pore pressure transducers are located along Mesh 1, Mesh 2, and Mesh 3 and three surface settlement plates which are connected to string potentiometers fastened to a frame located above the box.

Table 3-3: Sensor Type and Amount Installed during Testing

	Quantity
Instrument Sensors	PVD-1
P-Piezometers (PPT)	19
X-Acc (Ring and base) (AE, B)	19
Y-Acc (Ring and base (AE,B)	7
X-Potentiometers (H)	20
Z-Potentiometers (V)	3
Cameras (CA)	4

Unfortunately, a few sensors did not function properly during certain rounds of testing and will be noted in the results. The malfunctioning sensors were observed during data analysis. The sensors that recorded faulty data were removed when data analysis occurred.

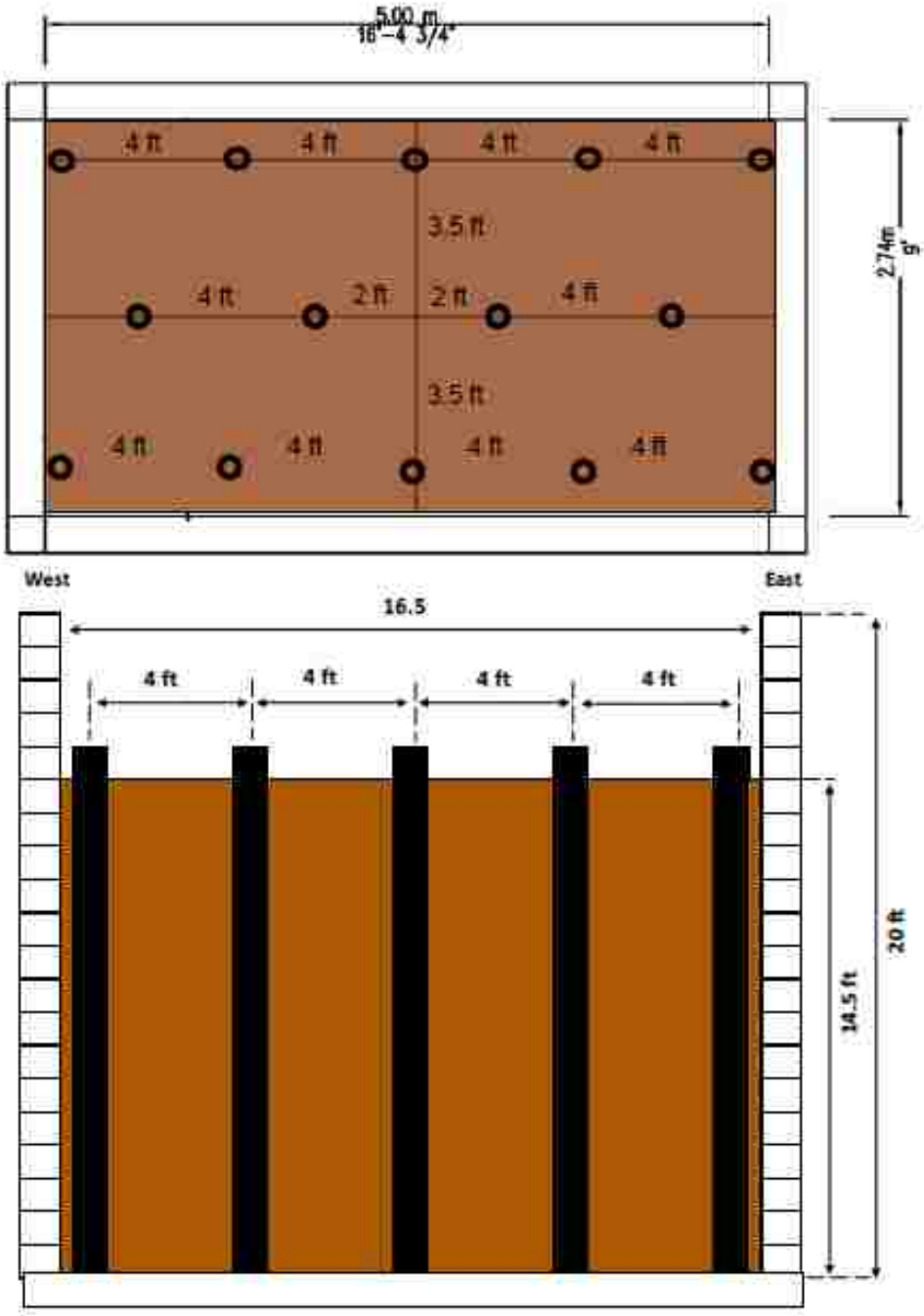

Figure 3-6: EQ Drains 4-ft Spacing Schematic

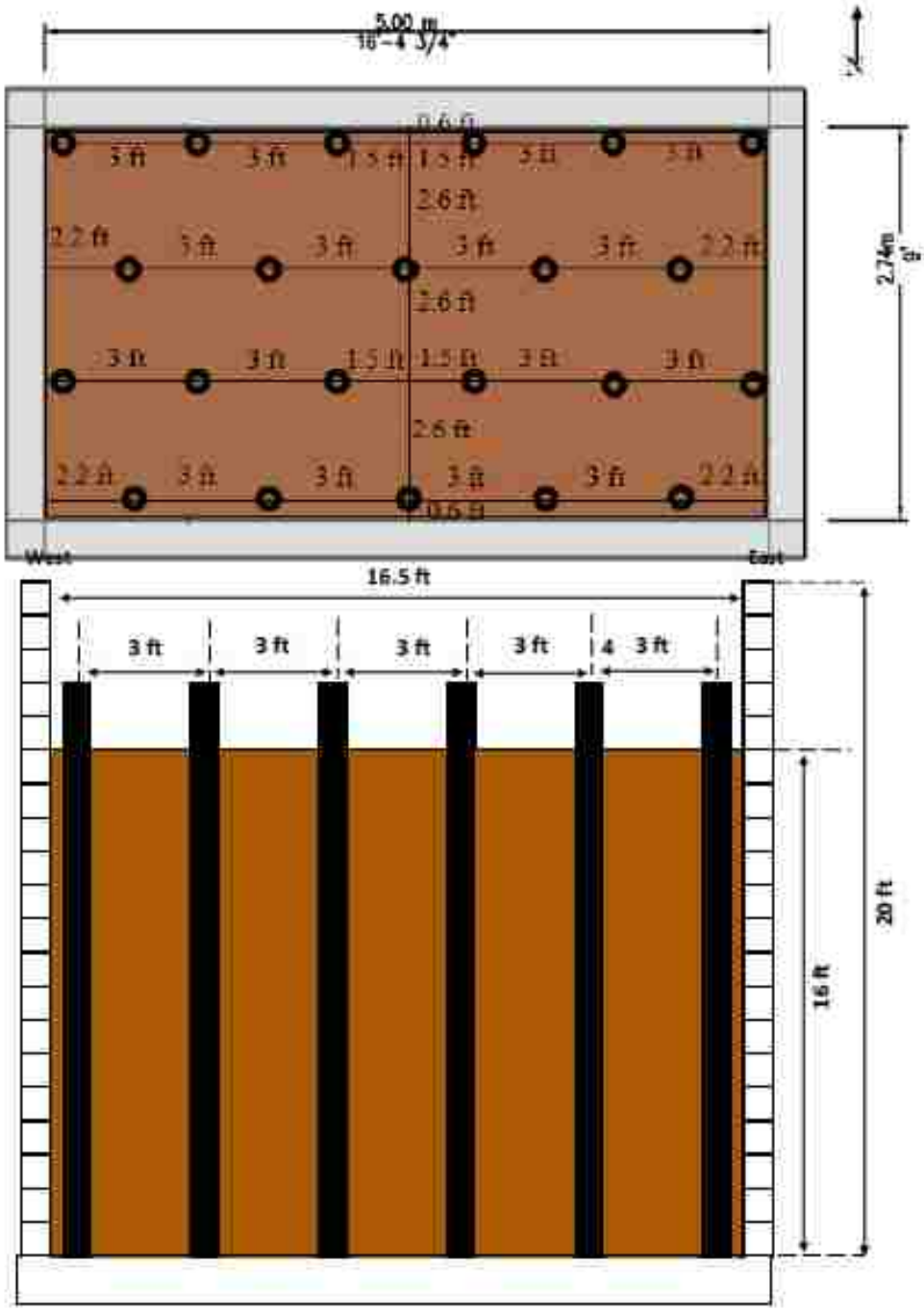

Figure 3-7: EQ Drains 3-ft Spacing Schematic

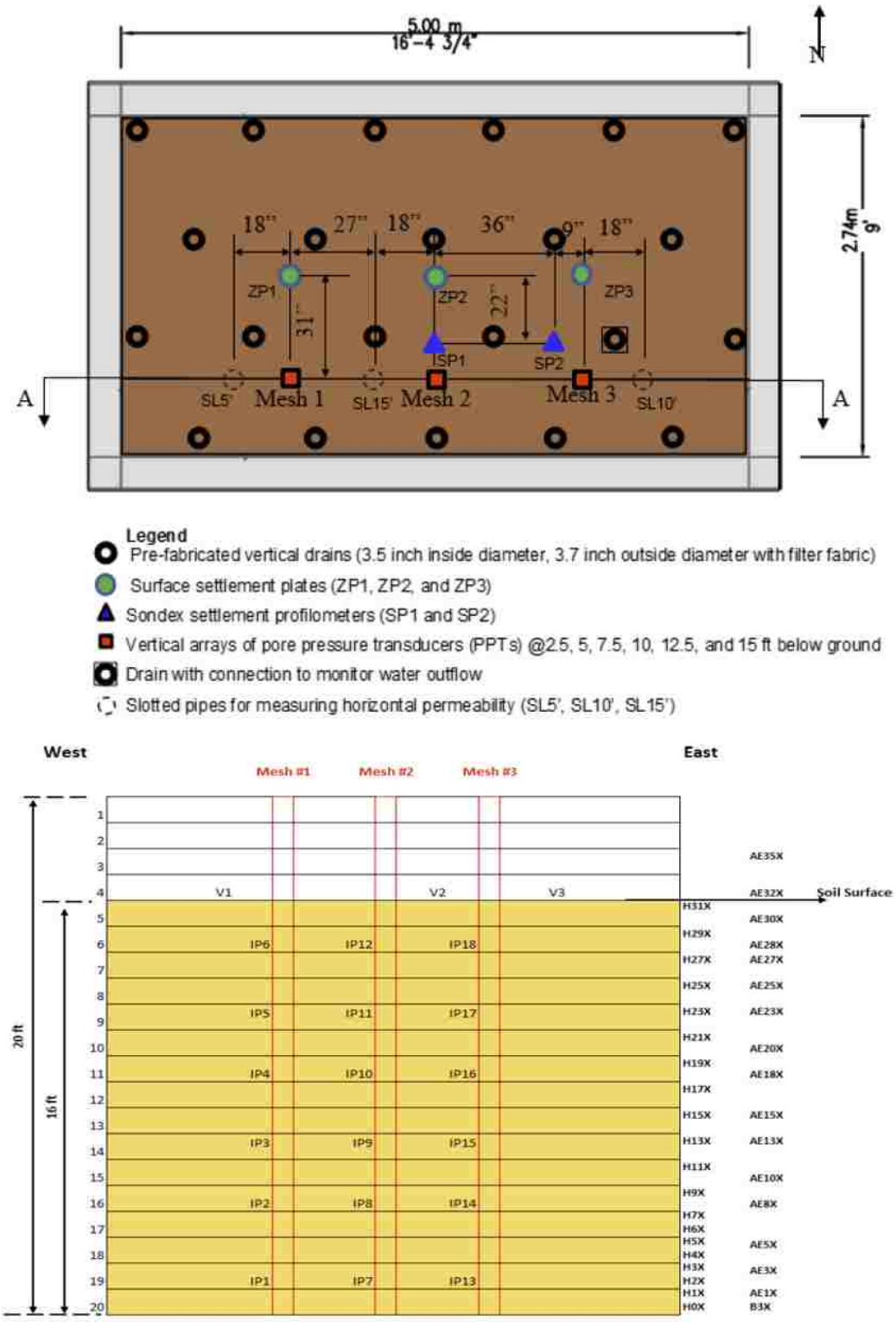

Figure 74 Profile View of Sensors Installed for PVD-2

Figure 3-8: Sensor Locations for 4-ft Tests

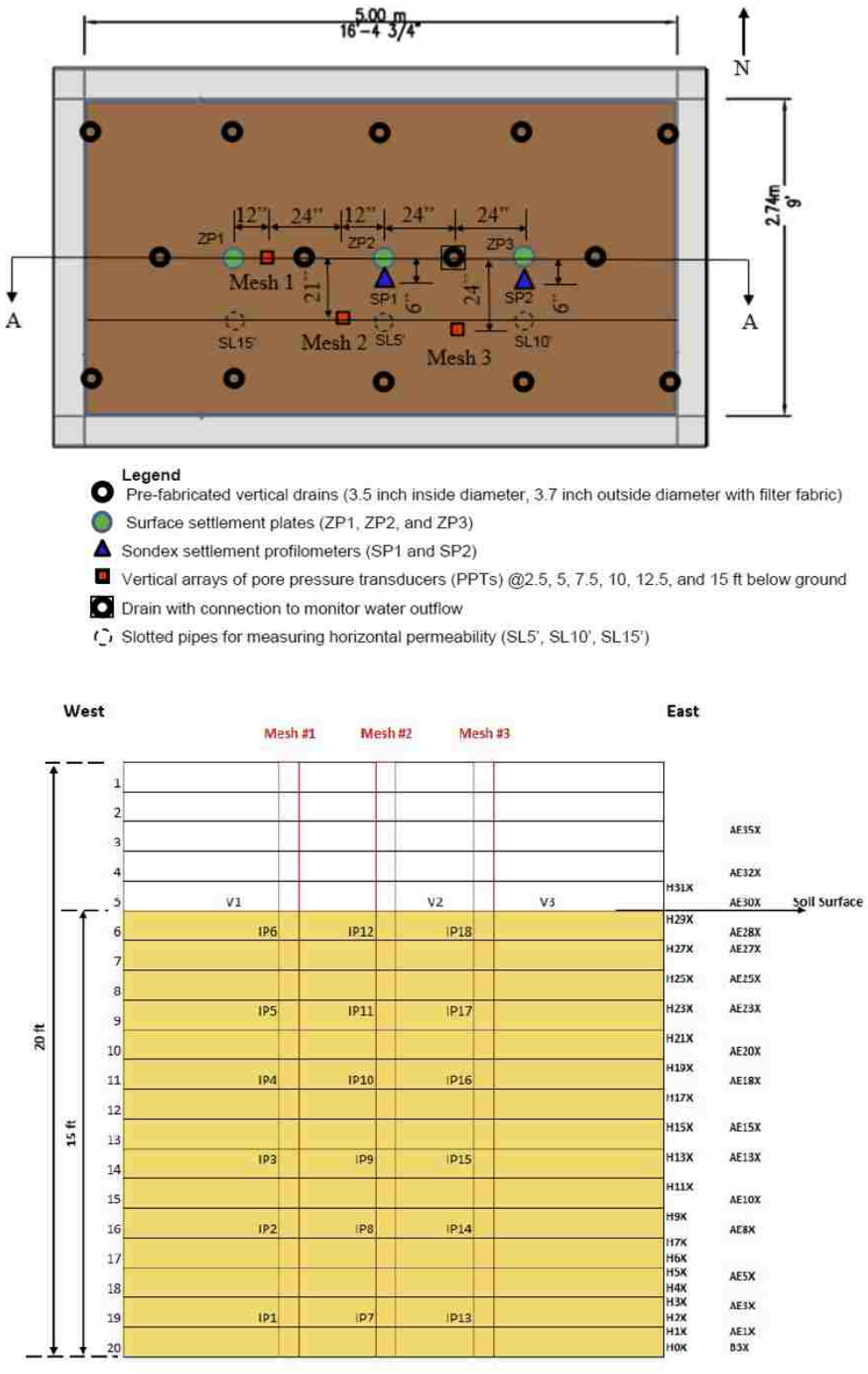

Figure 3-9: Sensor Locations for 3-ft Tests

3.5 Procedures

The laminar shear box and structure were stacked to the appropriate height. Each test used 40 stacked laminate rings lined with the membrane with the safety structures in place.

Drains and sensor arrays were secured as described in the schematic and arranged properly for each respective test. The drains were arranged in triangular grid, 3 feet and 4 feet from center, respectively, for each test. The prefabricated drains were fastened in a grid patterned to a frame work above the laminar shear box and the bottom of the laminar box. A plate was attached to the bottom of each drain to prevent the drain from buoying toward the soil surface during pluviation and shaking.

The laminar shear box was then filled with sand. The sand was mixed with water and then pumped to a spray slurry. The process of pluviating the sand and pumping it into the laminar shear box took three to five days to complete. The sand slurry was pluviated evenly to produce a saturated, loose sand.

Relative density was measured using two methods. The first method was lowering a pre-measured bucket into the laminar box set up. The can was filled by the pluviation and carefully lifted and measured. A picture of this apparatus is shown in Figure 3-5. It was difficult to avoid disturbing the sand and bucket during retrieval and measurement. This can change the measured relative density in relation to the actual pluviated sand. A modified cone penetration test (CPT) was driven into the sand. This was not a standard CPT and resulting resistance appeared lower than expected. This CPT test will not be included in the analysis of the results.

Shear wave velocity testing was performed before each round of testing. This was completed by using a hammer and steel plate. This test measured the approximate shear wave velocity of the soil, which correlates to max shear strength, or G_{max} or G_0.

A system check was performed. The input ground motion was 0.015-g maximum acceleration. This was only done to test that all equipment and sensors are working and to see if all safety measures were intact. If equipment and sensors were working correctly, the testing was initiated.

The testing was performed at differing accelerations. The sand was tested at 0.05-g, 0.1-g, and 0.2-g accelerations. Each acceleration had 15 cycles of movement. This frequency of 2 Hz is used to model a 7.5 magnitude earthquake, typically used for liquefaction studies. The planned accelerations can be viewed in Figure 3-10.

The sand was removed and replaced between each round of accelerations. The new sand was then tested again at the same accelerations. The 4-foot spacing PVD testing did not completely remove the sand between each round of tests, thus some of the behaviors observed do not coincide with the rest of the testing data. The 3-foot spacing completely excavated the sand after each round of shaking, thus avoiding the errors associated with the 4-foot tests.

The volume change in the tested soil was measure. The excess drained water was removed and measured. This allows the change in volume, or specifically, the volume of the voids, to be estimated due to the consolidation of the soil. The calculated relative density for each round of testing can be seen in Figure 3-11. Before a new round of testing, the soil was re-saturated and replaced by pluviation.

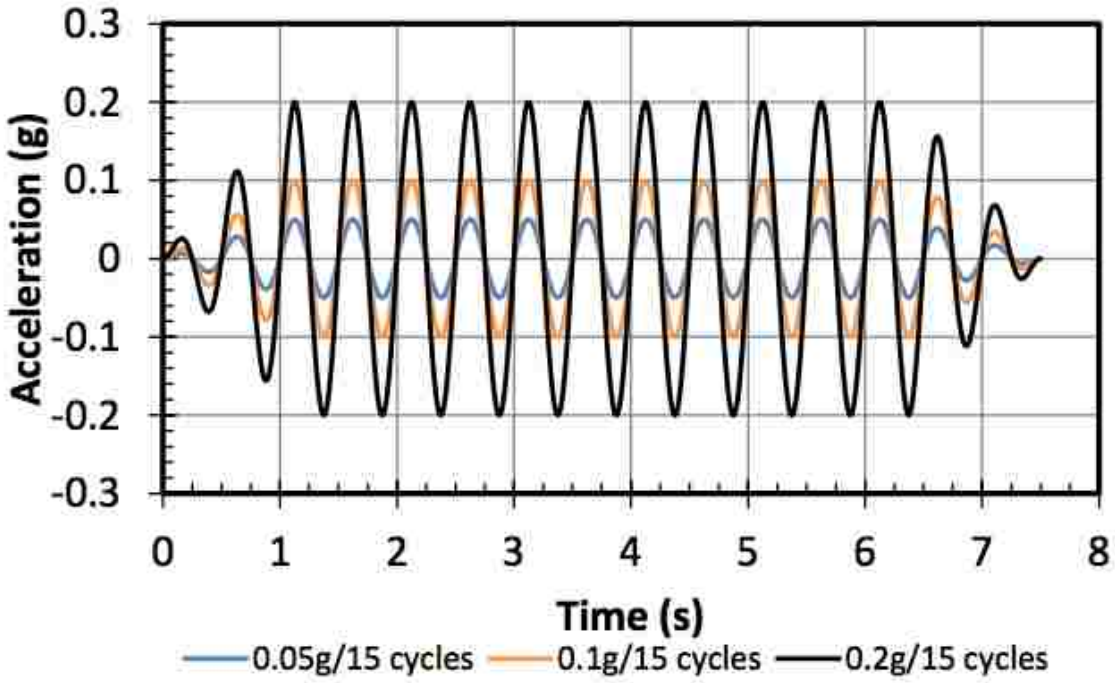

Figure 3-10: Planned Accelerations for Each Round of Testing

4 ft Drain Sapcing					3 ft Drain Spacing			
Base Acceleration	Round 1	Round 2	Round 3		Base Acceleration	Round 1	Round 2	Round 3
0.05g	27	47	58		0.05g	27	49	62
0.1g	33	50	59		0.1g	32	51	64
0.2g	39	54	61		0.2g	40	56	67

Figure 3-11: Calculated Relative Density for Each Round of Testing Based on Void Ratio

4 TEST RESULTS FOR LAMINAR SHEAR BOX TESTS WITH PREFABRICATED VERTICAL DRAINS

This section will show preliminary analysis. This analysis uses the data obtained by each of the testing done on 3-foot and 4-foot PVD spacing. The data obtained by Oakes (Oakes, 2015) was used for this analysis and is used for an in-depth analysis given in the next chapter.

The main effort for the previous study was to limit pore pressure generation, and to reduce the amount of settlement during a shaking event. The results presented in this section will focus on peak pore pressure ratio vs. time and depth; and settlement vs. peak pore ratio and volumetric strain. This was completed by Oakes (Oakes, 2015)and results are represented in the following sections.

4.1 Peak Pore Pressure

Pore water pressure is typically presented as a ratio to the effective stress in the soil. The expression is simply the excess pore water pressure divided by vertical effective stress at the location of the sensor. Therefore, if the ratio is nearing or equal to 1, the soil has, by definition, liquefied. This ratio is often used to describe liquefaction potential. Often a pore pressure ratio of 0.6 of 60% is considered liquefied for design purposes. Results for each test, both the 3-foot spacing and the 4-foot spacing, are discussed in the following sections.

4.1.1 Peak Pore Pressure Ratio vs. Time

Locations of the sensors vary by depth and vertical array. Sensor locations with accompanying vertical effective stress is shown in Table 4-1. The vertical effective stress is calculated by taking the soil unit weight minus water unit weight, due to the water level being higher than the soil surface, multiplied by the depth of soil at that sensor location. This information is used in calculating the pore pressure ratio.

The sensors took samples approximately every 0.0039 seconds. This created a large data file with varying levels of noise in the data recording. A moving average was applied to reduce noise and smooth data curves. An arbitrary number of 100 samples were used in creating a moving average. The effect of this moving average can be seen in Figure 4-1. By applying this, a clear and clear data curve was produced. This helped eliminate noise and establish realistic pore water pressures.

A few pore pressure ratios resulted in inaccurate numbers, for example calculations that resulted in pore pressure ratio higher than one. This means the sensor measured a greater pore water pressure than the assumed vertical effective stress. It is reasonable to assume that soil with a pore pressure ratio higher than one has fully liquefied can be treated as if the pore pressure ratio was one. The pore pressure calculations that results in numbers below zero, were treated as zero. This correction allowed the calculations to be within defined ranges.

The sensors were placed in three vertical arrays, with sensors approximately at the same depth. Therefore, a sensor from each vertical array was grouped and plotted in Figure 4-2. By grouping the plots, broken sensors or outliers were quickly identified. For example, sensor IP9 in Figure 4-2. IP9 was not used in further data analysis.

Table 4-1: Pore Pressure Transducer Locations and Vertical Effective Stress

3 ft. Testing

Sensor	Depth (ft)	Vert. Eff. Stress (Psf)
IP1	14.8	901.31
IP2	12.3	749.39
IP3	9.8	597.46
IP4	7.3	445.54
IP5	4.8	291.11
IP6	2.3	141.69
IP7	15.3	930.96
IP8	12.8	779.04
IP9	10.3	627.11
IP10	7.8	475.19
IP11	5.3	323.26
IP12	2.8	171.34
IP13	15.5	944.56
IP14	13.0	792.64
IP15	10.5	640.71
IP16	8.0	488.79
IP17	5.8	353.96
IP18	3.0	184.94

4 ft. Testing

Sensor	Depth (ft)	Vert. Eff. Stress (Psf)
IP1	12.5	758.98
IP2	10.0	607.06
IP3	7.6	461.44
IP4	5.3	319.04
IP5	3.0	182.31
IP6	0.5	30.39
IP7	12.6	764.50
IP8	10.1	612.58
IP9	7.0	425.39
IP10	5.3	319.04
IP11	3.0	184.13
IP12	0.8	45.58
IP13	12.7	773.01
IP14	10.2	621.08
IP15	7.8	474.75
IP16	6.0	364.62
IP17	3.3	197.50
IP18	0.9	54.69

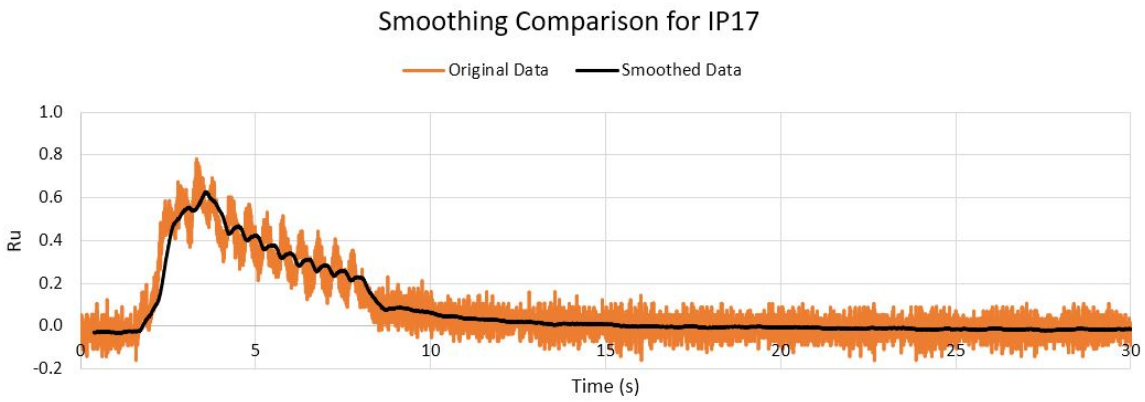

Figure 4-1: Comparison of Moving Average

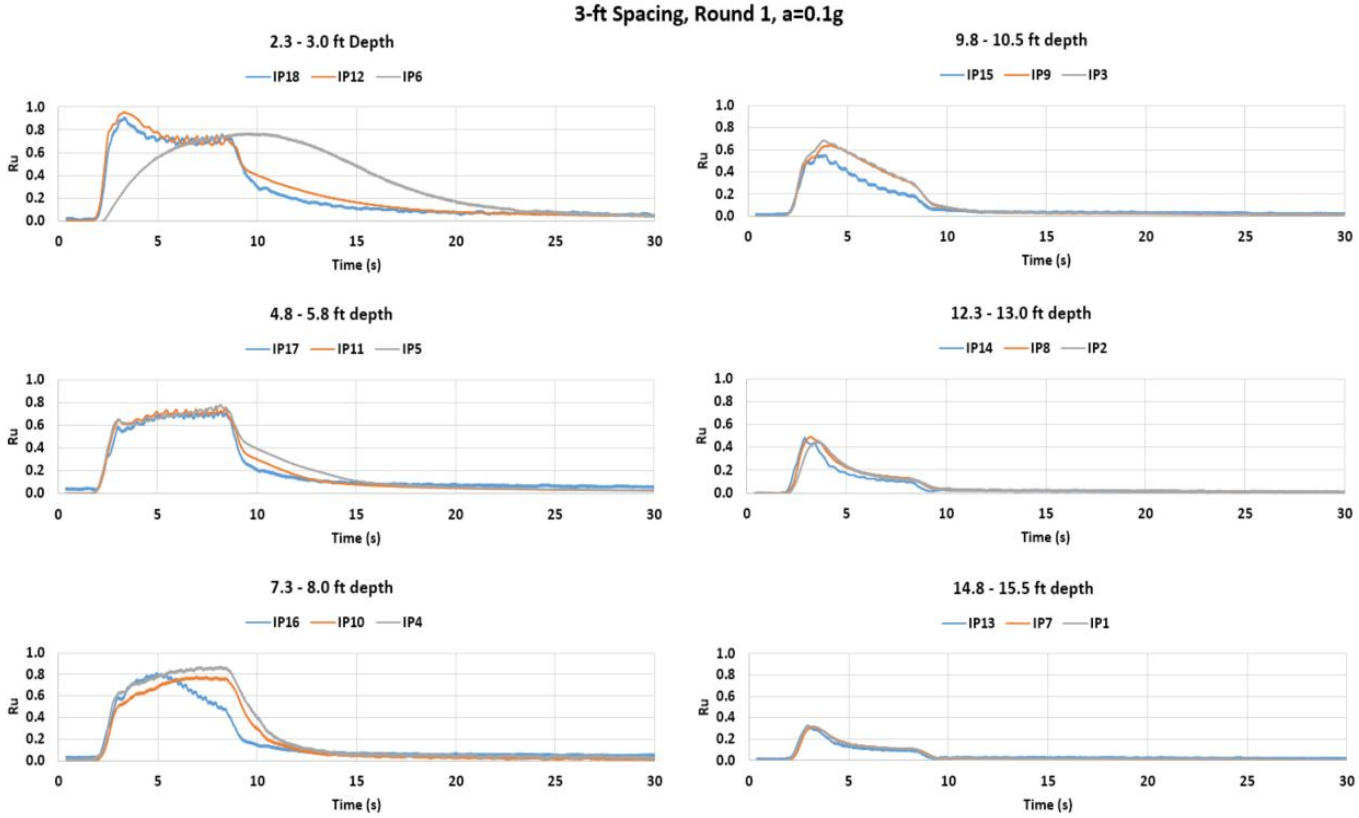

Figure 4-2: 3-ft Spacing, Round 1, a= 0.1-g Ru vs. Time

4.1.2 Peak Pore Pressure Ratio vs. Depth

Figure 4-3 and Figure 4-4 shows the peak pore pressure calculated vs. time for the 4-foot and 3-foot spacing test, respectively. The sensor locations were determined by taking the average depth of sensors in that area. These depths were assumed correct from the earlier test procedure and analysis completed by Oakes (Oakes, 2015). The average, maximum pore pressure ratio, R_u, was calculated and plotted at the average depths. The first sensors, located only an average of 0.72 feet below ground surface showed varied results. An assumption was made that these sensors were truly in liquefaction; therefore, the data points reflect a R_u value of one.

The trend for all tests is pore pressure ratios were higher at shallower depths, and lower at deeper depths. This is because of more effective vertical stress at lower depths, and the compressibility of the soil decreases with depth, making pore pressure generation more difficult. The upward flow of water causes the upper most layers of sand to have excess pore water to contribute with higher pore pressures. Some tests exhibited deeper soil layers with higher pore pressure than soil at a shallower depth. This also might be caused by the newly constituted soil being loose with varying densities, seen in rounds 3R2 and 3R3. The soil is also considered to not be uniform during and after shaking events, due to varying pore pressure generation, densification, and effects of liquefaction throughout the soil layers. Generally, a trend of higher pore pressure ratios at shallower depths and lower pore pressure ratios at deeper depths are observed.

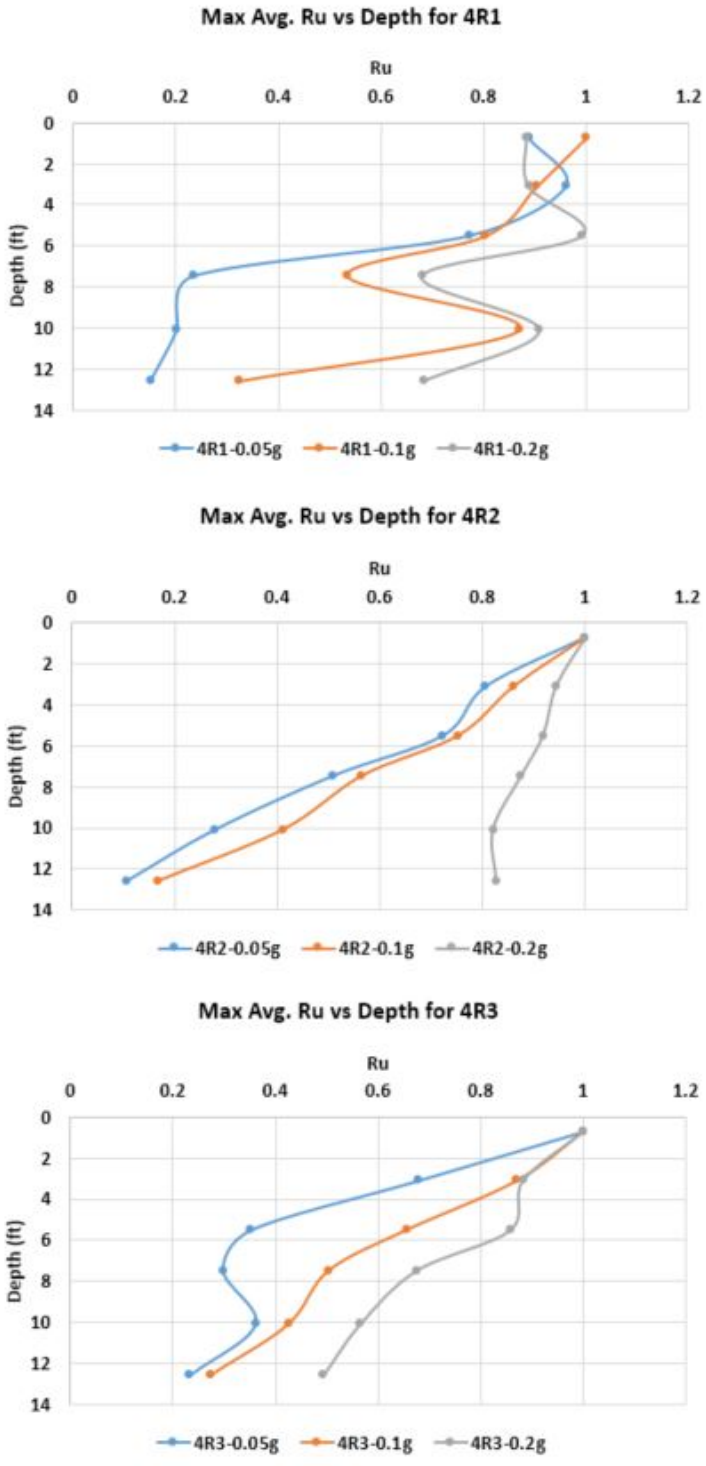

Figure 4-3: 4-ft Spacing, Ru vs. Depth

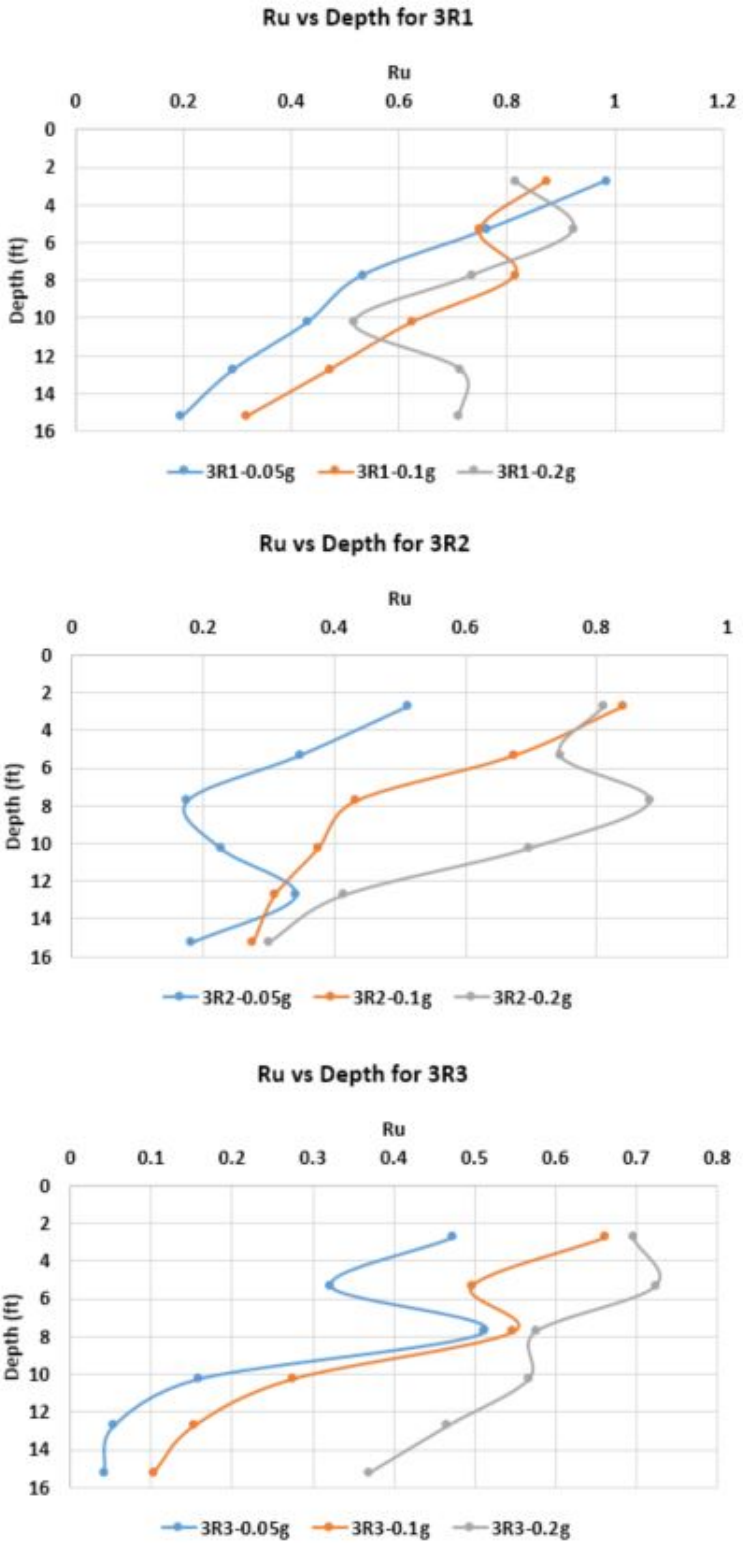

Figure 4-4: 3-ft Spacing Ru vs. Depth

4.2 Settlement

Settlement effects roadways, buildings, and utility lines. Settlement is a major concern and a large contributing factor to costly damages. Liquefaction mitigation focuses on eliminating or limiting settlement occurring in soils. Settlement occurs during liquefaction due to soil particle reconfiguration and the loss of void water space in the soil. The following data was prepared by Oakes (Oakes, 2015) on the UB-Suny testing. The results were presented in his thesis Please refer to the Oakes thesis study for more information, methods, and results. The details will not be discussed in this thesis.

Settlement calculations and data were collected by three different methods, string potentiometers on the soil surface, calculating the volume of drained water, and Sondex Tubes.

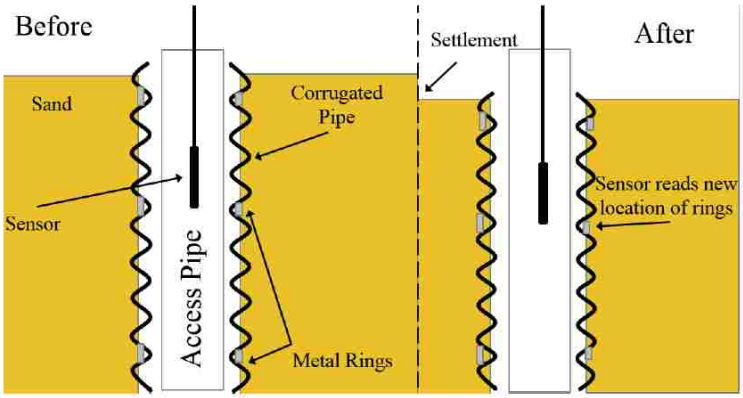

Figure 4-5: Schematic of Sondex Tubes

After each test, the water that was drained from the soil was measured. The string potentiometers measure the initial and final height of the soil, or how much the soil settled. The excess water is assumed to be completely removed from the volume of the voids in the soil. This can be used to estimate settlement of the soil. Two Sondex settlement profilometers contained measurements every two feet in depth.

4.2.1 Settlement vs. Depth

The prepared plots below in Figure 4-6 and Figure 4-7. show the measured settlement vs. depth and the surface settlement measured by the string potentiometers. The Sondex tube sensors at varying depths recorded the change in soil height or settlement.

The figures show the general trend of higher settlements at shallower depths and less settlement in each subsequent round. This correlates well with the R_u vs. depth data in Figure 4-3 and Figure 4-4. Deeper depths experienced less settlement due to higher effective stress. The drains appear to be more effective in reducing pore pressures at depth and upward flow of water reduces pressure at the bottom of a layer relative to the top of the layer. Each subsequent round had less settlement due to increased density from previous shaking events. Related, there is more settlement during the 0.2-g shaking than the 0.05-g shaking due to an increase shaking energy.

The collected data from the Sondex tubes have some errors in recording. The errors most likely was caused by the Sondex tubes bending within the soil. This causes the sensor to misread the current location and usually occurred at one point. The reading errors can be corrected by smoothing the curves. The Sondex tubes are discussed in greater detail in Section 4.2.2 Settlement vs. Volumetric Strain.

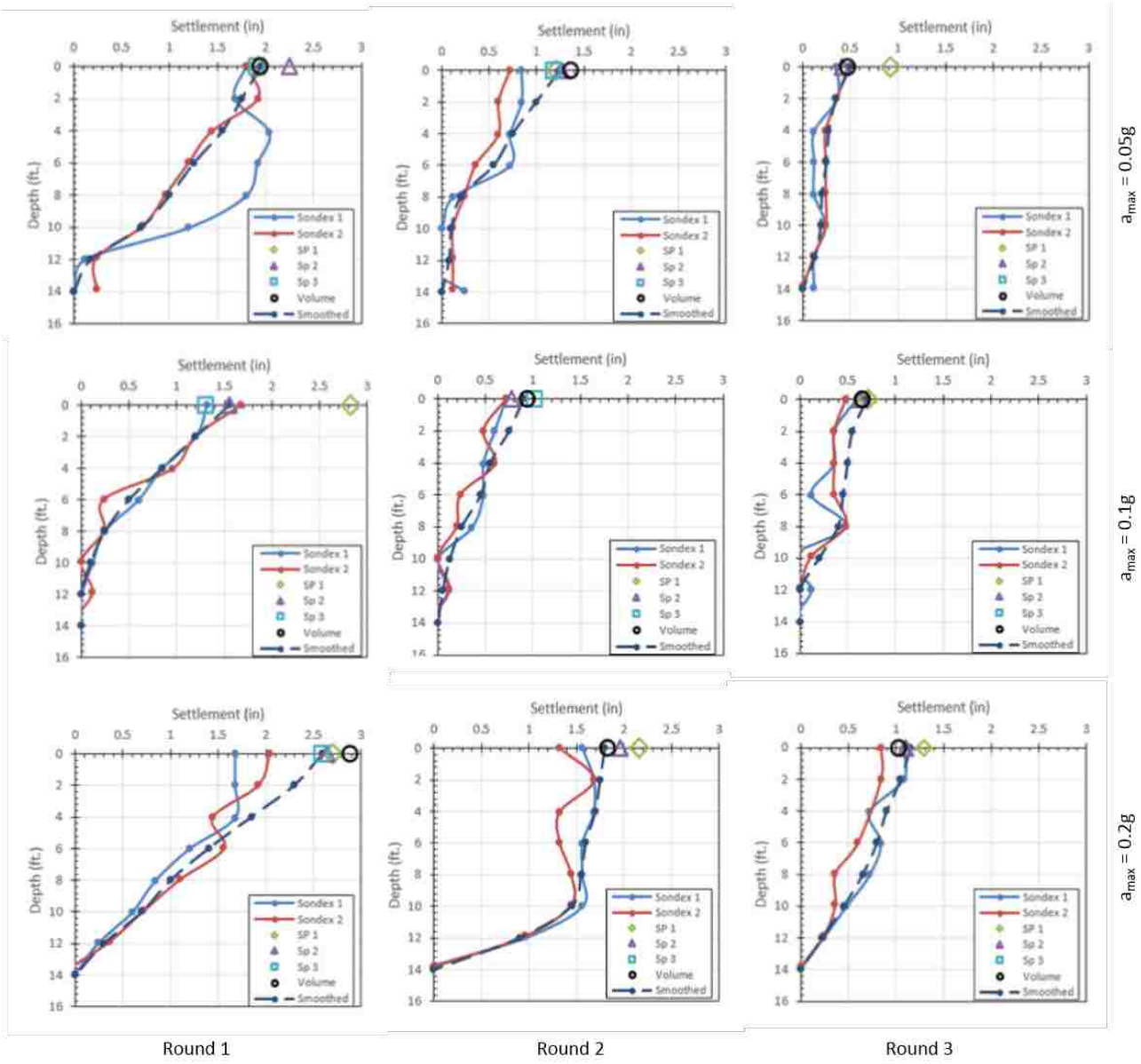

Figure 4-6: Settlement vs. Depth for 4 ft. Spacing

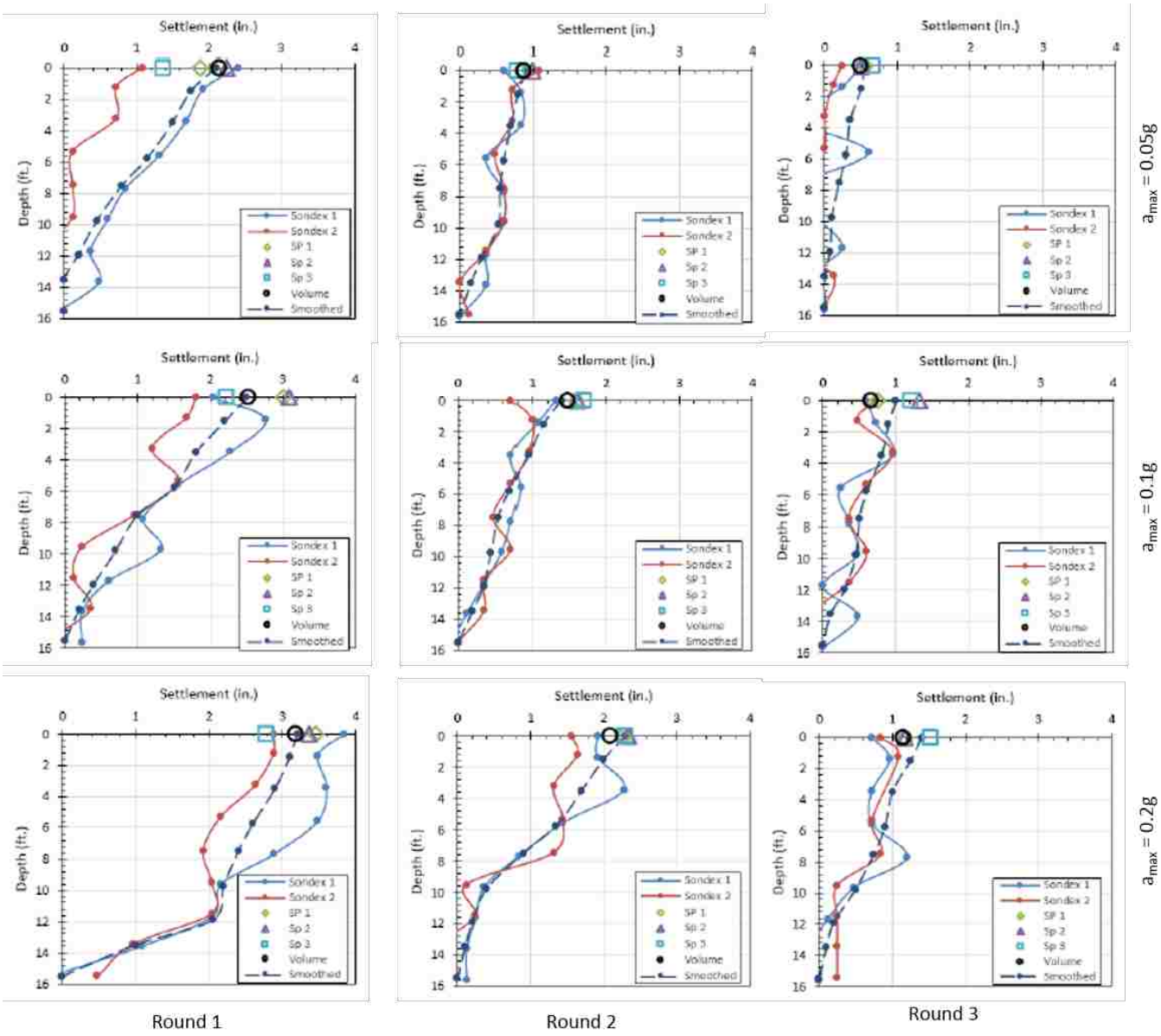

Figure 4-7: Settlement vs. Depth for 3 ft. Spacing

4.2.2 Settlement vs. Volumetric Strain

Volumetric strain was calculated by the Sondex tubes. This calculation was completed by Oakes (Oakes, 2015). A schematic describing how Sondex tubes function is shown in Figure 4-5. A sensor locates and reads metal rings around a flexible corrugated pipe. As the pipe compresses with the soil around it, the metal rings are displaced. The sensor then reads the new ring location. By taking the difference between initial and final ring placements, the settlement can be approximated by depth.

Volumetric strain is the change in volume divided by the initial volume. The volume was calculated using the change in height measure by the Sondex tube sensors multiplied by the space of soil around each Sondex tube sensor.

Figure 4-8 and Figure 4-9 show the calculated volumetric strain vs. the depth. The general trend being less volumetric strain was experienced with subsequent testing. In most testing, the higher shaking effort, i.e., 0.2-g acceleration, experienced higher volumetric strain. The volumetric strain varied by depth.

The observable aberrations in data trends may have resulted in Sondex tubes bending during shaking and inhibiting the movement of the sensor during shaking and giving incorrect positions of the metal rings. The volumetric strain measured at the lower depths in 4R2 0.2-g and 3R1 0.2-g do not fit data trends and can be considered outliers in this data analysis.

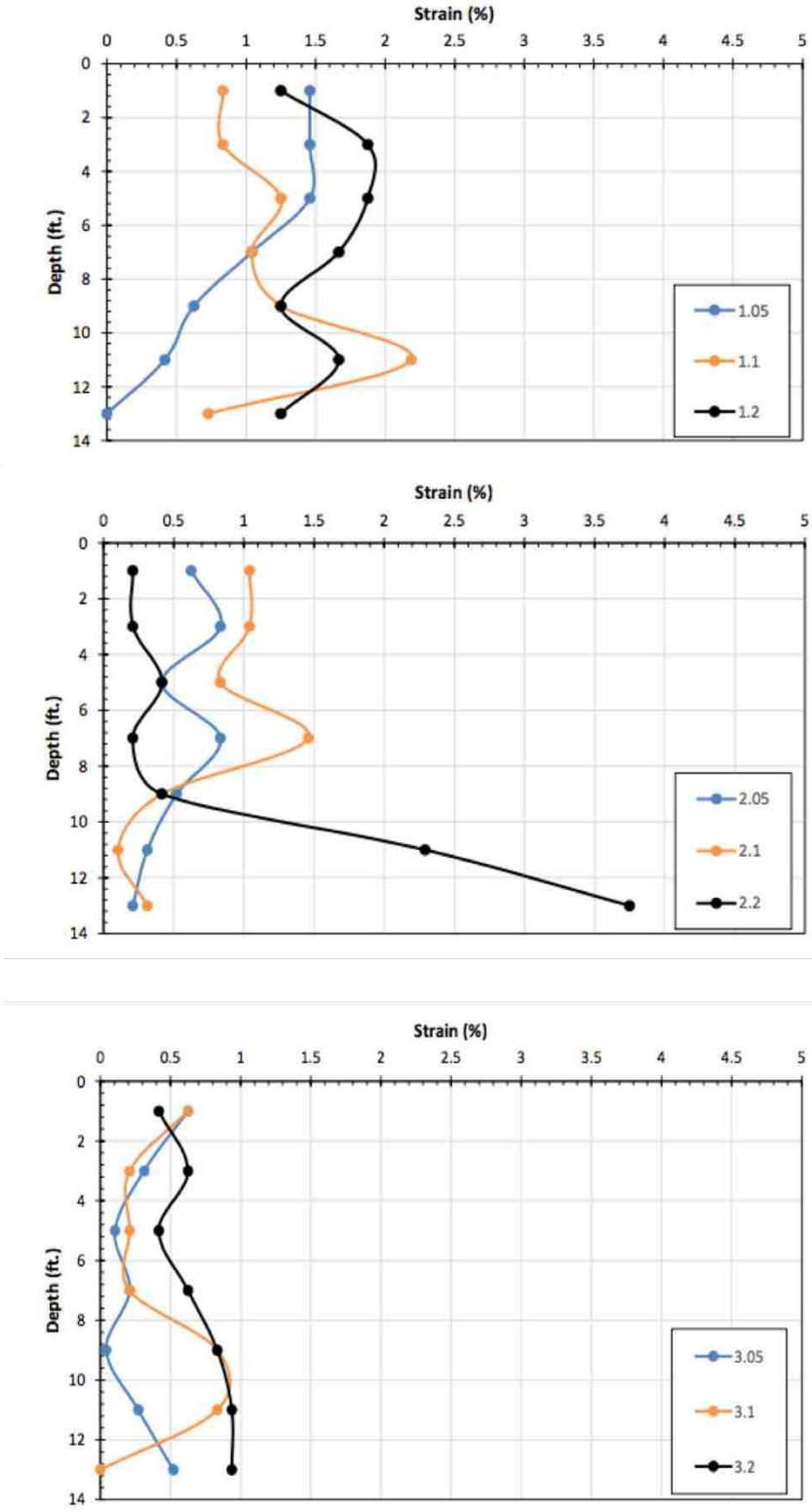

Figure 4-8: Volumetric Strain vs. Depth for 4 ft. Spacing

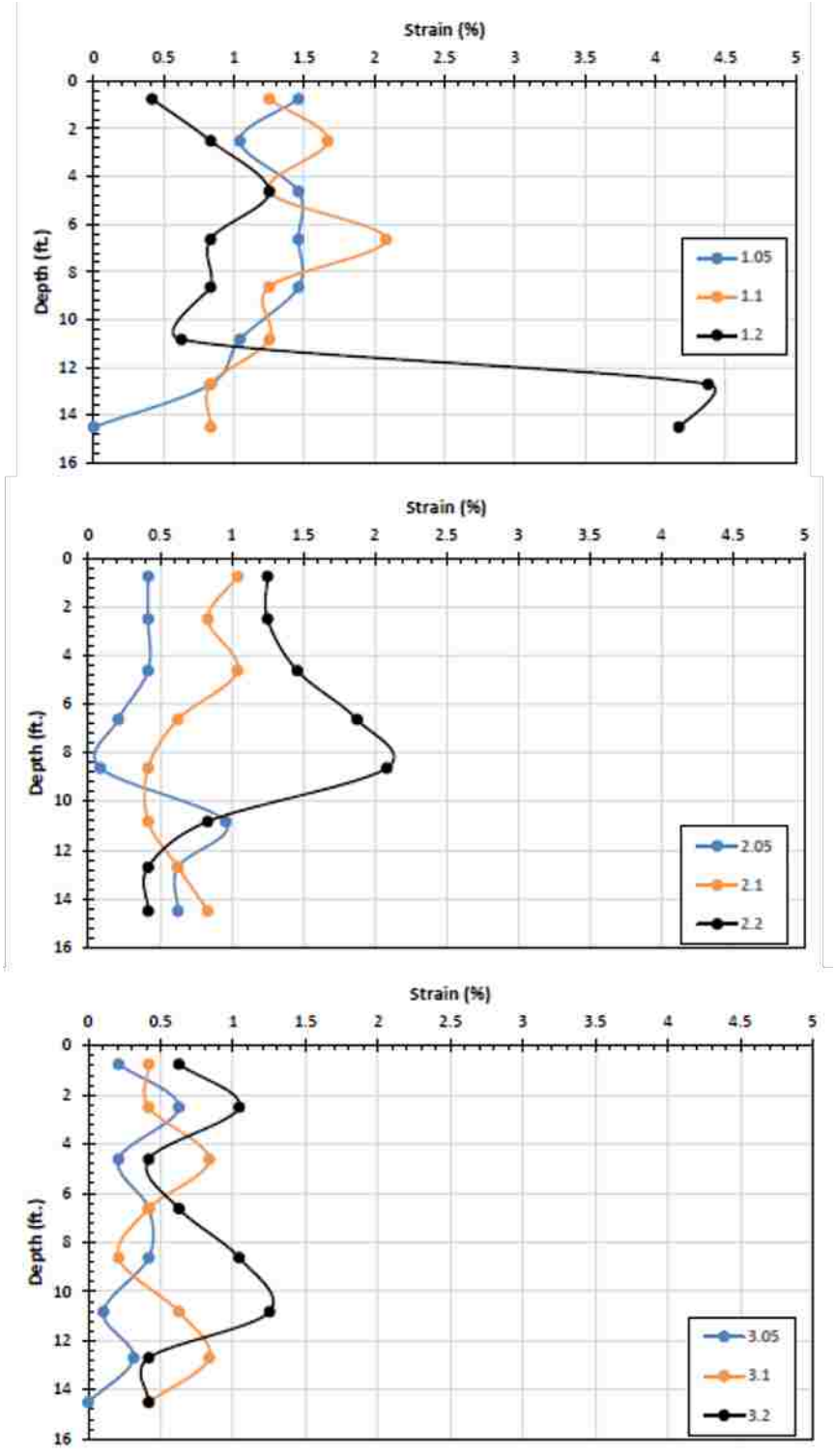

Figure 4-9: Volumetric Strain vs. Depth for 3 ft. Spacing

5 IN-DEPTH ANALYSIS

5.1 Introduction

The focus of this analysis is on shear modulus reduction at varying pore pressures and global effects of PVD drains in reducing settlement and pore pressure generation during laminar shear box testing. Comparisons will be provided between tests with drains conducted in this study and previously published results from similar tests without drains.

5.2 Soil Response Analysis within the Laminar Shear Box

This chapter provides an in-depth analysis of the soil response during laminar shear box testing based on the horizontal acceleration and displacement time histories measured on the laminar box along with measured excess pore pressures and settlement of the sand within the box. The acceleration and displacement time histories are subsequently used to develop shear stress vs. shear strain time histories at various depths in the soil column. Based on these measured and computed parameters, relationships will be developed to define (1) the generation of excess pore pressure ratios with shear strain, (2) the volumetric strain with excess pore pressure ratio, and (3) the reduction in shear modulus with shear strain curves as excess pore pressure ratios increase. Where possible, comparison will also be made with similar relationships developed for soil condition without drains.

5.2.1 Acceleration and Horizontal Displacement Measurements

Accelerations were recorded by accelerometers attached to the sides of the laminates as previously shown. The acceleration time histories experienced at different depths along the soil profile are presented in Figure 5-1 for round 1 test with the 3 foot drain spacing and horizontal movement results are presented in Figure 5.2 for the round 1 test with the 3 foot drain spacing.

For each shaking test the acceleration time histories are similar through all soil depths, with peak values only slightly increasing at the first 1-2-foot depths. The average peak acceleration of the soil column was approximately equal to the input ground motions. However, in some tests, the peak acceleration was above or below the peak value of the input ground motion. Laminates at very shallow depths and laminates near the actuator had varying accelerations. The acceleration time histories of each laminate approximate the average acceleration time history that the soil at that depth experienced during the shaking test.

Horizontal displacement time histories were also measured at the various depths on the laminates containing the soil column. Horizontal displacement is measured by potentiometers attached to the laminates. The displacement time history of each laminate is assumed to represent the average horizontal displacement of the sand column at that depth.

Measurements of acceleration time histories can be used to estimate the shear stress time histories at various depths within the soil profile while measurements of horizontal displacement time histories can be used to compute the horizontal shear strain time histories at the same depth in the soil profile as discussed subsequently. The shear stress and shear strain time histories can then be combined to define the shear stress vs. shear strain time histories.

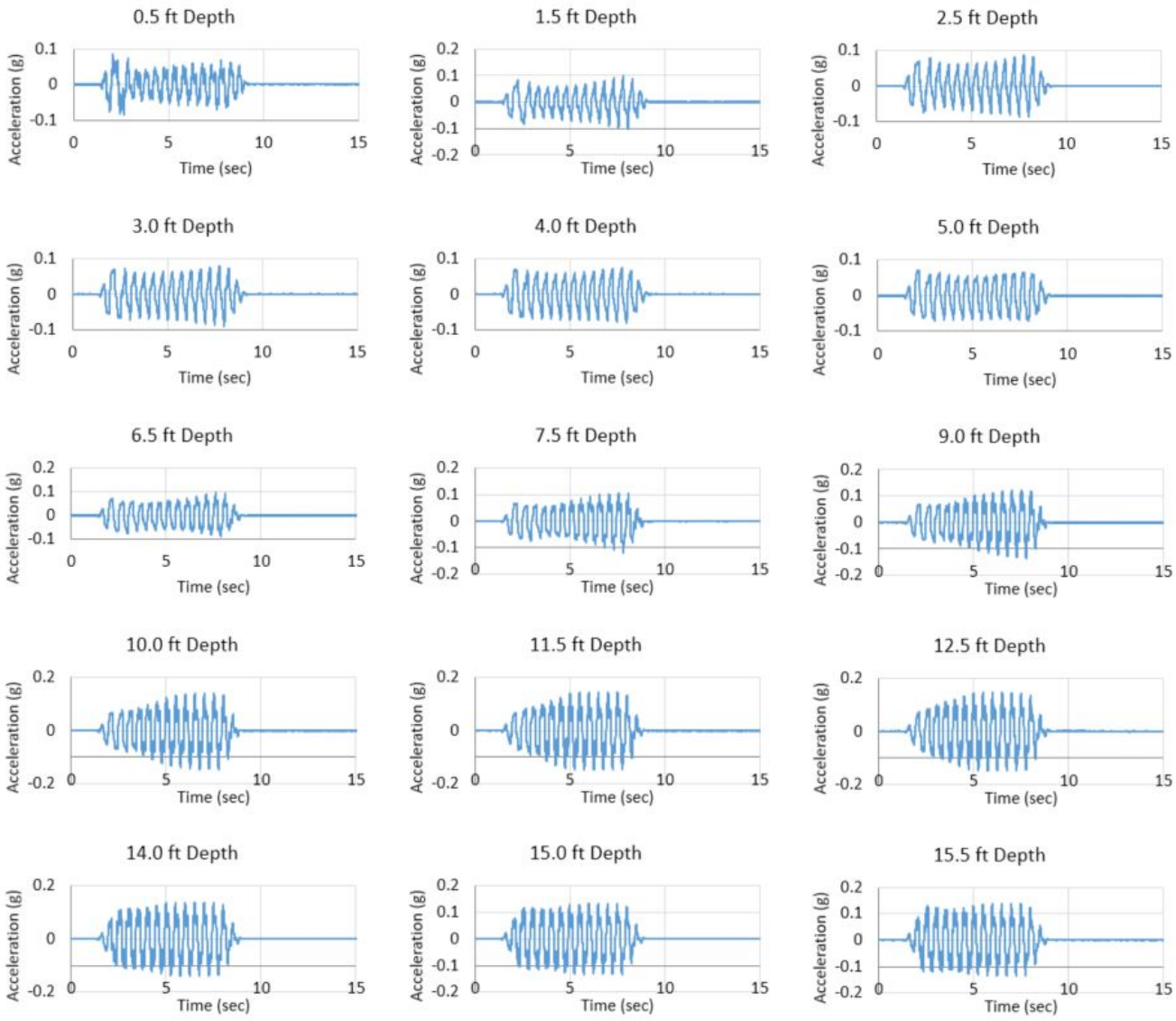

Figure 5-1: Accelerations for 3R1 - 0.1-g

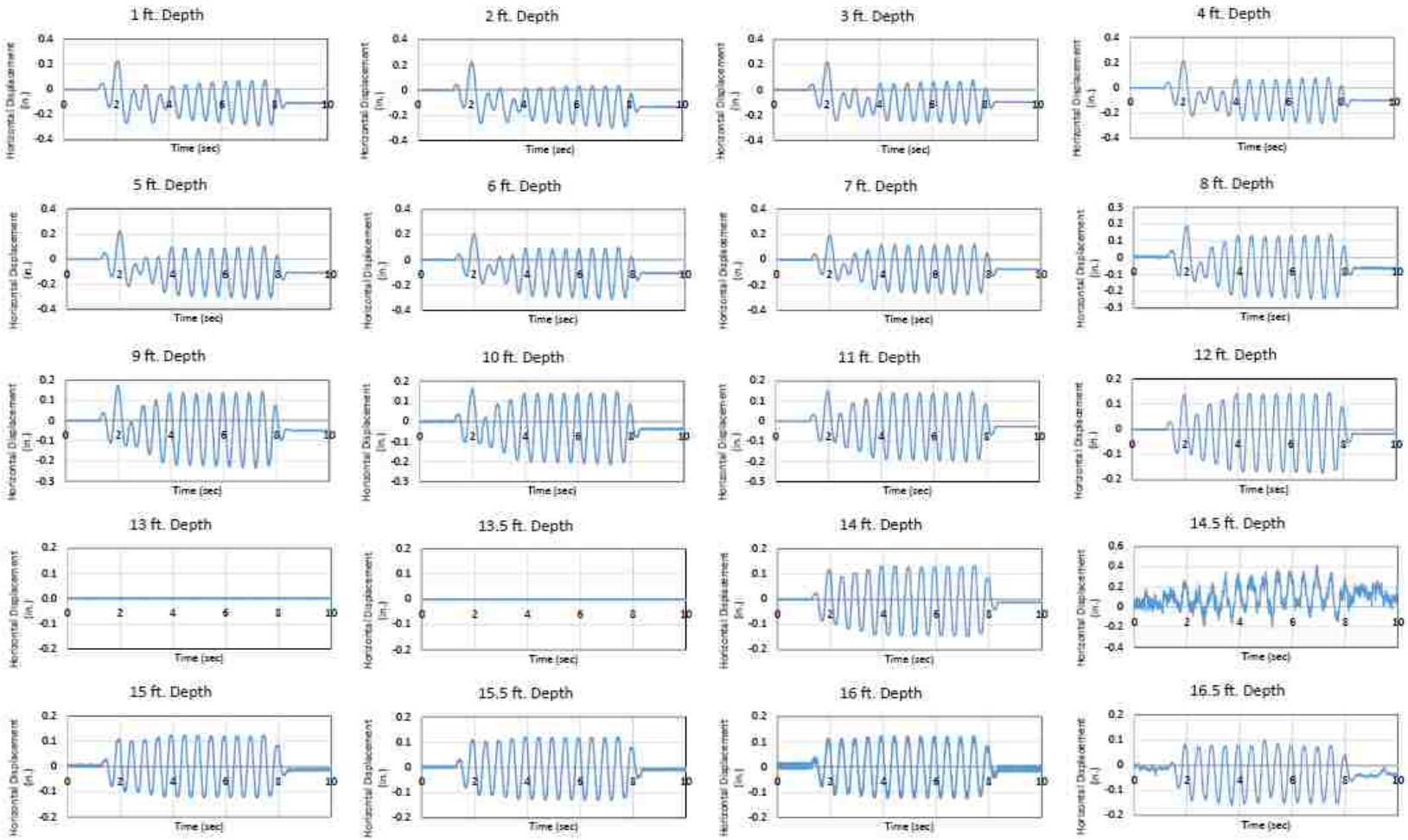

Figure 5-2: Horizontal Displacement for 3R1 0.05 g

5.2.2 Developing Shear Strain Time Histories

To produce the shear stress and shear strain time histories, shear stress and strain must first be calculated from the results of measured acceleration and displacement during the laminar box testing at UB-SUNY. These calculation procedures followed the procedures outlined in a preliminary report by Thevanayagam (Thevanayagam, Yeigan, Stokoe, & Youd, 2015) who performed laminar shear box testing on sands without drains immediately prior to the testing performed by Oakes (Oakes, 2015) at UB-SUNY. Shear strain is obtained by finding the lateral displacement difference between two adjacent laminates with respect to the vertical difference between the two laminates. The shear strain $\gamma(z,t)$ at any depth, z and time, t is given by the equation

$$\gamma(z,t) = \frac{d_{k+1}(t) - d_k(t)}{\Delta z_i} \tag{5-1}$$

where $d_{k+1}(t)$ and $d_k(t)$ represent lateral displacements at time t measured by adjacent displacement potentiometers and Δz_i is the vertical distance between the two potentiometers.

To demonstrate, the calculation for shear strain at laminate number 4 at a depth of 14 feet is given by the equation.

$$\gamma(z,t) = \frac{H5X - H4x}{6\ inches} \tag{5-2}$$

where H5X and H4X are displacement potentiometers on laminates at 14 and 14.5 feet below the ground surface and the distance between the two potentiometers is 6 inches. The vertical distance

between laminates varies depending on the location of the sensors. If sensors are placed farther apart, the vertical distance used in the calculation would increase. Due to the movement of the base actuators and the overlying laminates, the displacement can occur in both positive and negative directions from the initial reference point and. The sensors on the laminates measure the displacement in inches, therefore the shear strain from Equation 5-2 is pure strain and will remain unit-less; however, it can also be multiplied by 100% to yield percent strain. Selected strain time history plots developed for the round one test with an input peak acceleration of 0.05 g are provided at a variety of depths in Figure 5-3 .

The strain oscillates with time, mimicking the input acceleration time histories. Shallow depths typically have the highest strain while the deeper depths typically have the lowest strain which appears to be consistent with the increased confining pressure. Noise reduction was not applied to the calculated strain data.

After a shaking event, some of the sensors indicate residual strain as seen in the Figure 5-3 . This can be explained by the fact that the laminate rings experienced a residual horizontal offset after the shaking stopped. The residual strains and horizontal movements exhibited at certain locations appeared to be random through each round of testing, and the residual strain appears to have no permanent effect on subsequent rounds of testing. Therefore, it is assumed that each subsequent round of testing had no significant residual strain affecting the resulting calculated strains.

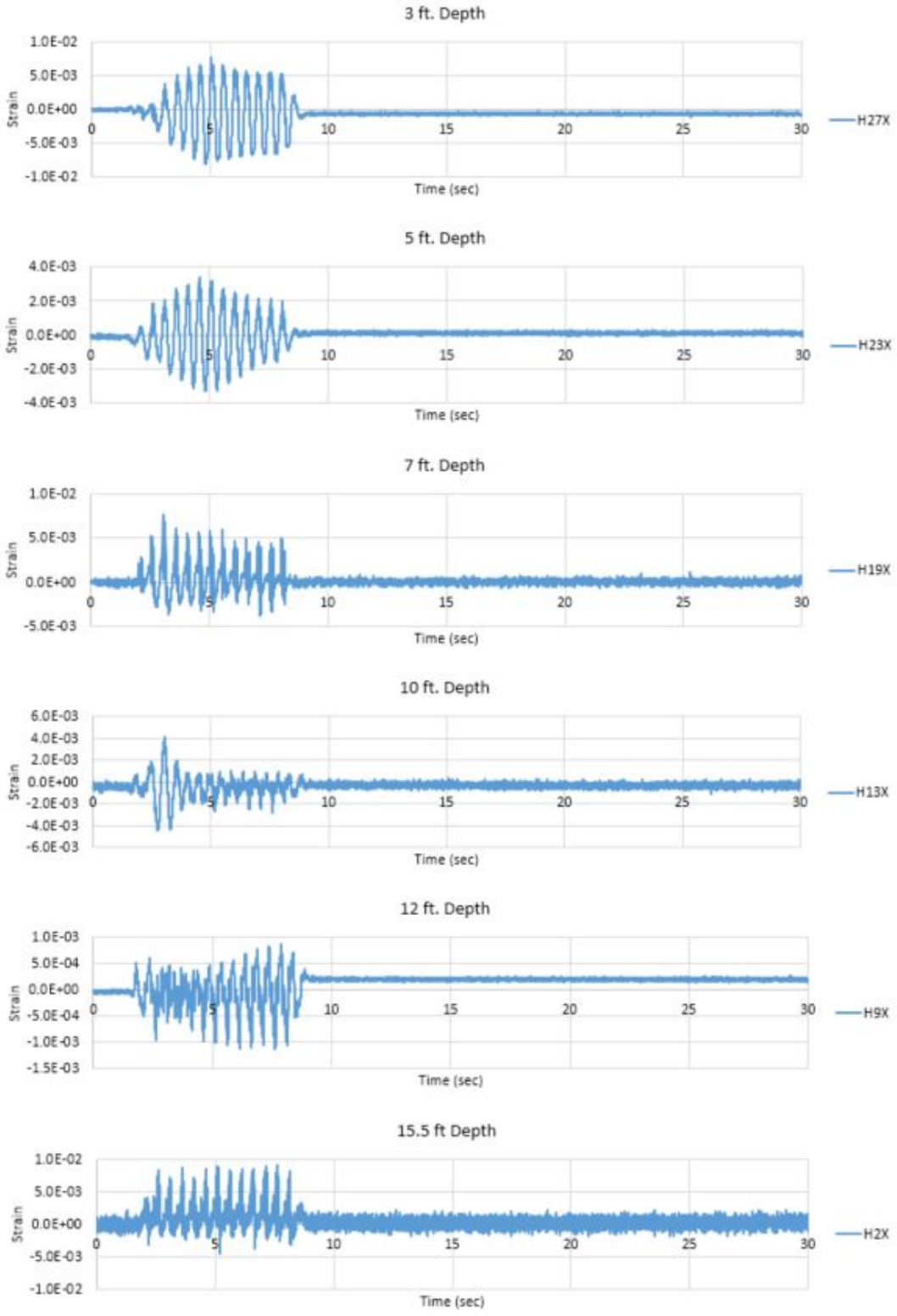

Figure 5-3: 3-ft Spacing, Round 3, a=0.05-g Strain Plots

5.2.3 Developing Shear Stress Time Histories

The shear stress, τ, is given by the equation

$$\tau = \frac{H}{A} \tag{5-3}$$

where H represents the horizontal shear force between two adjacent laminates and A represents the cross-sectional area of the soil between the laminates that the shear force is acting on.

The shear force, H, at any depth is given by the basic equation,

$$H = \sum_i^N m_i * a_i(t) \tag{5-4}$$

where m_i is the sum of the mass of each laminate and the soil within it above the layer of interest and $a_i(t)$ is the acceleration of each laminate at time *t*. Recognizing that the mass is equal to the weight divided by the acceleration of gravity, the equation for H can be given by

$$H = \sum_i^N \frac{(W_{si}+W_{Li})}{g} a_i(t) \tag{5-2}$$

where W_{si} is the weight of the soil within each laminate *i* above the depth of interest, W_{Li} is the weight of each metal laminate above the depth of interest, *g* is the acceleration of gravity, and a is the acceleration of each laminate *i* above the depth of interest.

The weight of the metal laminate W_{Li} was found to be equal to 24004.5 lbs. or a mass of 1107 kg. The weight of the soil within each laminate, W_{si} was given by the equation

$$W_{si} = \gamma_{soil} * H * A \tag{5-3}$$

where γ_{soil} is the unit weight of the soil (122.9 lbs/ft^3), H is the height of the laminate (0.5 ft) and A is the cross-sectional area of the soil (147.6 ft^2 = 9 ft. width by 16.4 ft. length) within the laminate. This leads to a weight for the soil of 9069 lbs or a mass of 4117.3 kg. The horizontal

force H computed in Equation 5-5 can then be divided by the cross-sectional area to obtain the shear stress.

Therefore, to calculate shear stress at a certain laminate location, the mass from each laminate above that level must be multiplied by the associated acceleration. For example, the equation for calculating the shear stress at laminate #27 would be given by

$$\tau = \frac{\left((m_{k_{27}} * AE_{x_{27}}) + (m_{k_{28}} * AE_{x_{28}}) + \left(m_{k_{29}} * AVG(AE_{x_{28}}, AE_{x_{30}})\right) + (m_{k_{30}} * AE_{x_{30}}) + \left(m_{k_{31}} * AVG(AE_{x_{30}}, AE_{x_{32}})\right) + (m_{k_{32}} * AE_{x_{32}})\right) * g}{A}$$

where m_{ki} is the mass of a laminate and included soil, AE_{xi} is the measured horizontal acceleration associated with the mass in g's, g is the acceleration of gravity, and A is the cross-sectional area of the soil. In some cases, it was necessary to average accelerations from adjacent laminates to get the appropriate acceleration time history for a given laminate.

Shear stress time histories computed at several depths for the first round of shaking tests with an input acceleration of 0.05 are plotted in Figure 5-4 as an example. Similar to the strain time histories, the shear stress time histories oscillate from positive to negative as a result of the input motions. Shear stress increases at deeper depths because of the increase in mass of the overlying laminates and soil along with the increase in effective stress.

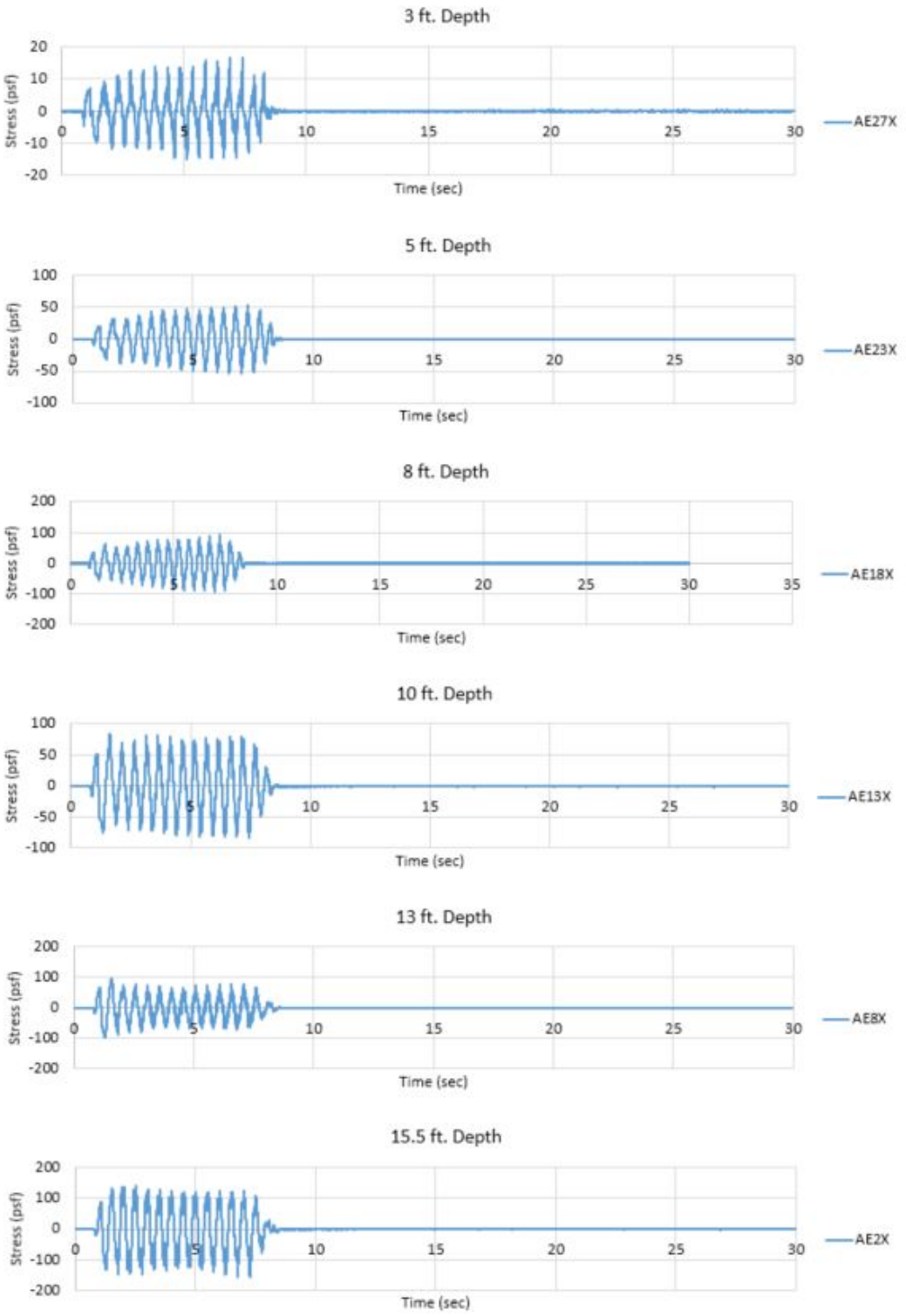

Figure 5-4: 4-ft Spacing, Round 1, 0.2-g Stress Plots

5.2.4 Shear Stress vs. Strain Curves

Shear stress and shear strain plots were created at corresponding acceleration sensors and horizontal displacement sensors. The sensors are located on the same laminate or adjacent laminates. Using this procedure, stress-strain curves were computed at five or six depths within the profile providing information and analysis for the entire soil profile. An example of shear stress-strain plots can be seen in Figure 5-5. Shear stress was plotted in pounds per square foot (psf), and shear strain as unit-less pure strain. Some sensors where not chosen for analysis due to error in capturing data.

At each depth, the shear stress and strain were plotted for an average of 0.5 seconds of shaking. One complete cycle of an individual hysteretic loop was completed in approximately 0.5 seconds. The 0.5 second time frame was large enough to capture the complete hysteretic loop for most plots and was used to analysis varying shear modulus.

A shear stress-strain curve was plotted from 0.5 secs to 9.5 secs for each depth. For the 3-foot. and 4-foot. spaced testing, nine and eight depths were analyzed, respectively. This analysis was completed for each acceleration and each round. The total number of shear stress-strain plots generated for analysis was **2,754**. This is a tremendous amount of data to analyze and to develop patterns and trends.

To help analyze the stress and strain curves, the average calculated pore pressure ratio at the given time step and depth were combined with stress-strain data, and the stress-strain curves were color coordinated. The pore pressure ratio color code is summarized in Table 5-1. Generally, the cooler colors indicate the lower pore pressure ratios, while the hotter colors indicate the highest pore pressure ratio

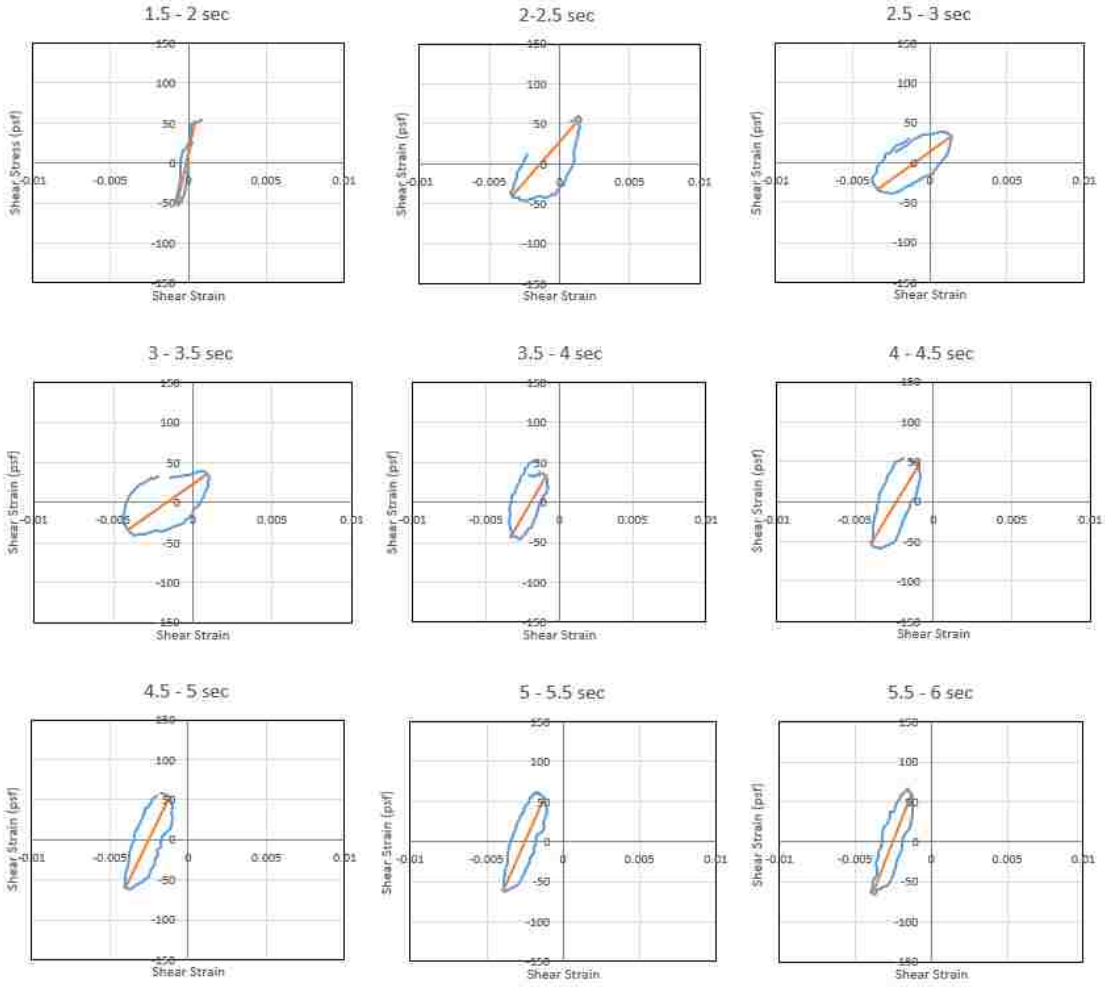

Figure 5-5: Selected Stress-Strain Curves from 3R1 0.05-g at 7.5 ft. Depth

Table 5-1: Pore Pressure Ratio Color Code

Pore Pressure Ratio Color	
Color	Pore Pressure Ratio
	0.0 – 0.2
	0.2 – 0.3
	0.3 – 0.4
	0.4 – 0.5
	0.5 – 0.6
	0.6 – 0.7
	0.7 – 0.8
	0.8 – 0.9
	0.9 – 1.0

An example of liquefaction developing within the analyzed time is presented in Figure 5-6 along with the effect of excess pore pressure ratio on shear strain and shear modulus. In Figure 5-6, individual shear stress-strain curves are plotted for 0.5 second time windows which captures each cycle of motion. The stress-strain curves show the soil at a depth of 2.5 feet. remaining relatively stiff and linear with low pore pressures ratios during the first two seconds of shaking. However, as the shaking continues, the soil decreases in stiffness as increases in pore pressure ratio develop. As a result, peak shear strains increase to between 5 and 8% as the soil liquefies and starts straining excessively. Shear strains of about 3.5% are typically associated with liquefaction in cyclic triaxial tests.

The effects of earthquake drainage can be observed in multiple stress-strain curve analysis. In Figure 5-7, pore pressures decrease, and stiffness increases with time during the shaking event. The pore pressure ratio reaches the range of 0.5 to 0.6 within 2.5 seconds but decreases as shaking continues. The reduction in pore pressure can be attributed to the earthquake drains effectiveness in mitigating pore pressures.

The effects of earthquake drainage may apply to other interesting observed stress-strain curves. In Figure 5-8, pore pressures remained low, below R_u of 0.4, while shear strains reached over two percent and stiffness was reduced to near zero. The lack of pore pressure generation may be attributed to the effectiveness of the earthquake drains in mitigating pore pressures despite the high level of strain experienced.

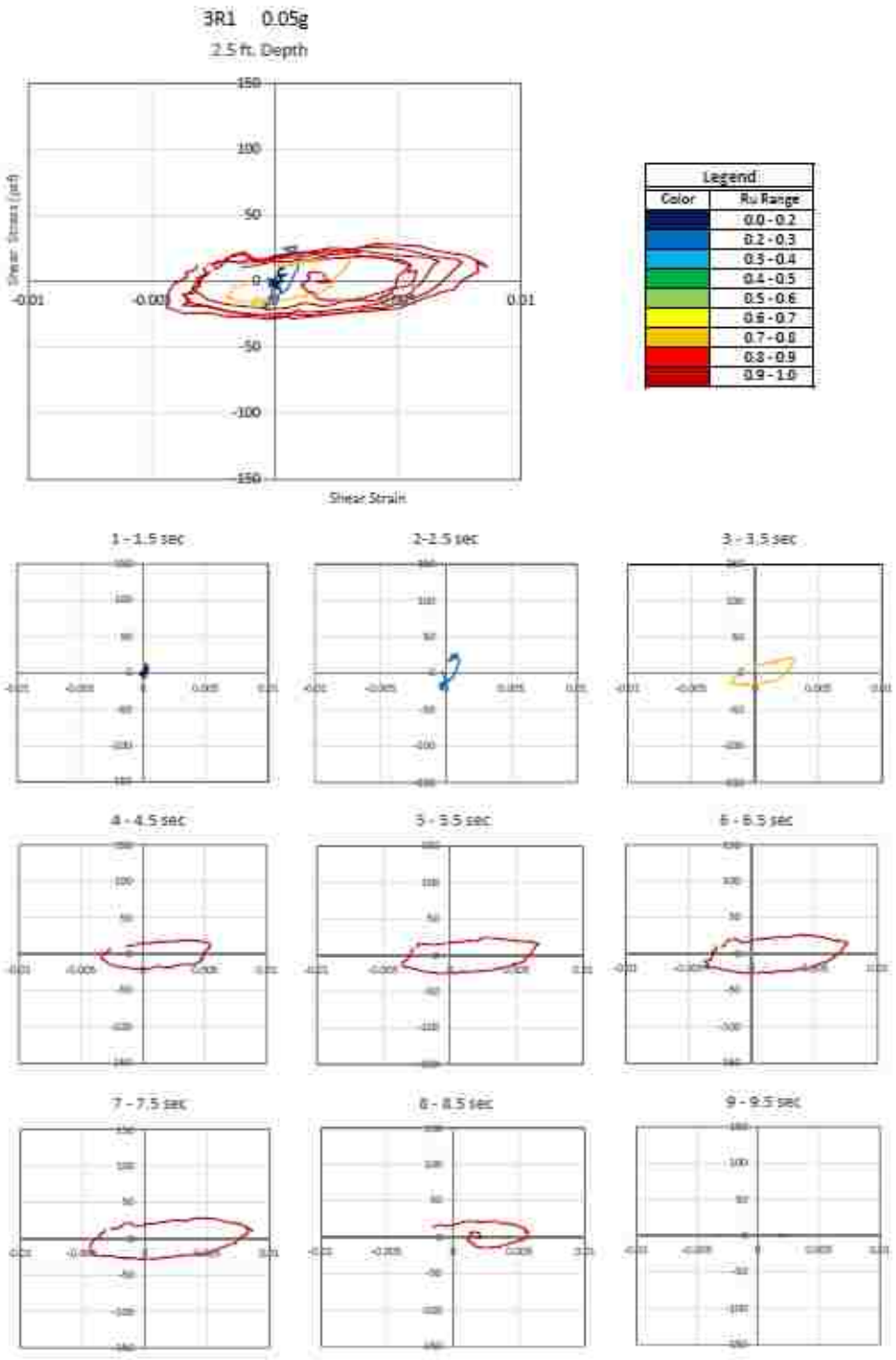

Figure 5-6: Computed shear stress-shear strain curves plotted in 0.5 second time windows (one cycle of motion) along with a plot showing all curves for all cycles at a depth of 2.5 ft. during round 1 with a peak acceleration of 0.05-g for the 3-foot drain spacing (3r1). Plots are color-coded based on the average measured Ru during the cycle according to the legend.

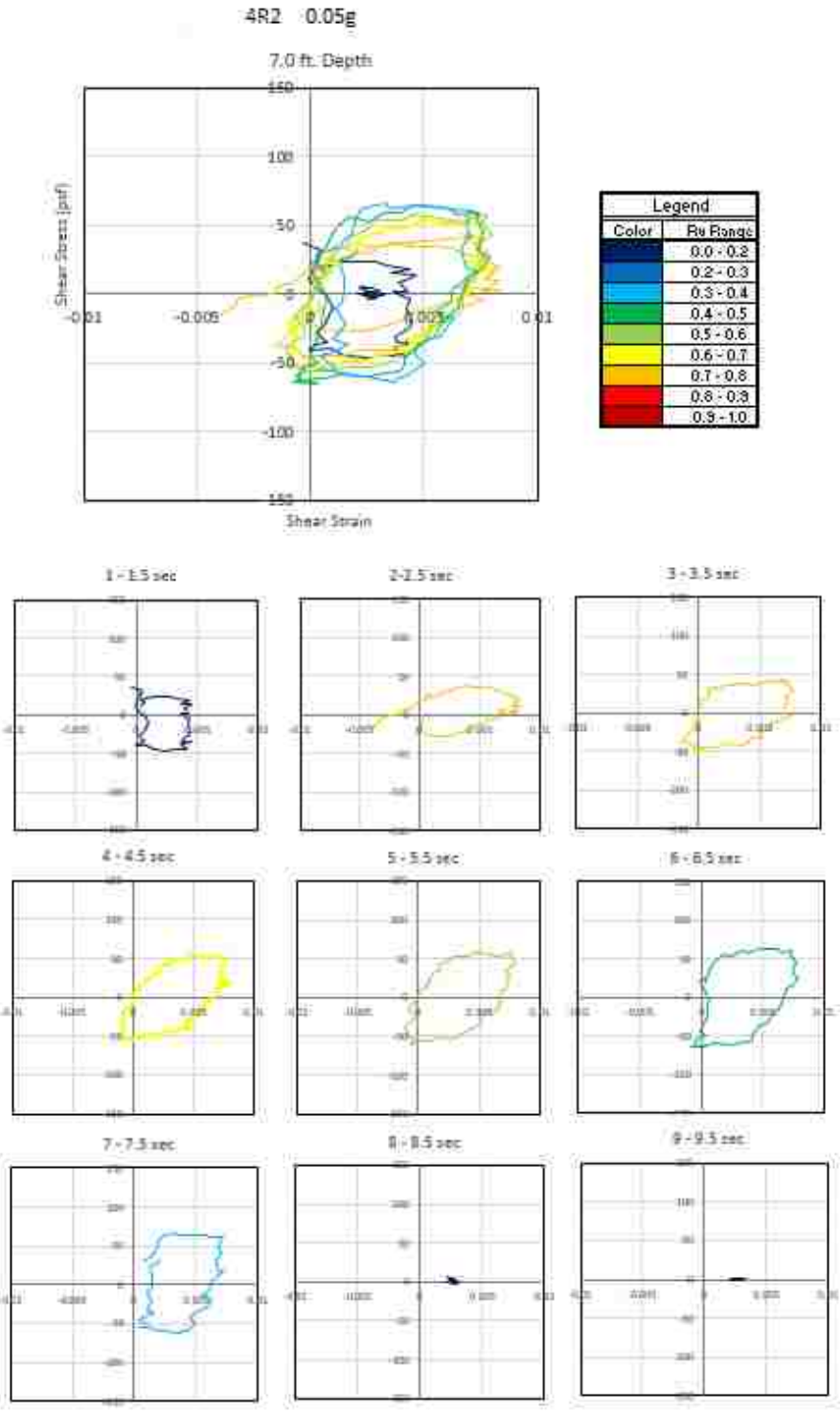

Figure 5-7: Computed shear stress-shear strain curves plotted in 0.5 second time windows (one cycle of motion) along with a plot showing all curves for all cycles at a depth of 7.0 ft. during round 1 with a peak acceleration of 0.05-g for the 4 foot drain spacing (4r1). Plots are color coded based on the average measured Ru during the cycle according to the legend.

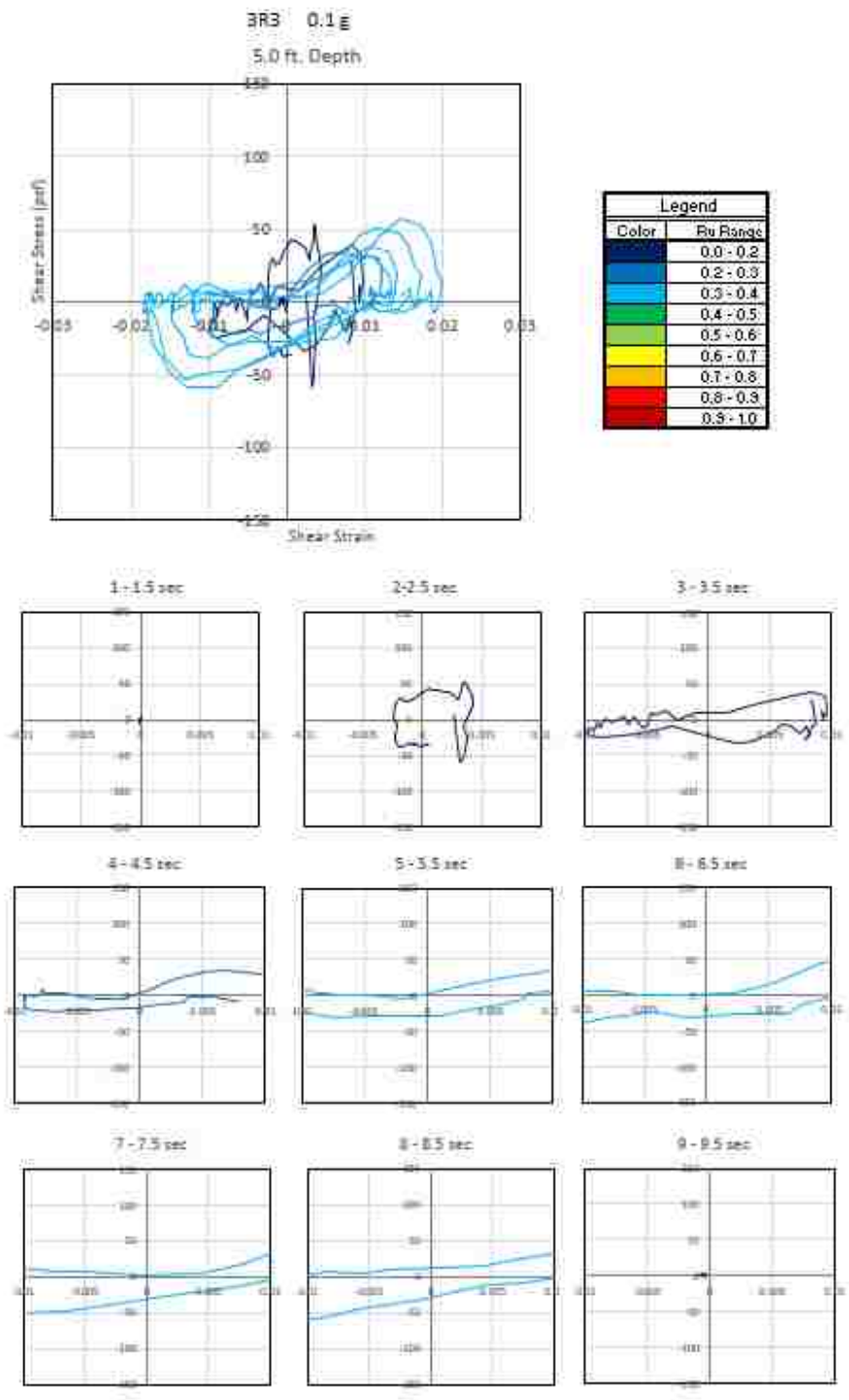

Figure 5-8: Computed shear stress-shear strain curves plotted in 0.5 second time windows (one cycle of motion) along with a plot showing all curves for all cycles at a depth of 5.0 ft. during round 1 with a peak acceleration of 0.1-g for the 4 foot drain spacing (4r1). Plots are color coded based on the average measured Ru during the cycle according to the legend.

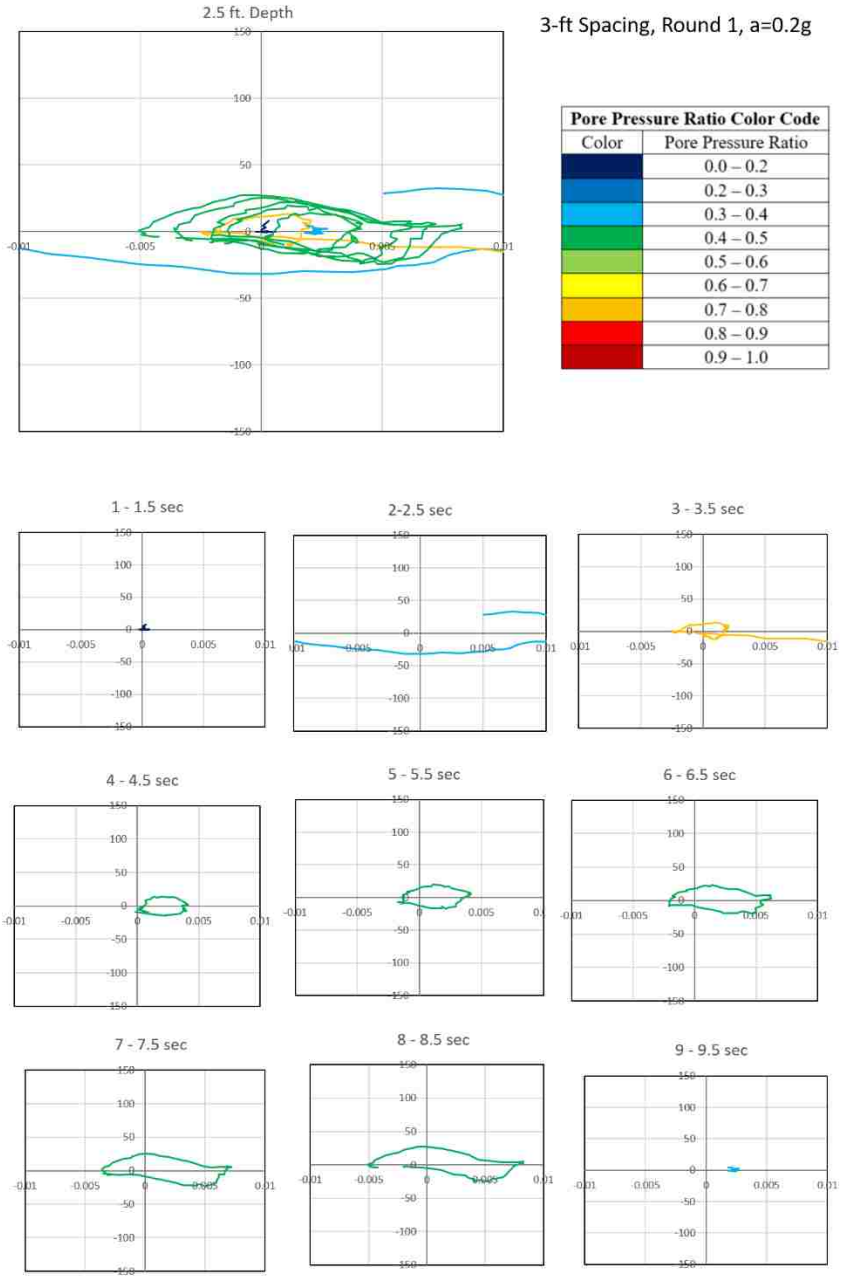

Figure 5-9: Computed shear stress-shear strain curves plotted in 0.5 second time windows (one cycle of motion) along with a plot showing all curves for all cycles at a depth of 2.5 ft. during round 1 with a peak acceleration of 0.2-g for the 3 foot drain spacing. Plots are color coded based on the average measured Ru during the cycle according to the legend

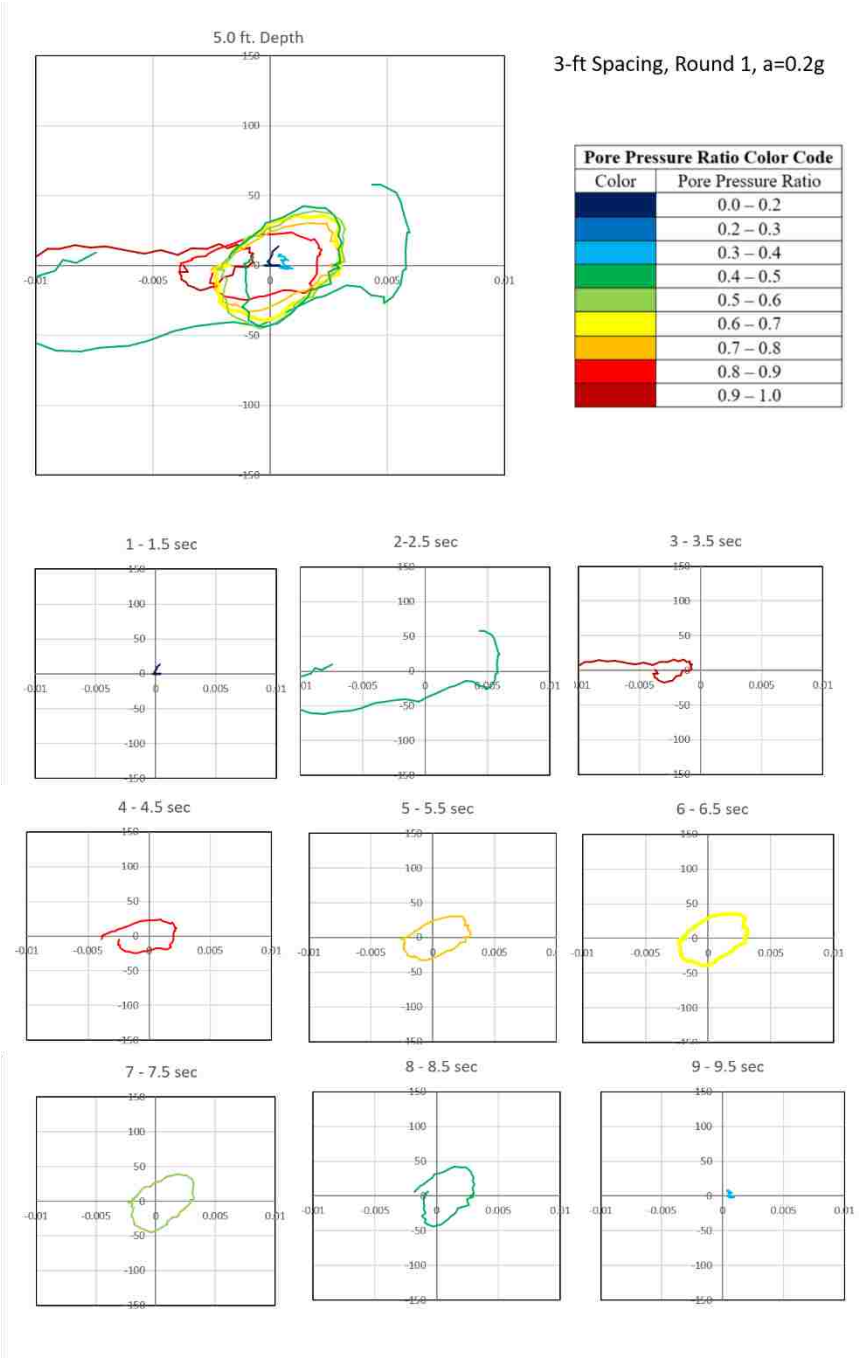

Figure 5-10: Computed shear stress-shear strain curves plotted in 0.5 second time windows (one cycle of motion) along with a plot showing all curves for all cycles at a depth of 5.0 ft. during round 1 with a peak acceleration of 0.2-g for the 3 foot drain spacing. Plots are color coded based on the average measured Ru during the cycle according to the legend

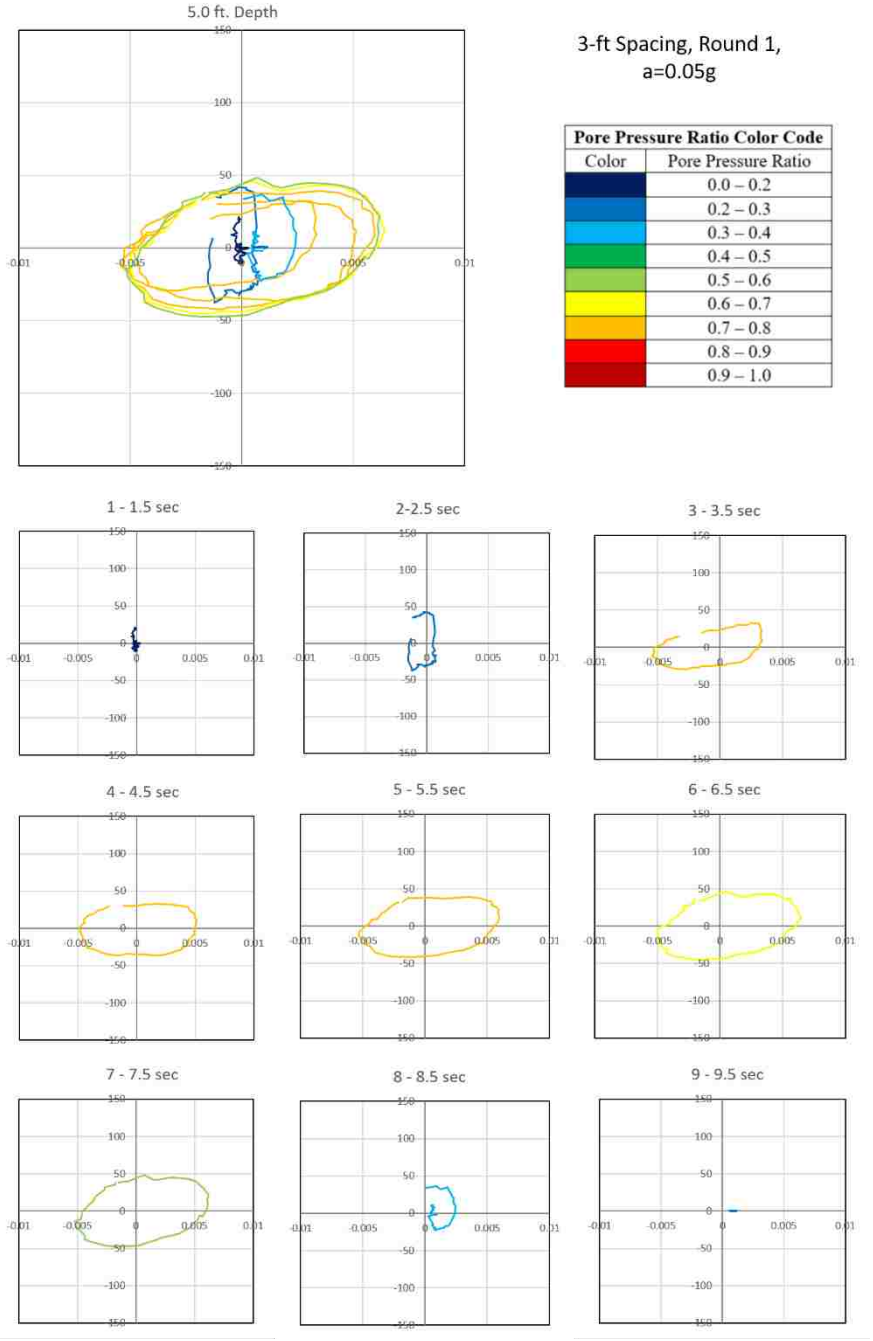

Figure 5-11: Computed shear stress-shear strain curves plotted in 0.5 second time windows (one cycle of motion) along with a plot showing all curves for all cycles at a depth of 5.0 ft. during round 1 with a peak acceleration of 0.05-g for the 3 foot drain spacing. Plots are color coded based on the average measured Ru during the cycle according to the legend.

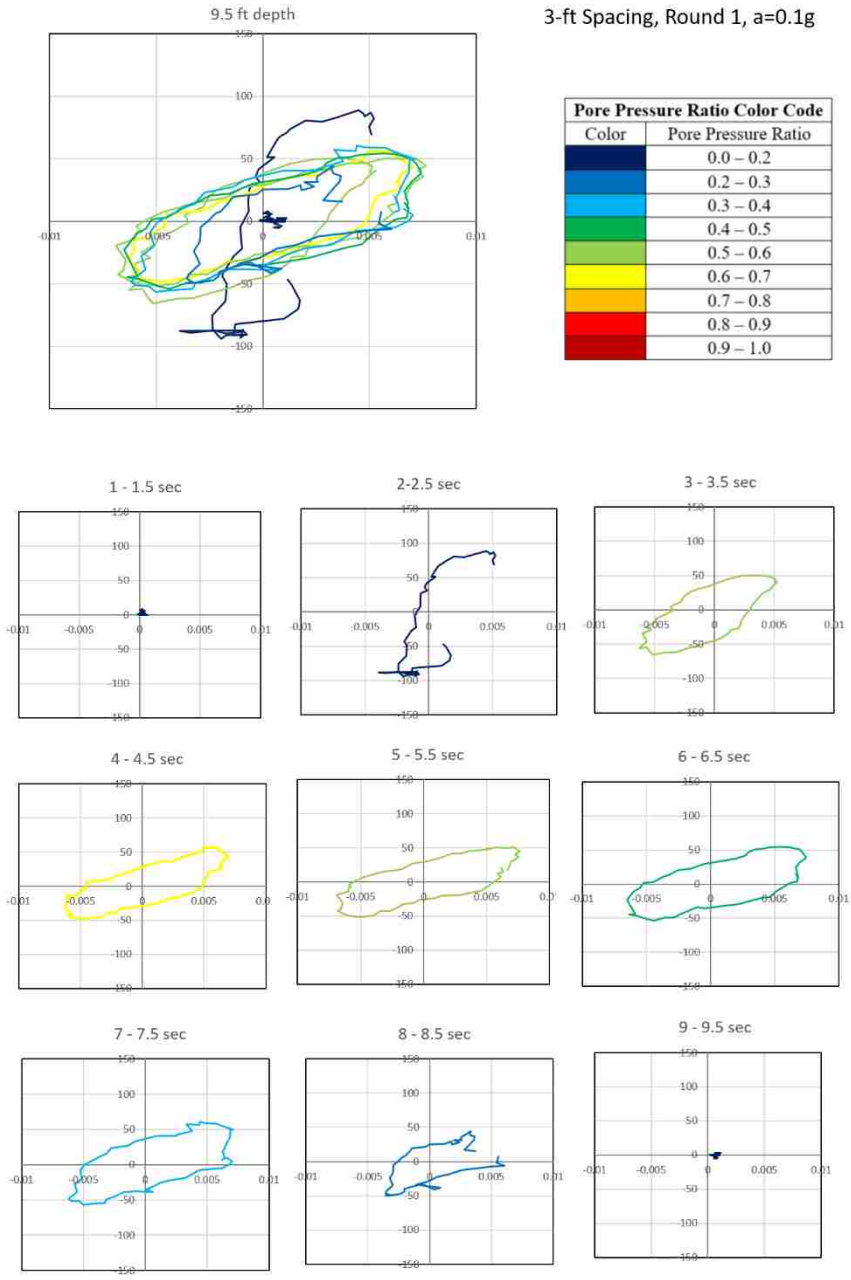

Figure 5-12: Computed shear stress-shear strain curves plotted in 0.5 second time windows (one cycle of motion) along with a plot showing all curves for all cycles at a depth of 9.5 ft. during round 1 with a peak acceleration of 0.1-g for the 3 foot drain spacing. Plots are color coded based on the average measured Ru during the cycle according to the legend

A brief examination for each round at 3 seconds and 6.5 seconds of shaking were developed for each depth. The stress-strain hysteretic loops were also color coded by R_u values at time interval. This gave an overall picture of what was occurring during each shaking event. These can be seen in Figure 5-13, Figure 5-14, Figure 5-15, Figure 5-16, Figure 5-17 , and Figure 5-18

During each round and shaking event, the shallow depths, 0.0 feet to 3.0 feet, were very inconsistent. Very large strains were measured, especially in subsequent testing. This inconsistency may be from the excess water being deposited at or near the surface through the earthquake drains. This excess water made the soil develop into "soup," with no soil particle interaction that could be measured correctly.

Generally, the deeper the depth, the lower pore pressure generation. The lower depths have higher vertical effective stress, causing the pore pressure ratio to be lower. Also, each subsequent round experienced lower pore pressure generation. This is because each shaking event densifies the soil structure, increasing the soil's resistance to further shaking events.

Occasionally, layers or pockets of sand will densify at different times during the shaking. Observing 3R1 at 0.2-g, depths of 12.5 feet and 15.5 feet experienced higher pore pressures than that of 9.5 feet. Although action was taken to create a uniform sand layer, each shaking event would create varying densities in response to the shaking.

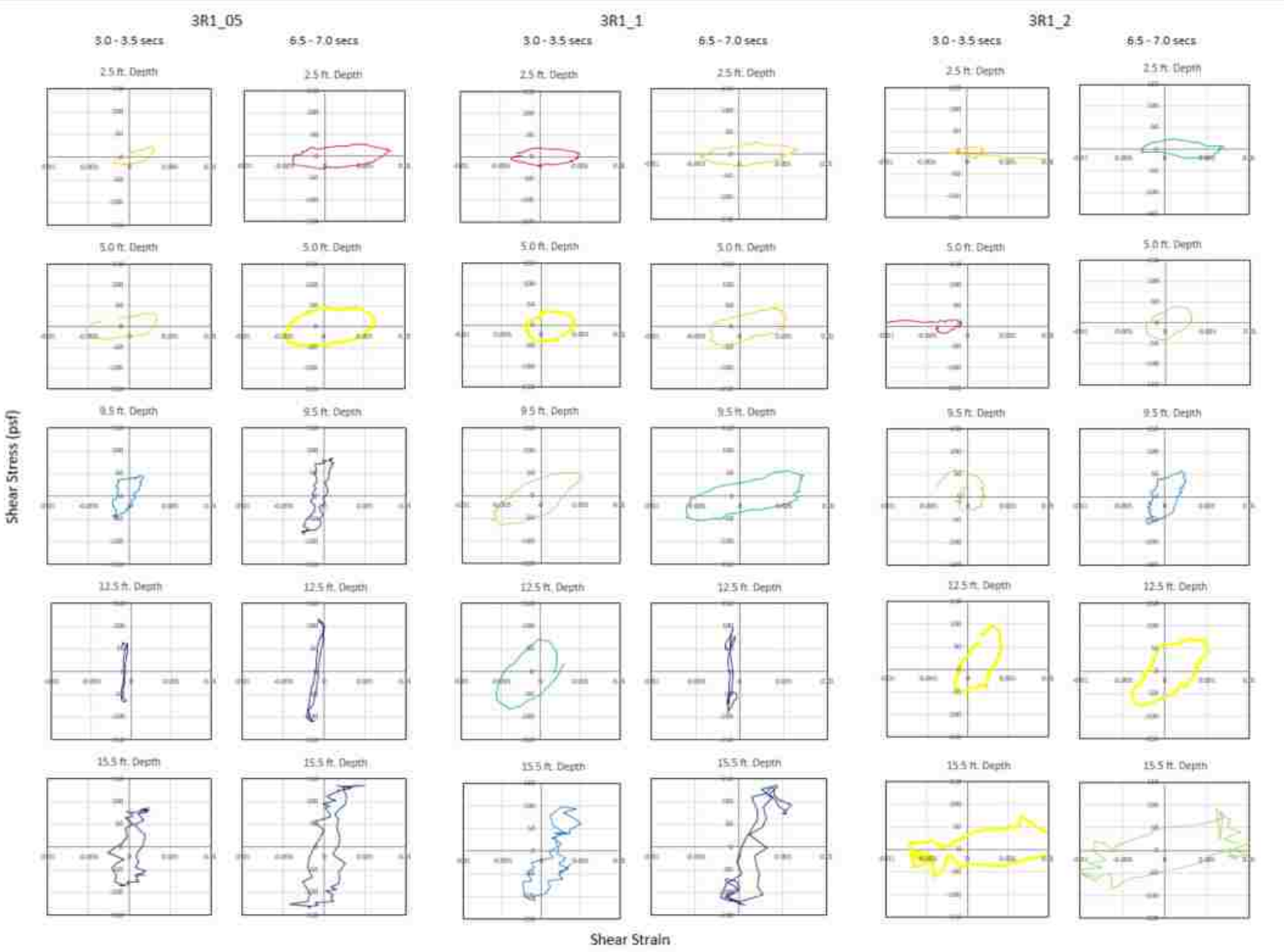

Figure 5-13: 3R1 Shear Stress-Strain Summary

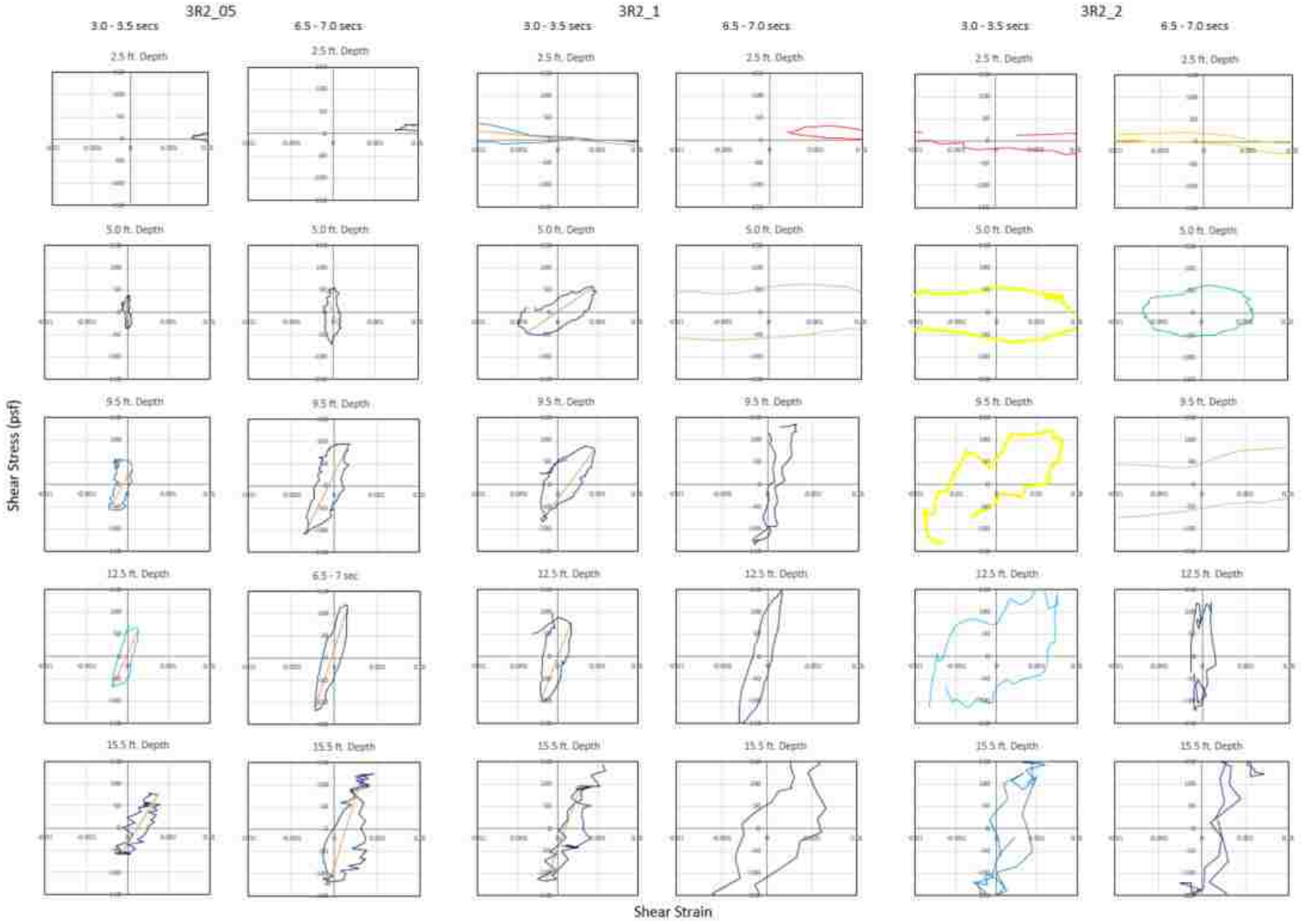

Figure 5-14: 3R2 Shear Stress-Strain Summary

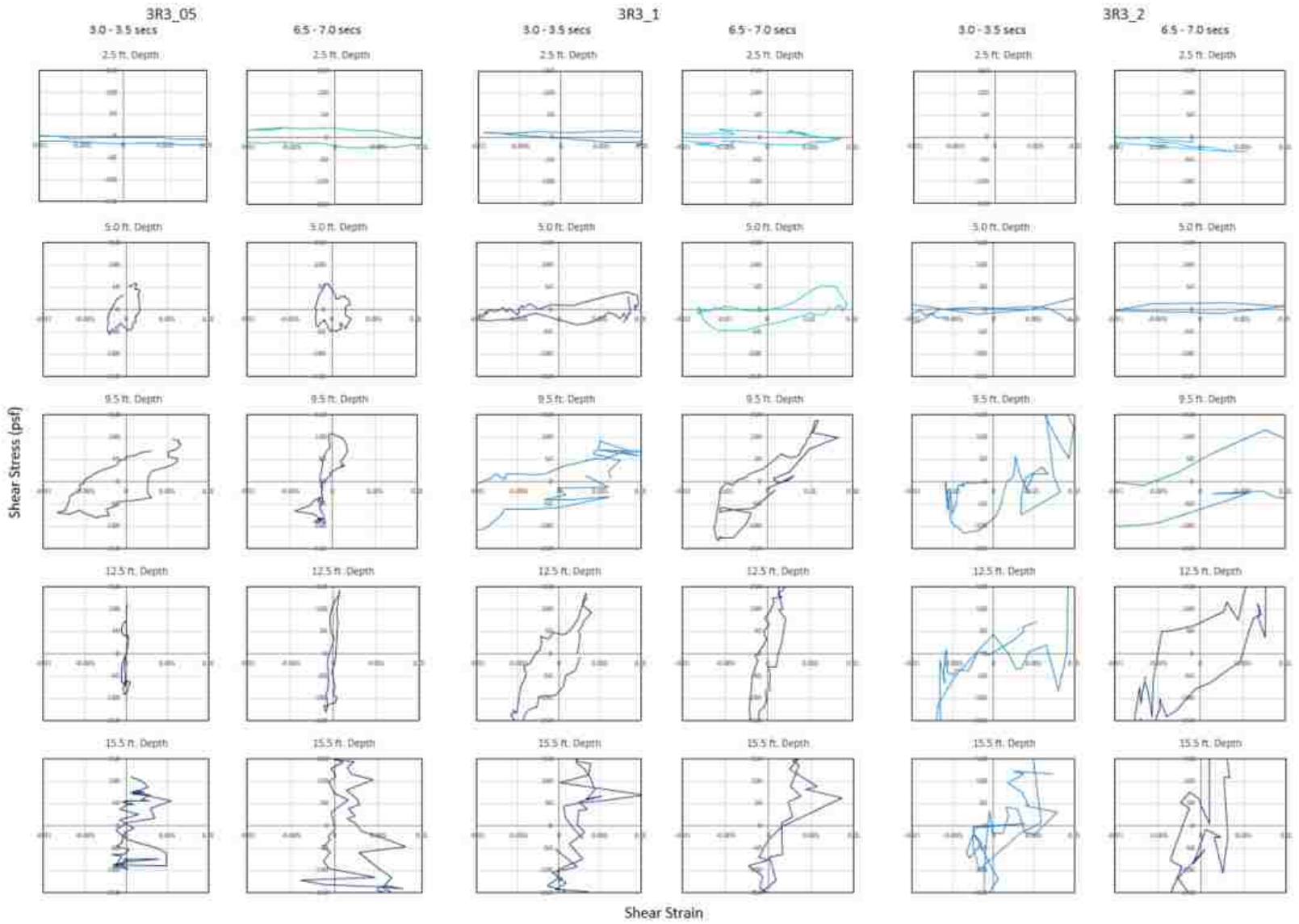

Figure 5-15: 3R3 Shear Stress-Strain Summary

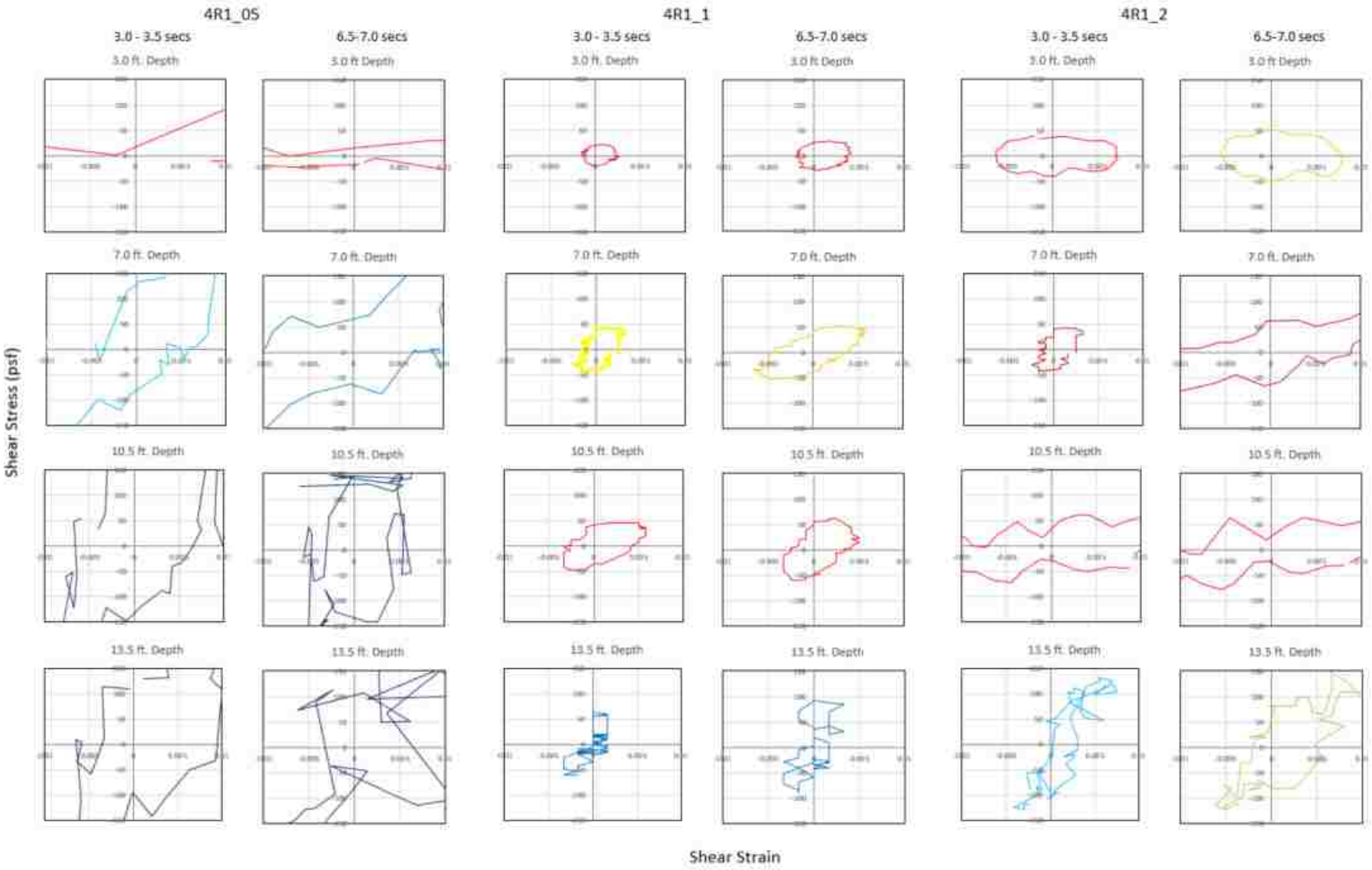

Figure 5-16: 4R1 Shear Stress-Strain Summary

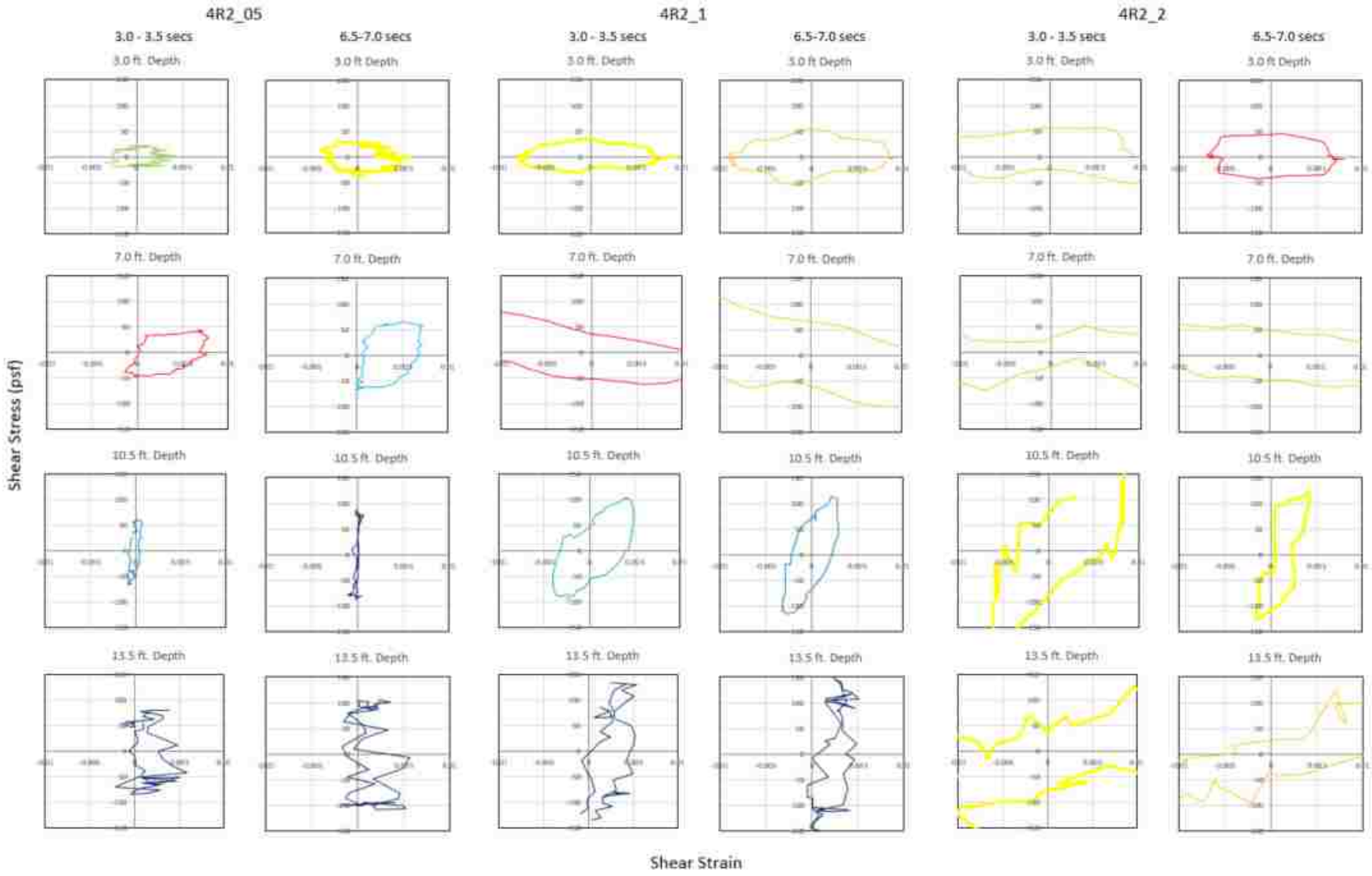

Figure 5-17: 4R2 Shear Stress-Strain Summary

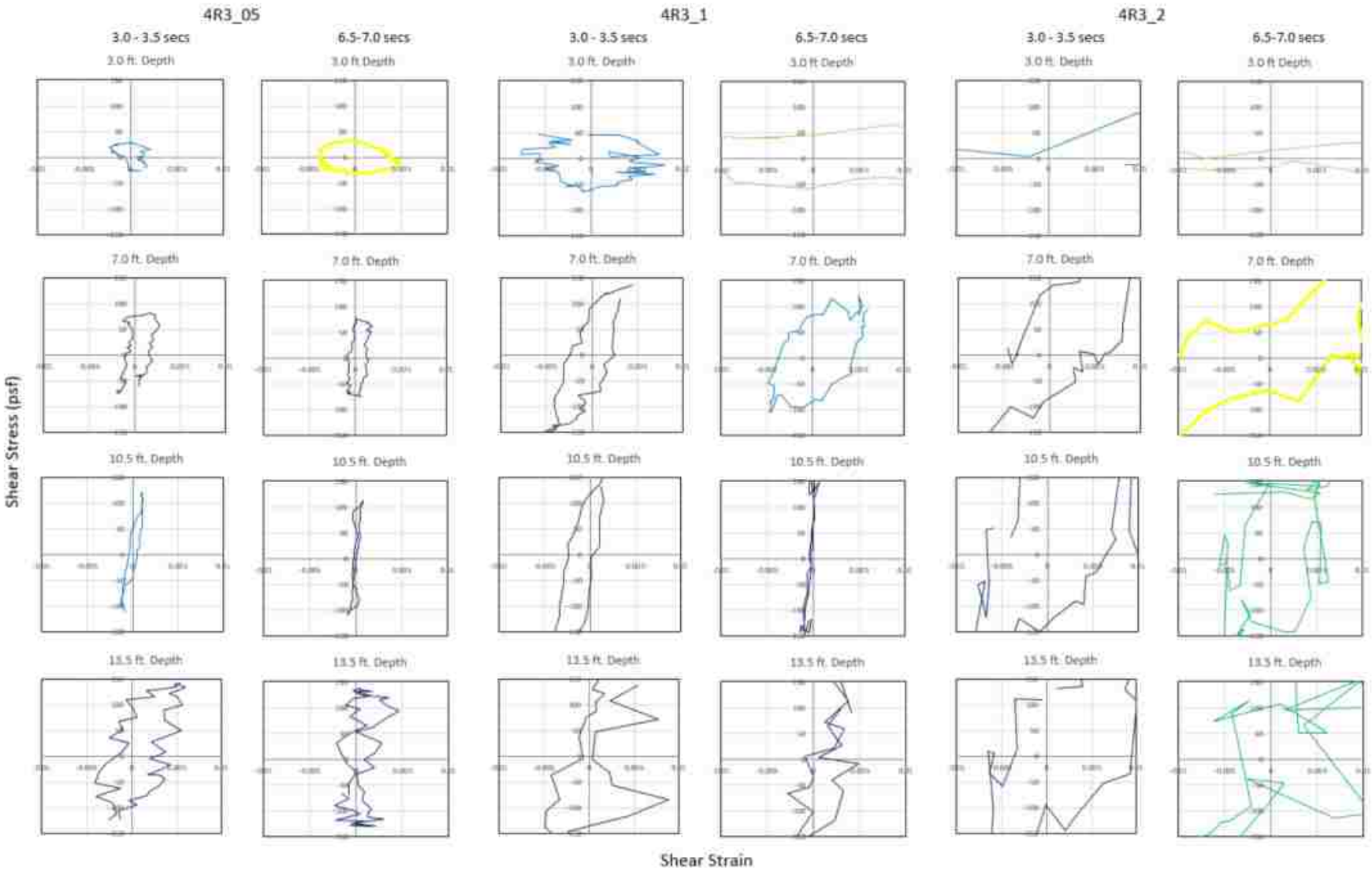

Figure 5-18: 4R3 Shear Stress-Strain Summary

5.3 Shear Modulus Analysis

Shear modulus is a ratio developed to describe the soil's stiffness. To analysis the effects of pore pressure generation and the potential effects of earthquake drains, shear modulus was calculated for each of the stress-strain plots described in Section 5.2.4 Shear Stress vs. Strain Curves.

5.3.1 Calculated Shear Modulus

Shear modulus, G, is defined as the slope of the secant line of a hysteretic loop if plotted in pure strain. A manually fitted line was inserted in each plotted hysteretic loop judiciously. This manually inserted line was used to approximate the slope of the secant line and therefore the shear modulus at each period. This process was repeated for each 0.5-time step, for each round and test. The shear modulus changes could visibly and quantitatively be observed.

Small strains were difficult to capture by the sensors used in this testing. The sensors were not sensitive enough to pick up the small strains and the soil. The resulting stress-strain plots with small strains were problematical to interpret and were not included in further data analysis. An example of small strain stress-strain curve can be found in Figure 5-19.

Some of the hysteretic loops were difficult to distinguish suitable points when measuring shear modulus, as seen below in Figure 5-20. Most of these points are reasonable within the spread of the data and were used despite difficult interpretation.

Each of the manually fitted shear modulus lines were used to calculate the shear modulus. A rise over run slope equation was used to calculate the slope. This slope is assumed to be the

shear modulus at the given time frame. This calculation is shown in Figure 5-21. The units of the calculated shear modulus are pounds per square foot.

Shear modulus calculations were completed for each depth analyzed, at 0.5-time steps, for each acceleration and each round. The calculated shear modulus was grouped with the stress-strain data, and the pore pressure ratio data by depth and time step.

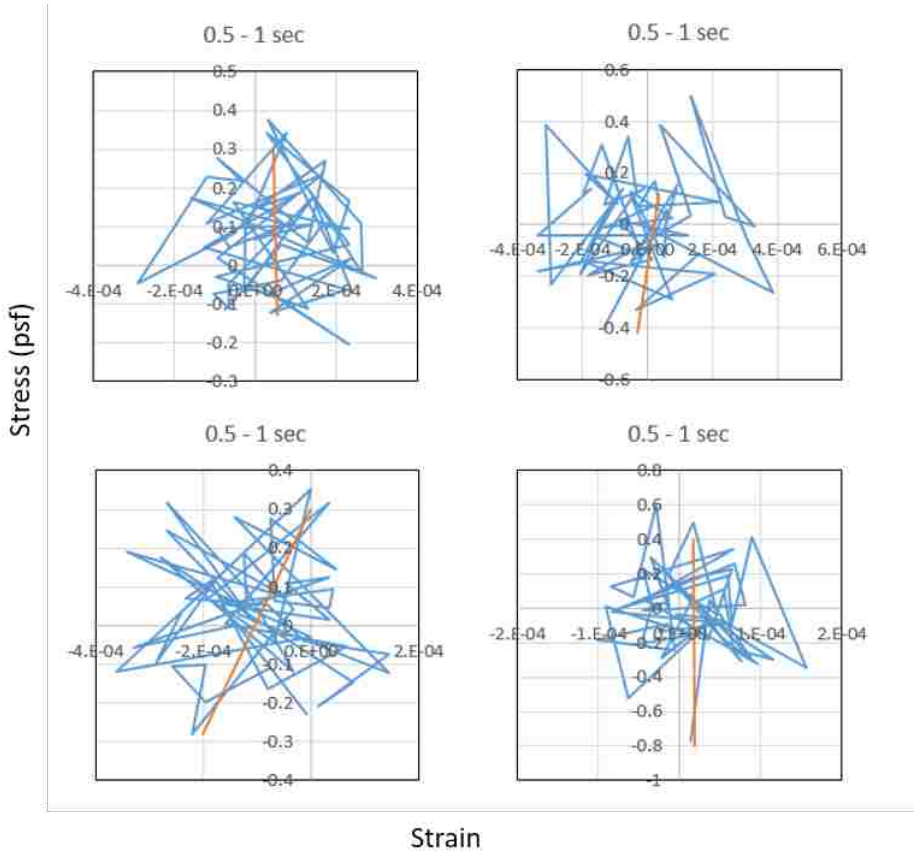

Figure 5-19: Difficult Shear Modulus Interpretation at Small Strains

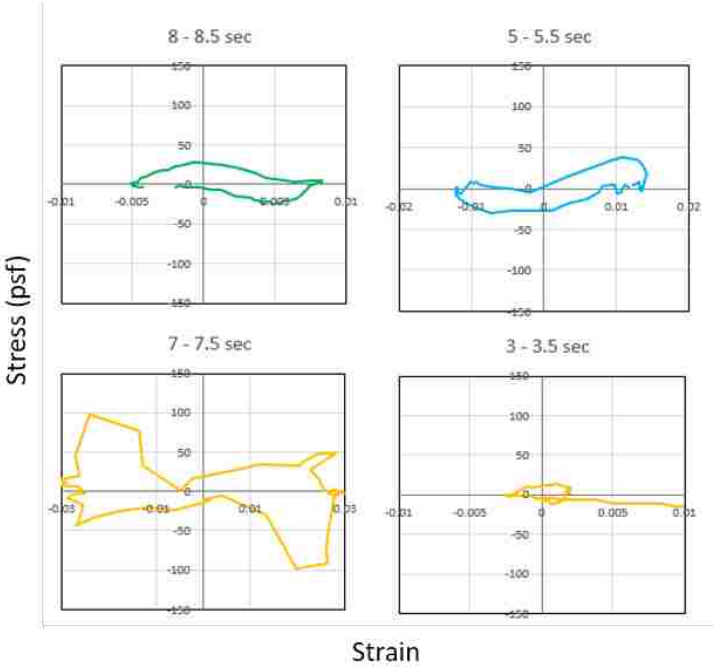

Figure 5-20: Difficult Hysteretic Loops to Interpret

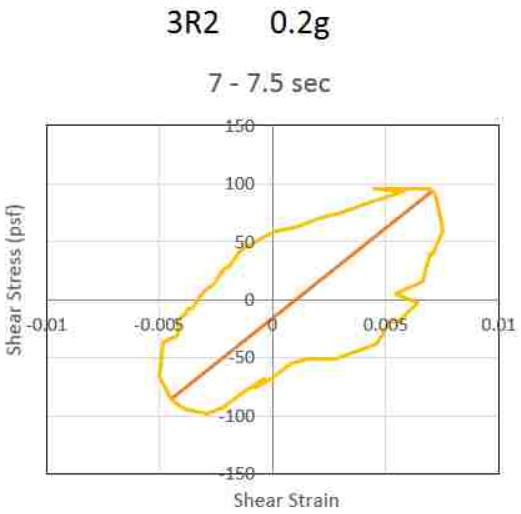

G (shear modulus)		Stress	Strain
		7 - 7.5 sec	
AE18x - H19x	Max	92.000	0.00700
	Min	-84.000	-0.00440
	G	15438.60	

Figure 5-21: Shear Modulus Calculation

5.3.2 Normalized Shear Modulus vs. Cyclic Shear Strain

The shear modulus was than normalized by the initial or maximum shear modulus. The initial shear modulus was difficult to estimate due to the sensors poorly measuring small shear strain, as seen in Figure 5-19 Due to the difficulty of interpreting the shear modulus plots, an estimation of initial shear modulus was used and applied to the analysis. The estimated shear wave velocity is typical of loose, clean sands.

The 100 m/s shear wave was used to estimate the shear modulus at that time. Testing completed previously at UB-SUNY by Thevanayagam (Thevanayagam, Yeigan, Stokoe, & Youd, 2015) used CPT tests to calculate the shear wave velocity. Shear wave velocity tends to increase with the increase of density in the soil. This was not considered during analysis of the data obtained by Oakes large scale shaker table. The initial shear wave values for Thevanayagam testing is show in Figure 5-22.

This was based on average shear wave velocities measured in sands. The value of 100 m/s shear wave velocity was used. This can be converted to shear modulus by the equation below.

$$G = \rho * V_s^2 \tag{5-7}$$

By using the initial shear wave velocity of 100 m/s (or 328 ft/s), using $\rho = g / \gamma$, and assuming the unit weight is $\gamma = 123.17$ pcf, the calculated G_{max} or G_o is 411.7 ksf. This value was used in all shear modulus analysis, regardless of acceleration or round of testing.

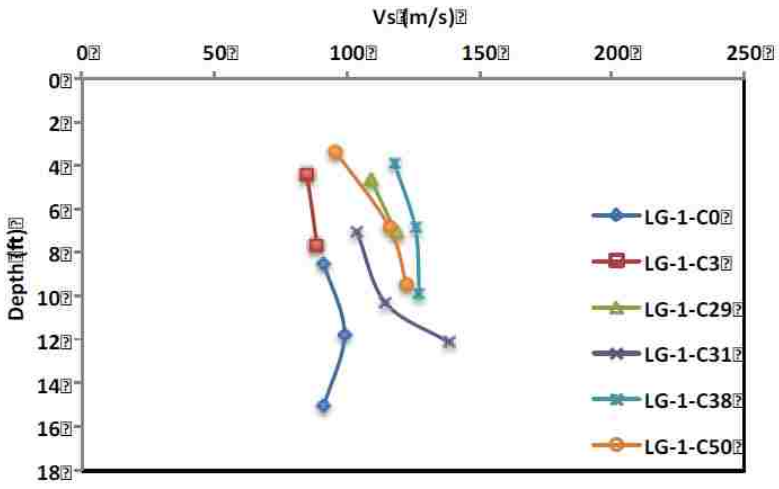

Figure 5-22: Initial Shear Wave Velocity for Thevanayagam Testing (Thevanayagam, Yeigan, Stokoe, & Youd, 2015)

Figure 5-23 shows normalized shear modulus vs. cyclic shear strain. These data points are the estimated shear modulus and theoretical maximum cyclic shear strain experienced for each timeframe and each depth analyzed. The data is compared against the typical upper and lower bounds presented by Seed and Idriss (Seed & Idriss, 1970)

Most of the data points obtained through this testing had high shear strain. This is due to the soil being new and very loose and quickly straining. Small strain data had a large amount of noise and was difficult for interpretation, and therefore, removed from this analysis. This analysis was then separated by excess pore pressure ratio ranges, dictated in Table 5-1. The resulting plot can be seen in Figure 5-24.

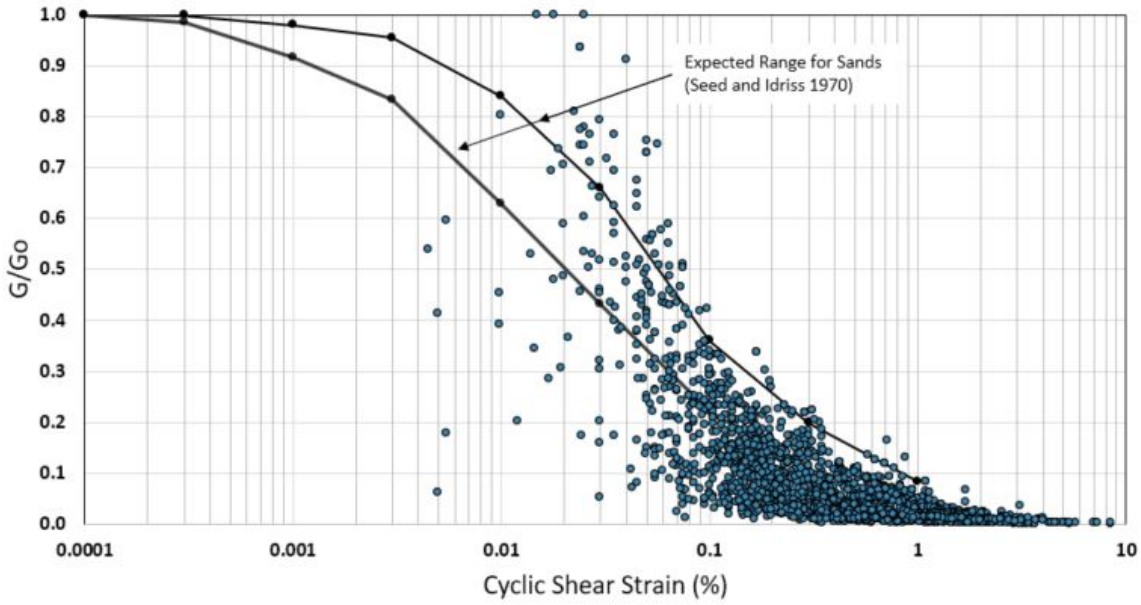

Figure 5-23: All Data Points for G/Go vs. Cyclic Shear Strain

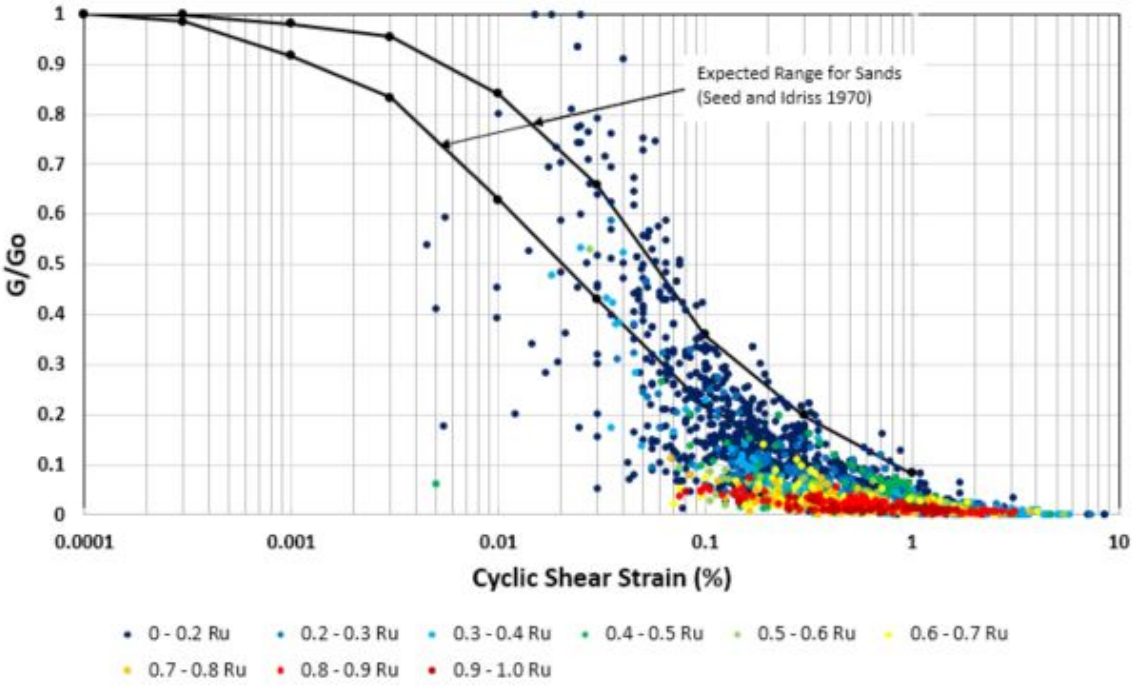

Figure 5-24: Normalized Shear Modulus vs. Cyclic Shear Strain Color-Coded by Pore Pressure Ratio

By separating into pore pressure ratio ranges, the effect of pore pressure generation on shear modulus can be observed. The normalized shear modulus decreases with increasing pore pressure ratio. The effects of pore pressure generation can be captured and used in design.

With ratios above 0.6, which is considered near- or liquefied, the shear modulus approaches zero but does not reach the value of zero. This is important to note, because liquefied soil is assumed to have zero shear strength in design. But results from this testing show that the soil still has shear strength at high R_u values, and pore pressure generation was mitigated potential by the earthquake drains even pass threshold cyclic shear strains.

5.4 Shear Wave Velocity vs. Excess Pore Pressure Ratio for Blast Liquefaction Tests

Due to the insensitivity of the LVDTs and accelerometers, small strains could not be accurately resolved during the shaking events. As a result, all computed small shear strain data points were considered inconclusive and were removed from the data set owing to high noise and difficulty in interpretation. To develop G/Go curves for the varying pore pressure ratios (R_u), additional data was needed, primarily in low to very low shear strains ranges, 10^{-3}% to 10^{-4}%.

To supplement this data set, shear wave velocity and pore pressure ratio information was gathered from multiple test sites where shear wave velocity was measured after blast-induced liquefaction. These test sites include: Treasure Island Blast Test (Jelinek & Bay, 2000); (Rollins, Lane, & Gerber, 2005); Maui Blast Tests (Rollins K. M., Lane, Nicholson, & Rollins, 2004); Christchurch Blast Tests (Wentz, van Ballegooy, Rollins, Ashford, & Olsen, 2015); (Rollins & Hollenbaugh, 2015); and (Cox and Roberts, personal communication, 2014); Mirabello Blast Test (Amoroso & et al, 2017); and (Amoroso and Rollins, personal communication, 2014); and

Turrell Arkansas Blast Liquefaction Test (Kevan, 2017); (Rollins and Amoroso, Personal communication, 2014).

5.4.1 Treasure Island Blast Tests

The Treasure Island blast tests were performed on Treasure Island in the San Francisco Bay (Rollins, Lane, & Gerber, 2005). The main purpose of the testing was to investigate the effect of liquefaction on the lateral resistance of piles and drilled shafts.

The soil profile for the Treasure Island blasts tests was obtained from soil borings and CPT testing. The soil profile can be seen in Figure 5-25. The upper 8 meters of the profile consists of poorly-graded sand which classifies as SP according to the Unified Soil Classification System.

After the blast, the excess pore pressure was measured by vertical and horizontal arrays of transducers surrounding the pile group and drilled shaft foundations as illustrated in Figure 5-26. The shear wave velocity before and after the blast liquefaction experiment was measured with cross-hole techniques using a source and a receiver at a depth of 5 to 6 feet below the ground surface. Liquefaction was induced using rings of eight blast holes around both the pile group and the drilled shaft.

The explosives consisted of 0.5 kg charges in each hole located at a depth of about 3 meters below the ground surface that were detonated two at a time. The shear wave velocity immediately prior to the blast provided the velocity at a shear strain of 10^{-4}% for the static water pressure condition (excess pore pressure ratio of 0%). Shear wave velocities were then measured shortly after the blast as excess pore pressure ratios reached 100%, or liquefaction, and at several time intervals afterwards as excess pore pressures dissipated, and R_u values decreased back to

0%. The shear wave data and pore pressure data were combined to produce a plot of normalized shear wave velocity as a function of R_u in Figure 5-27. The shear wave velocity was normalized by the initial velocity when R_u had returned to zero. The normalized shear wave velocity decreases as the pore pressure ratio increases and reaches a minimum value of about 0.40 when R_u reaches 1.0.

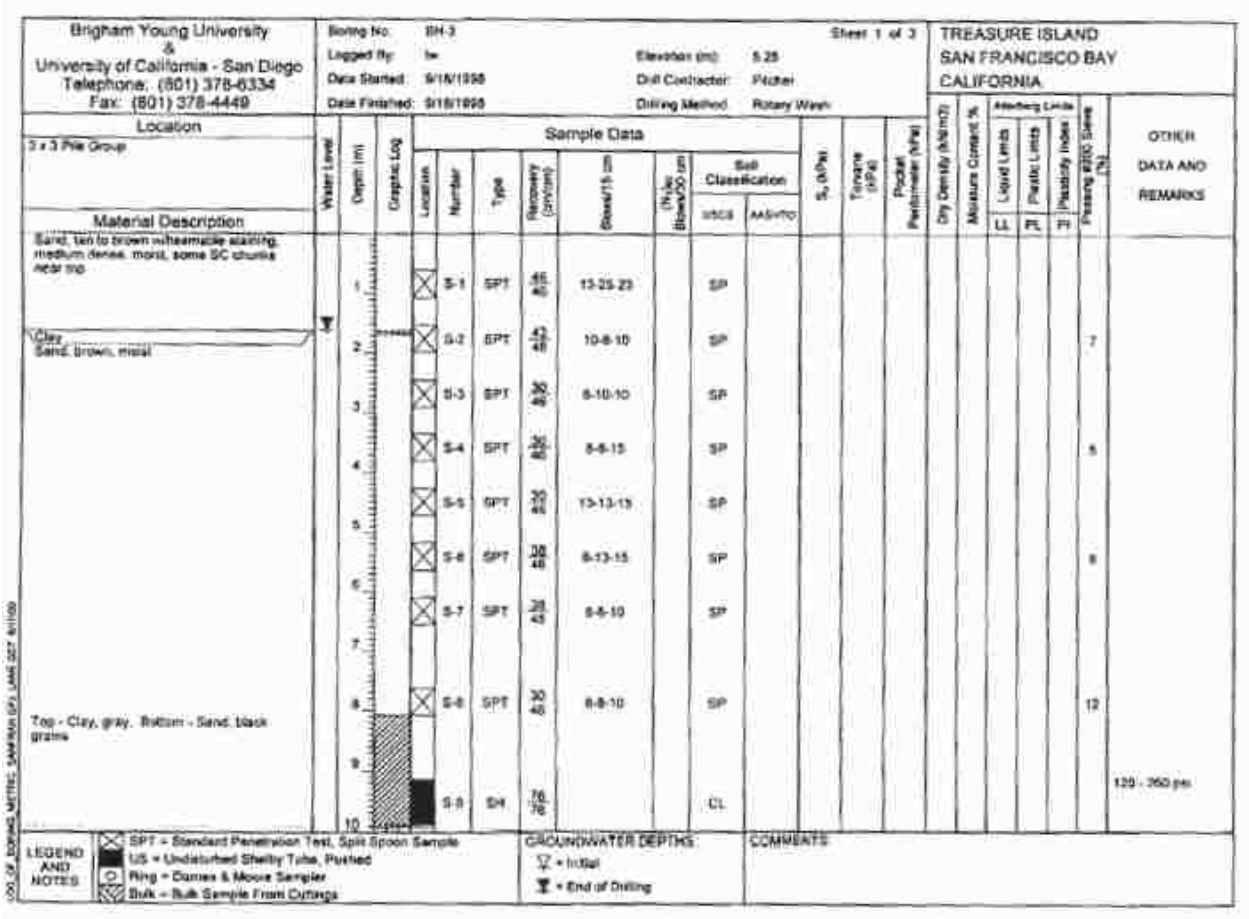

Figure 5-25: Treasure Island Soil Profile (Jelinek & Bay, 2000)

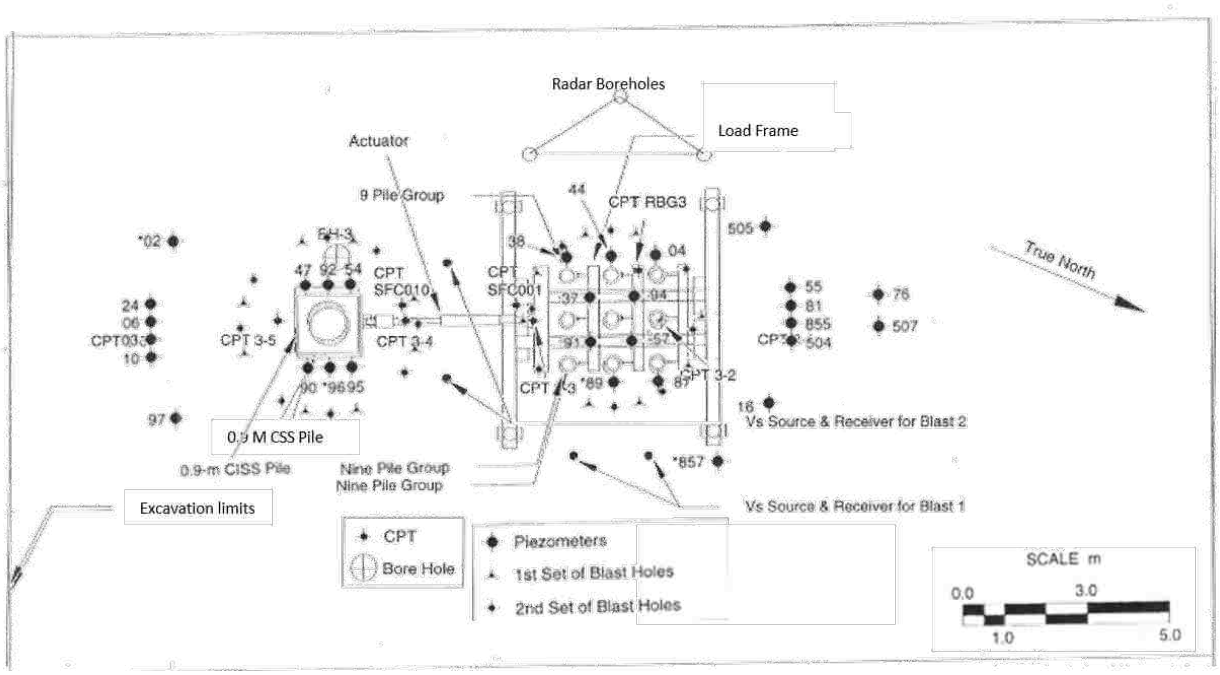

Figure 5-26: Treasure Island Test Layout (Jelinek & Bay, 2000)

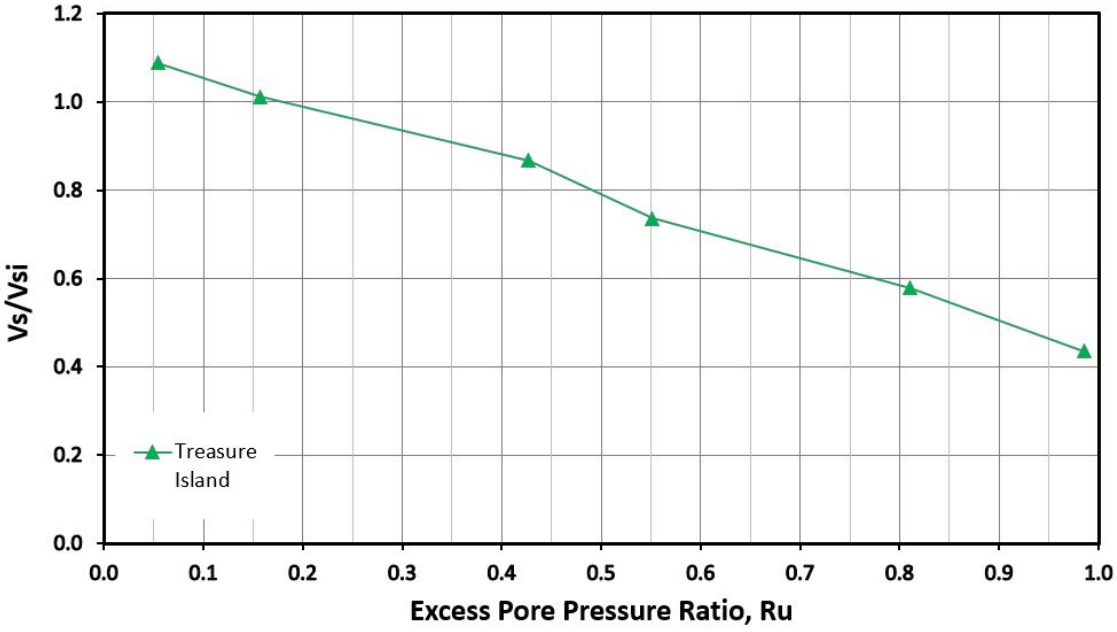

Figure 5-27: Normalized Shear Wave Velocity vs. Pore Pressure Ratio from Treasure Island Blast Test

5.4.2 Maui Blast Tests

Testing was performed in Maui, Hawaii to evaluate the potential for liquefaction in coralline sands and gravels relative to that of conventional sands (Rollins K. M., Lane, Nicholson, & Rollins, 2004). Two bore holes were drilled to define the soil profile at the testing location. The soil profile is presented in Figure 5-28. The soil consisted of clayey silt underlain by fine volcanic sand which was in turn underlain by coralline sand and gravel, at a depth of 3.8 m extending to 8 m.

The test layout, provided in Figure 5-29, shows the location of the data measuring sensors and the blast locations. Two blast sequences were initiated, the first sequence used a line of charges located 5.35 meters from the test center, and the second sequence used a line located 4.11 meters from the test center. In each test, a total of eight 0.45 kg charges were detonated at a depth of 5.35 meters with a delay of 500 msec between each detonation. Instrumentation included piezometers, downhole accelerometers, downhole geophones, blast seismographs, string potentiometers, and settlement stakes. Piezometers were placed at a depth of 5.35 meters.

Two hardened geophones were also installed at a depth of 5.35 meters on opposite sides of the centerline of the test area at a spacing of 2.13 meters (see Figure 5-29). The geophones were connected to steel pipes which extended through a mudded hole and above the ground surface. The P- and S-wave velocities could be measured as a function of pore pressure change. The velocity testing and the data analysis were conducted by Prof. James Bay and Kurt Jelenik of Utah State University. P- and S-wave velocity measurements were made prior to blasting to determine the initial values.

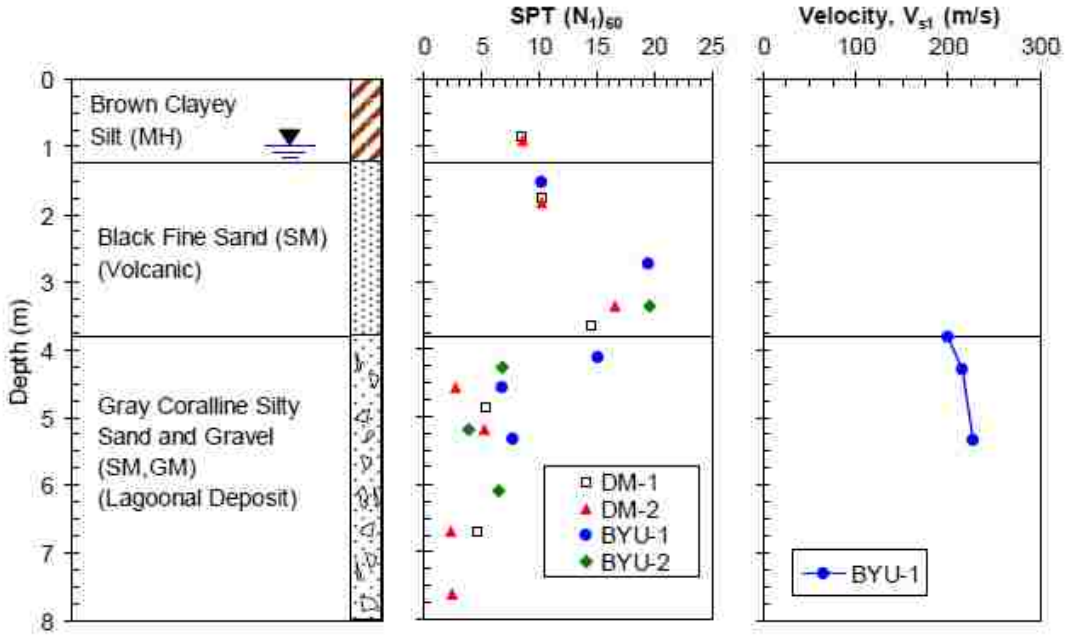

Figure 5-28: Soil Profile for Maui Testing (Rollins K. M., Lane, Nicholson, & Rollins, 2004)

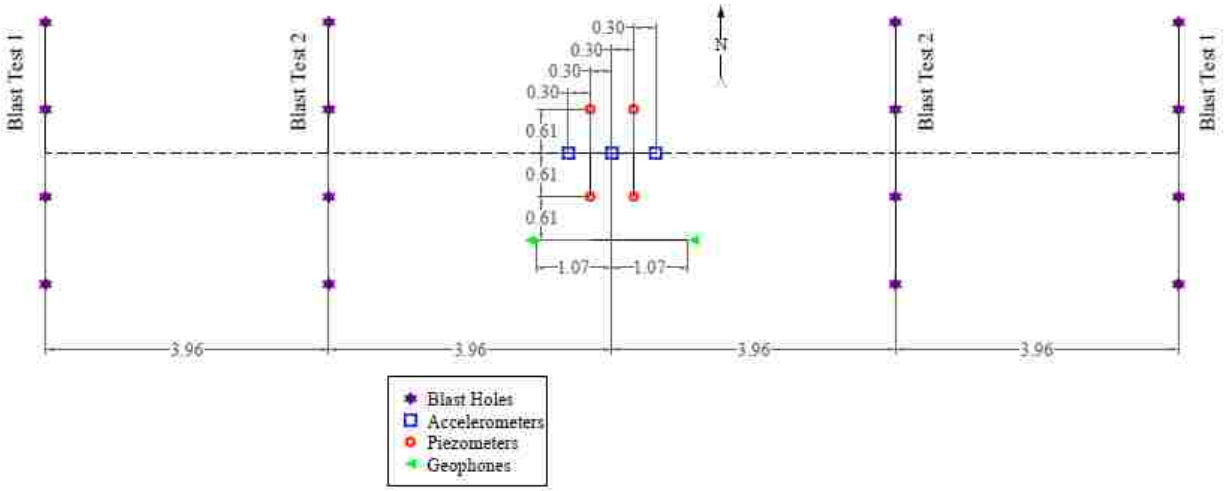

Figure 5-29: Maui Test Layout (Rollins K. M., Lane, Nicholson, & Rollins, 2004)

As soon as possible after the blasting, the compression and shear wave velocities were measured within the testing area using the cross-hole method. Figure 5-30 shows a plot of the measured normalized shear wave velocity normalized by the initial velocity prior to blasting vs. the excess pore pressure ratio, R_u. As R_u reached the maximum of approximately 0.9, signifying that the coralline sands had essentially liquefied, the shear wave velocity decreased to about 50% of its pre-blast value for the first blast and about one-third of its value for the second blast. This decrease is similar to the 65% decrease in velocity recorded following liquefaction in non-coralline sands at Treasure Island for similar blast test experiments. This is equivalent to reducing the shear modulus (G_{max}) to about 11% of its original value. The P-wave velocity remained relatively constant after blasting indicating that de-saturation was not occurring. (Rollins K. M., Lane, Nicholson, & Rollins, 2004)

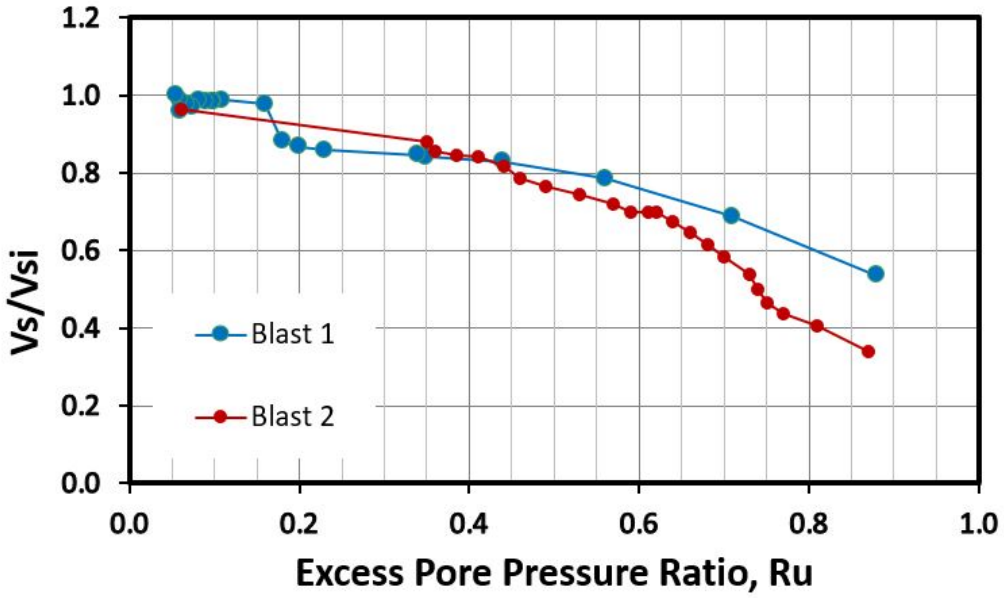

Figure 5-30: Shear Wave Velocity vs. Pore Pressure Ratio

For the first blast test, the shear wave velocity after re-consolidation (R_u = 5%) was essentially equal to that prior to blasting. However, for the second blast test, the shear wave velocity after re-consolidation (R_u = 5%) was only about 90% of its pre-blast value. This result suggests that the blasting process may have permanently disrupted weakly cemented bonds in the coral sands thereby decreasing the shear wave velocity.

5.4.3 Christchurch Blast Tests

In the aftermath of the Christchurch, New Zealand earthquakes in 2010-2011, liquefaction testing was performed to better understand the liquefaction that affected Christchurch and techniques for mitigating the hazard. The Earthquake Commission (EQC) of New Zealand sponsored a series of field trials to evaluate the effectiveness of various ground improvement methods for creating a stiff surface layer over the liquefied sand below. During one of these trials, three ground improvement methods were being tested along with an unimproved control section as shown Figure 5-31. The subsurface soils at the test site consisted of approximately 2 meters of loose silt/sandy silt overlying generally loose to medium dense silty sand/sand. Relatively clean, predominantly medium dense sand was consistently present below a depth of about 4 meters across the test site.

As illustrated in Figure 5-31, double rings of blast holes were installed in blast casings around each test panel; an inner 10-meter diameter ring and larger outer 15-meter diameter ring. Ten blast casings were evenly spaced around the perimeter of each ring (at approximately 3.1 meters center-to-center spacing). Each blast casing contained three levels or "decks" of gelignite charges consisting of 2.8 kg at 11.5 meters, 2.4 kg at 7.5 meters, and 0.55 kg at 4 meters depth. A

total of 396.8 kg of explosives were distributed around the 4 test panels in two separate blast sequences (Wentz, van Ballegooy, Rollins, Ashford, & Olsen, 2015)

Pore pressure transducers were located at 2.3, 3,3, 4.3, 5.3, 7.3, 8.3 and 11.3 meters below the ground surface near the center of each blast ring. At three locations throughout the test area, two vertical pipes were installed at depths of 2.875 meters, 4 meters and 5 meters, with a distance of a few meters between them. A remotely activated hammer was used to strike one pipe generating a wave, while a geophone on the second pipe was used as a receiver so that P- and S-wave velocities could be measured by the cross-hole method as was done at Treasure Island and Maui. The velocity testing was performed by Dr. Julia Roberts and Prof. Brady Cox of the Univ. of Texas at Austin.

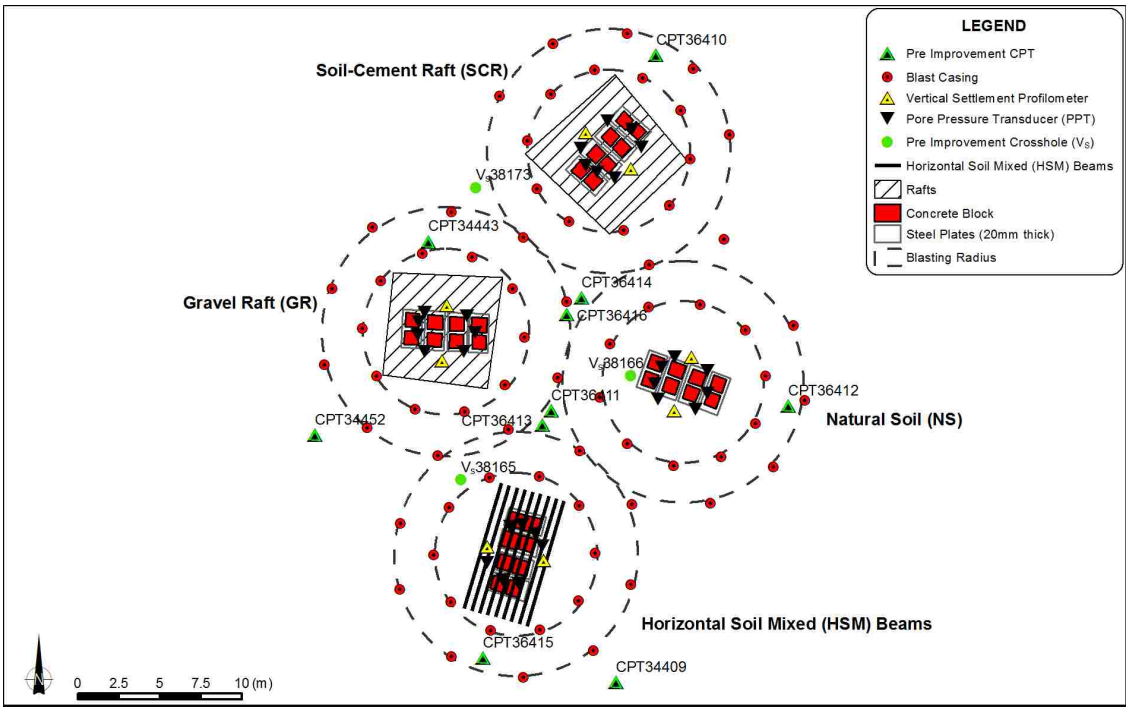

Figure 5-31: Test Panel Locations and Subsurface Investigation, Instrumentation and Charge Layouts (Wentz, van Ballegooy, Rollins, Ashford, & Olsen, 2015)

In addition to the ground improvement tests, three test piles were instrumented to measure negative skin friction and downdrag following liquefaction and after pore pressure dissipation. The test site was located in Avondale, near the Avon River in Christchurch, New Zealand. CPT soundings and a SPT boring were performed at the test site to define the soil profile. Based on the field and laboratory testing the idealized soil profile in Figure 5-33 was developed (Rollins & Hollenbaugh, 2015)

The test piles were 0.6-meter diameter auger-cast piles with lengths of 8.5 meters, 12 meters, and 14 meters. The test layout is illustrated in Figure 5-32. The three test piles located at a radius of 2 meters from the center were surrounded by a ring of blast holes having a radius of 5.0 meters. In each of 8 blast holes, explosive charges were detonated one at a time at approximately 0.2 second intervals beginning with the eight 2.7 kg charges at 8.5 meters followed by the eight 1.1 kg charges at 4.0 meters. depth. Pore water pressure transducers were located around a ring with a radius of 2 meters from the center as shown in Fig. 5.27. Liquefaction was produced between depths of about 4 m and 14 m.

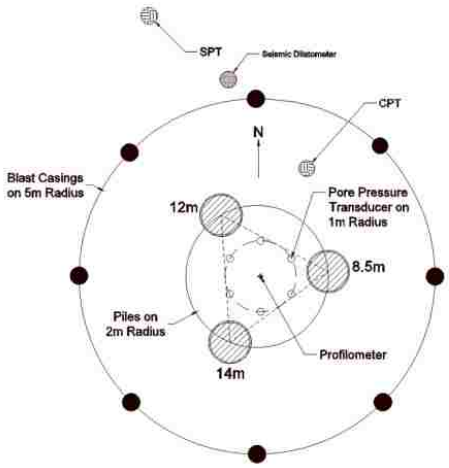

Figure 5-32: Test Layout for Christchurch Testing (Rollins & Hollenbaugh, 2015)

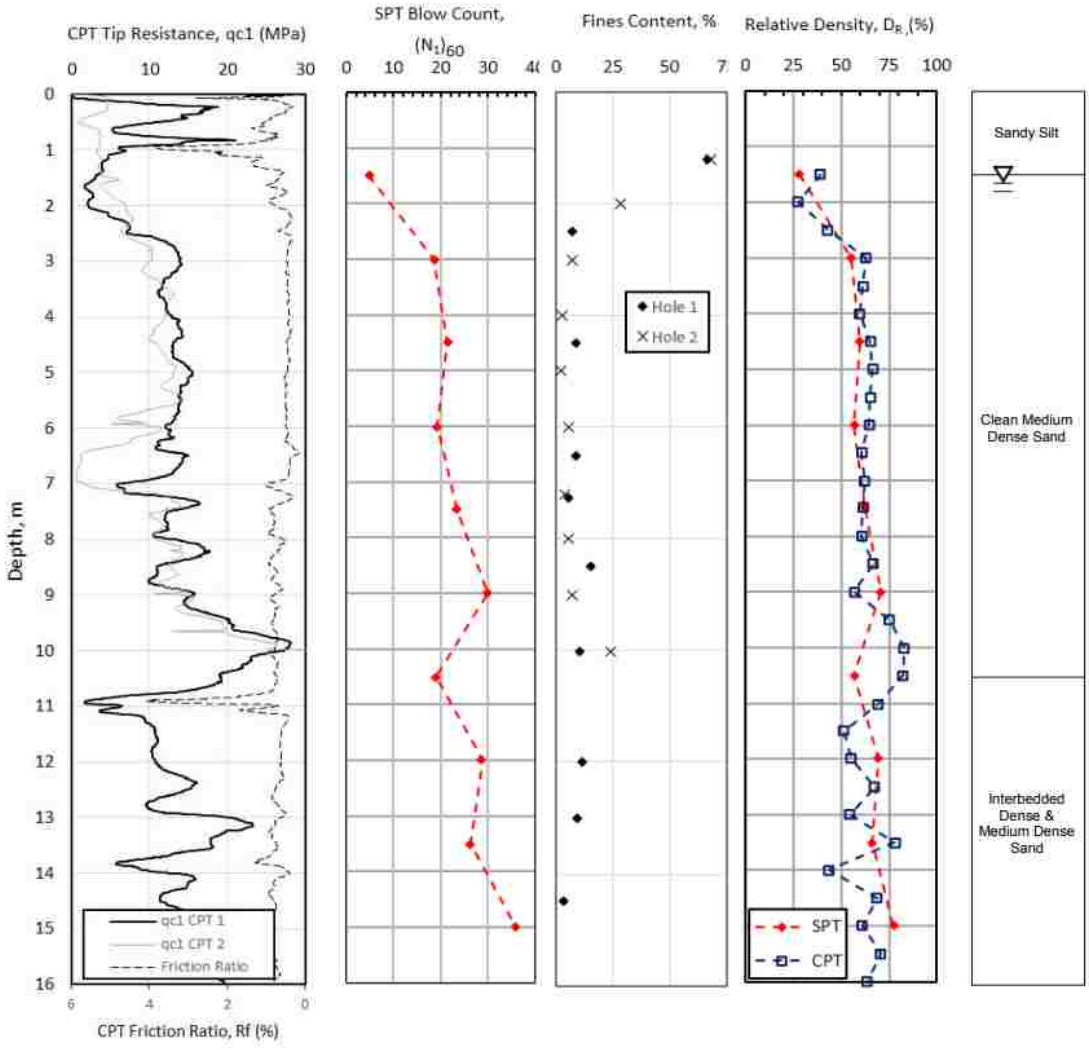

Figure 5-33: Soil Profile for Christchurch Testing (Rollins & Hollenbaugh, 2015)

The shear wave velocity before and after blasting was measured using a seismic dilatometer (SDMT) with a small hammer that was designed to impact a steel plate at the ground surface in the horizontal direction. The SMDT, located a depth of 6.5 meters, measured the resulting wave arrival times at two different receivers located 0.5 meters apart in the vertical direction. As shown in Figure 5-32, the SDMT was located at a distance of 3.5 meters from the center of the blast array. Using a cross-correlation algorithm, *VS.* was obtained as the ratio between the difference in distance between the two receivers (0.5 meters) and the delay ΔT in

arrival time from the first to the second receiver. The porewater pressure before and after blasting was measured using the DMT sensor located just below the seismic receivers. The SDMT testing was conducted by Dr. Sara Amoroso of Instituto Nazionale di Geofisica e Vulcanologia (INGV) of Italy.

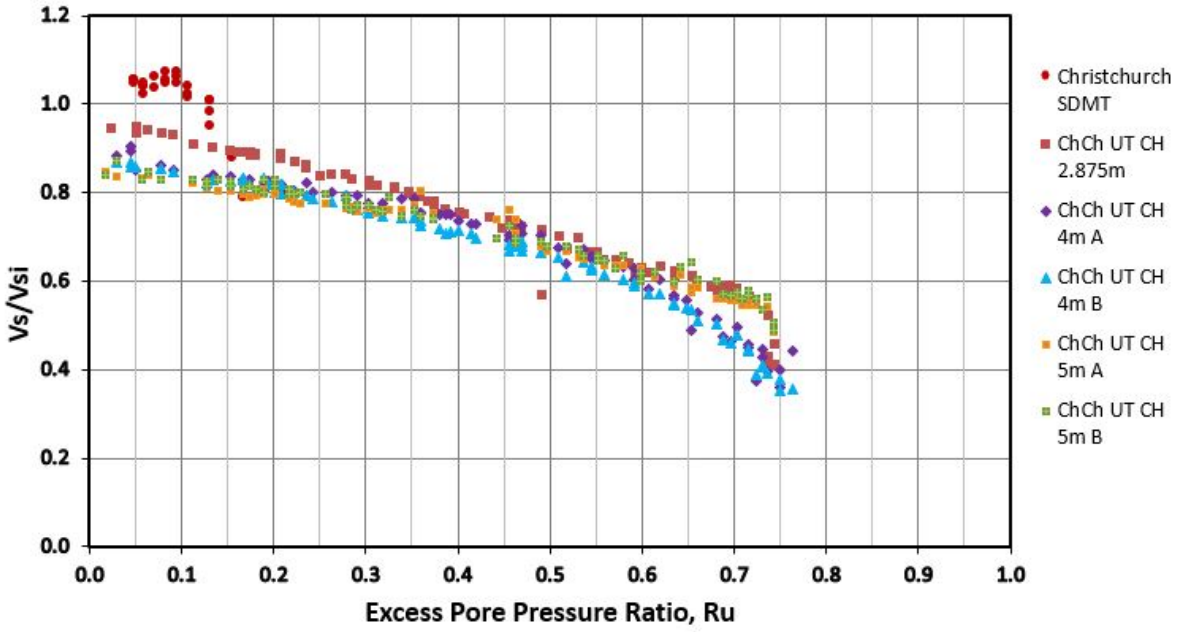

Figure 5-34: Christchurch Shear Wave Velocity vs. Pore Pressure Ratio

The measured shear wave velocity normalized by the initial velocity is plotted vs. R_u in Figure 5-34. Although liquefaction developed within the blast ring, the R_u at the location of the SDMT was only 0.21 by the time that post-blast Vs. measurements could be made. Therefore, the Vs/Vsi did not decrease below about 0.75. Despite the lower Ru values for this test, the observed Vs/Vsi vs. Ru trend is consistent with that for the other tests at the site where higher Ru values developed. However, in contrast to the other five tests in Christchurch, the Vs. value after pore pressure dissipation was about 5% high than the initial value rather than lower. This is

likely a result of the lower Ru that developed in this test which was apparently insufficient to destroy the soil structure but may have caused some densification.

5.4.4 Mirabello Blast Test

The significant settlement that can occur from liquefaction is of immense importance in engineering design. This test site was chosen due to the multiple earthquake events that occurred in the surrounding area in 2012. Liquefaction had been observed in this area previously. A piezocone test (CPTu) and four standard penetration tests (SPT), were performed to develop a soil profile, which can be seen in Figure 5-35.

The test layout is also shown in Figure 5-36. The blast charges were distributed in eight blast holes around a 5-meter radius. In each blast hole, 1.875 kg and 2.5 kg charges were located at 7-meter and 11-meter depths, respectively. The two charges in the same hole were planned to detonate almost simultaneously (delay of detonation 42 ms), while the delay of detonation between each of the eight holes was fixed at 200 ms.

Eight pore pressure transducers were installed at depths from 6 meters to 11 meters on a ring about 1 meter from the center of the blast array to measure pore pressure generation. Shortly after the blasting, shear wave velocities were measured using the seismic dilatometer (SDMT) as described previously. The SDMT testing was conducted by Dr. Sara Amroso of INGV. The dilatometer was located at a depth of 7.25 meters below the ground surface and at a distance of about 2.5 meters from the center of the blast circle. The hammer at the ground surface was operated remotely to obtain measurements as soon as possible after the completion of the blast sequence.

A plot of the V_s/V_{si} vs. R_u is plotted in Figure 5-37. The trend is similar to that observed in other liquefaction tests where the shear wave velocity decreases with increasing R_u. At the maximum R_u of 0.65, the measured shear wave velocity is about 35% of its initial value. Even after the dissipation of the excess pore pressure ($R_u = 0$), the shear wave velocity is still only about 70% of its initial value prior to blasting. This significant reduction in velocity is likely a result of a breakdown of the soil structure owing to liquefaction. In addition, the high fines content of this profile (30 to 80% fines) appears to have delayed the re-development of stiffness relative to a clean sand (see Treasure Island). SDMT testing conducted two months after the blast do show that the silty sand layer at 6.5 meters did eventually regain its initial velocity.

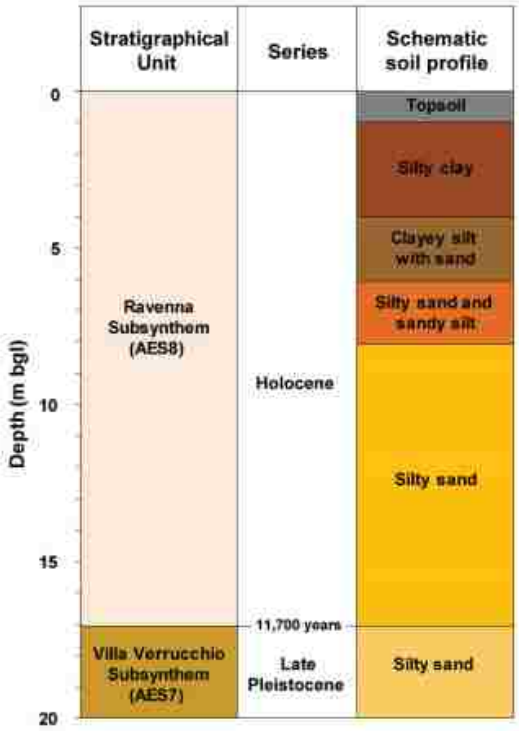

Figure 5-35: Mirabello Soil Profile (Amoroso & et al, 2017)

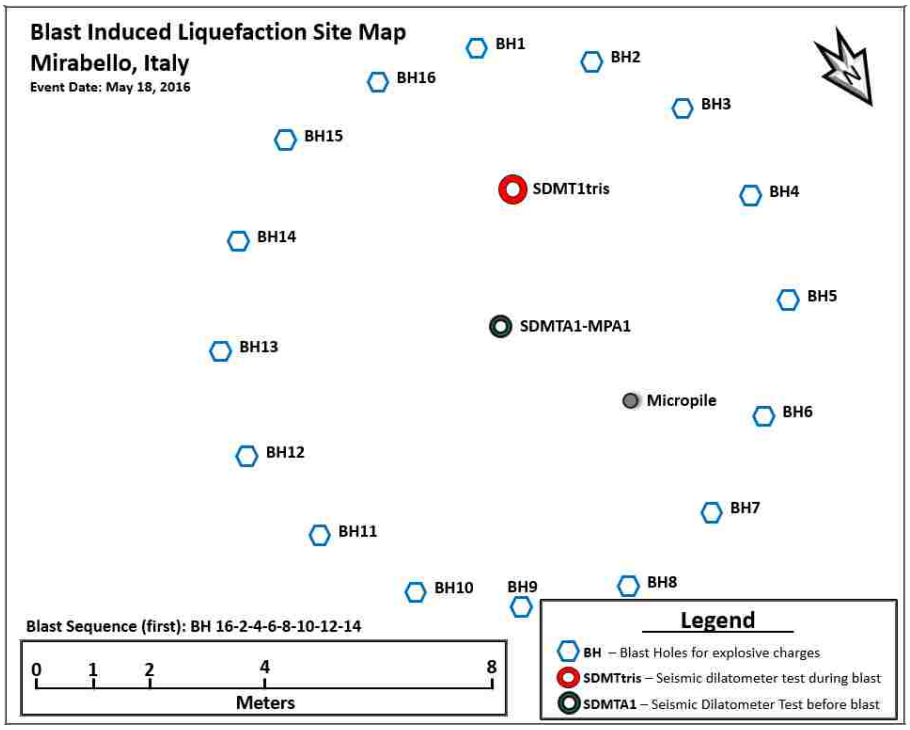

Figure 5-36: Test Layout for Mirabello (Amoroso and Rollins, Personal Communication 2016)

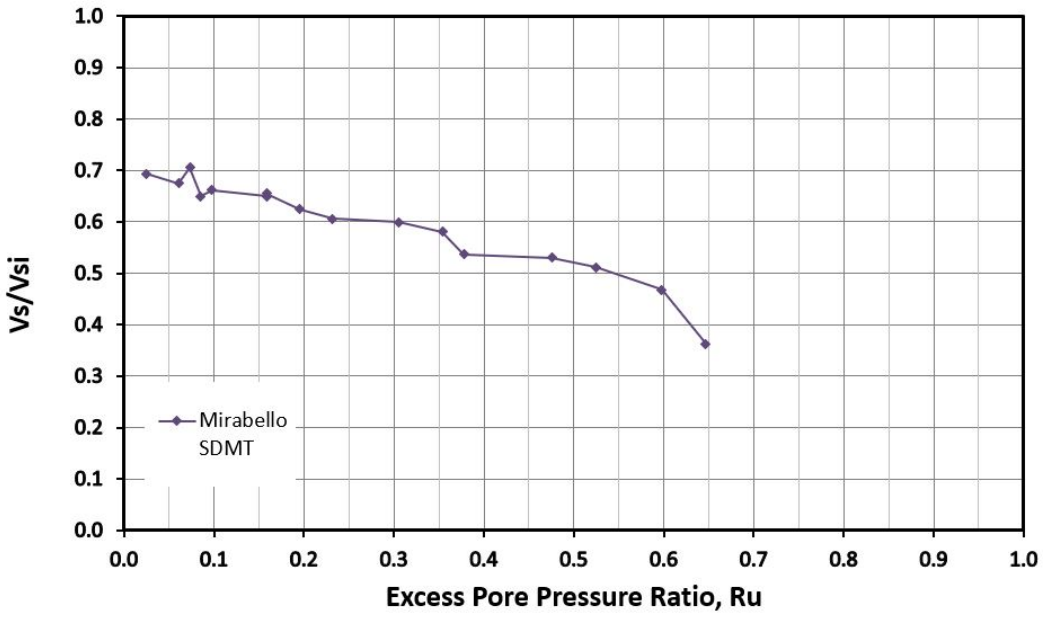

Figure 5-37: Shear Wave Velocity vs. Pore Pressure Ratio for Mirabello Blast Test

5.4.5 Turrell Arkansas Blast Liquefaction Test

A series of three blast liquefaction tests was performed at a highway interchange near Turrell, Arkansas (about 15 miles west of Memphis, Tennessee) in 2016. The test program was organized by Prof. Richard Coffman of the University. of Arkansas in collaboration with Prof. Kyle Rollins of Brigham Young University (Ishimwe, Coffman, & Rollins, 2016) (Kevan, 2017). The test site is located on the west side of the Mississippi river and the soil profile consisted of about 30 feet of cohesive soil underlain by sand and silty sand layers as shown in Figure 5-38.

The Figure 5-39 provides a plot showing the test layout and the location of the SDMT in near two of the blast rings. For the first blast the SMDT was located one meter from the center of the blast ring and 3 meters from the center for the second blast. In both blast tests the SDMT was located at a depth of 34.75 feet. Pore pressure measurements were made using a vertical array of pore pressure transducers at depths of 30, 33, 36, 39, 42, 46, 56 and 62 feet.

In addition, pore pressure measurements were made with the DMT. Shortly after the blasting, shear wave velocities were measured using the seismic dilatometer (SDMT) as described previously. The SDMT testing was conducted by Dr. Sara Amroso of INGV. A hammer at the ground surface was operated remotely to obtain velocity measurements as soon as possible after the completion of the blast sequence.

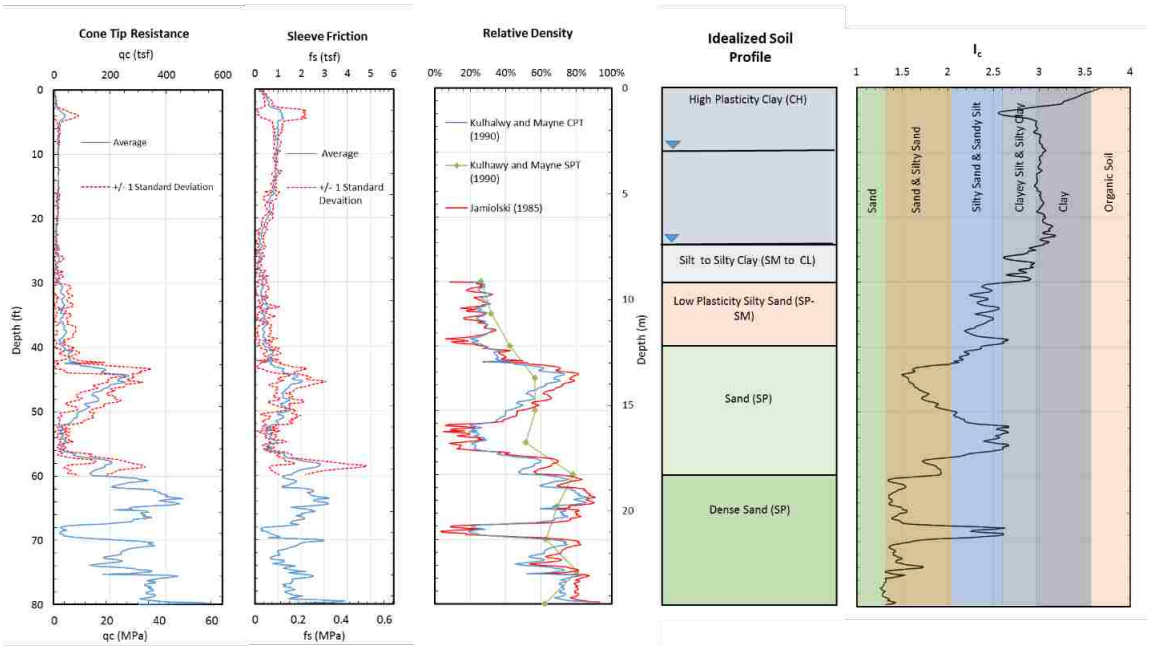

Figure 5-38: Turrell Blast Test Soil Profile (Kevan, 2017)

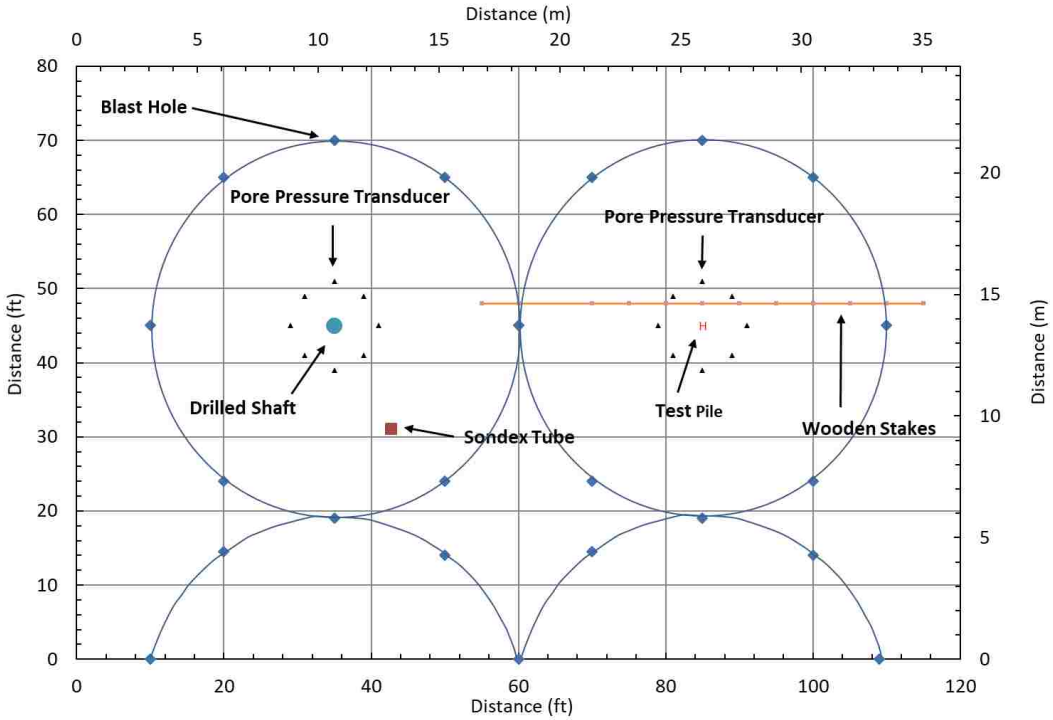

Figure 5-39: Turrell AR Blast Test Layout (Kevan, 2017)

A plot of the V_s/V_{si} vs. R_u is shown in Figure 5-40. The trend is similar to that observed in other blast liquefaction tests where the shear wave velocity decreases with increasing R_u. At the maximum R_u of 0.53, the measured shear wave velocity for blast one is about 70% of its initial value, and about 50% of its initial value for blast two. Even after the dissipation of the excess pore pressure ($R_u = 0$), the shear wave velocity is about 105% of its initial value prior to blasting for blast one, and about 80% of its initial value for blast two.

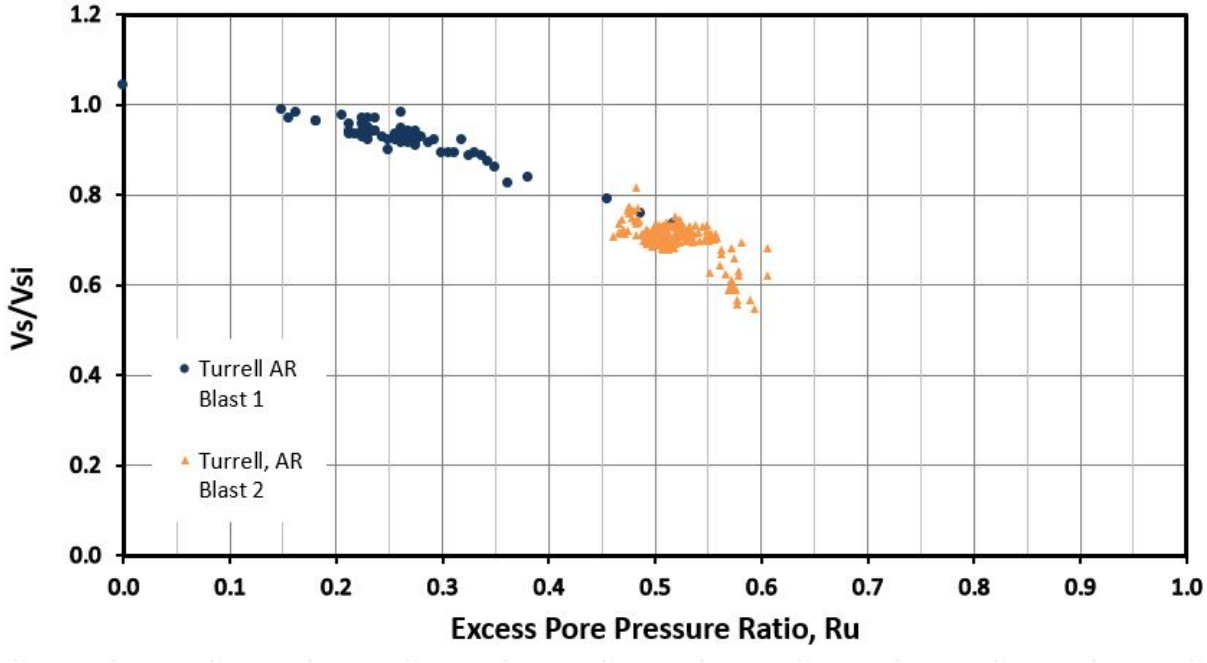

Figure 5-40: Turrell AR Blast-Induced Tests, Vs/Vsi Vs vs. Ru

5.4.6 Summary of Pore Pressure Effects on Shear Wave Velocity and Shear Modulus for Small Strain Conditions on Blast Liquefaction Tests

The results from all the blast liquefaction tests are summarized in Figure 5-41, with shear wave velocities being normalized by the initial shear wave velocity at each site. The shear wave velocities after reconsolidation (to $R_u \approx 0$) following blasting end up being higher or lower than

the initial velocity leading to V_s/V_{si} values ranging from 0.7 to 1.1. The higher ratios V_s/V_{si} ratios appear to be associated with loose, relatively clean sands where the blasting leads to increased density after reconsolidation. In contrast, the lower V_s/V_{si} ratios appear to be associated with silty sands where the breakdown in the soil structure does not completely recover at the end of re-consolidation presumably owing to the lower hydraulic conductivity of the soil or the extent of the disruption to the soil structure. The measured shear wave velocity data before, during, and after the blast induced liquefaction are summarized in Table 5-2.

To combine the results from the blast liquefaction tests with the G/G_o vs. cyclic shear strain results from the laminar shear box testing, shear wave velocity ratio (V_s/V_{si}) must be converted to a G/G_o ratio. To do this, an assumption was made that the velocity measurements were obtained at very small shear strain, on the order of 10^{-4}%, because shear waves were measured before and after the blasting event. With this assumption, the field blast liquefaction tests provide G/G_o vs. R_u values at small strain that can be combined with the data measured at large strain in the laminar shear box testing presented previously in this thesis.

It is important to note that the data with high pore pressure ratios are assumed to occur after the shaking event, therefore with no shear strain, but before the pore pressures dissipate. The pore pressure ratio has already formed before additional cyclic shear strain would be applied. When the blast liquefaction data is plotted with the laminar shear box data, the assume small strain data should not be interpreted as the cyclic shear strain causing the high pore pressure ratio.

The G/G_o ratio is computed for each V_s/V_{si} curve using the equation

$$\frac{G}{G_0} = \left(\frac{V_s}{V_{si}}\right)^2 \tag{5-4}$$

A plot of G/G_o vs. R_u based on the V_s/V_{si} measurements for each blast test is presented in Figure 5-42 For comparison purposes, a theoretical G/G_o vs. R_u relationship proposed by (Kramer & Greenfield, 2017) is also presented with the measured curves in Figure 5-42. The equation for G/Go is shown below.

$$\frac{G}{G_0} = (1 - R_u)^{0.5} \qquad \textit{(At small shear strain} \approx 10^{-4}\%) \tag{5-9}$$

The G/G_o values are typically lower than the theoretical curve proposed by Kramer (Kramer & Greenfield, 2017). This discrepancy could be attributed to the fact that the Kramer equation only accounts for decreases in the vertical effective stress caused by excess pore pressure generation; however, it does not account for possible degradation of the soil structure produced by liquefaction prior to reconsolidation. Nevertheless, the reduced shear wave velocities following reconsolidation strongly suggest that soil structure is being degraded by the liquefaction process.

The $V_s/V_{s.\,max}$ vs. R_u curves for each blast test are presented in Figure 5-43 and it can be clearly seen that this normalization process has produced a relatively narrow band of data points with scatter increasing somewhat at higher R_u values. This normalization has been effective in minimizing the effects of density and soil structure degradation on the test results.

Once again, the $V_s/V_{s.\,max}$ curves from Figure 5.38 were converted to G/G_o curves using Equation 5-8. The resulting G/G_o vs. R_u curves for all the blast liquefaction tests are plotted in Figure 5-44 along with the theoretical curve proposed by (Kramer & Greenfield, 2017). The measured data points generally fall below the theoretical curve; however, the discrepancy between the measured and theoretical values is much smaller. Nevertheless, the discrepancy between the measured and theoretical G/G_o values appears to increase as the R_u increases

Table 5-2: Blast Liquefaction Test Summaries

	Before Blast	During Blast			Post Blast	
Site	**Initial Vs**	**Max Ru**	**Min. Vs**	**Min Vs/Vs_i**	**Max. Vs**	**Vs_{max}/Vs_i**
Treasure Island	346 ft/s	0.98	150 ft/s	0.44	376 ft/s	1.09
Maui Blast No. 1	655 ft/s	0.88	351 ft/s	0.54	655 ft/s	1.0
Maui Blast No. 2	655 ft/s	0.87	222 ft/s	0.34	632 ft/s	0.96
Christchurch SDMT	155 ft/s	0.21	109 ft/s	0.71	163 ft/s	1.06
CHCH 2.875 m	120 m/s	0.74	50 m/s	0.41	114 m/s	0.90
CHCH 4m A	140 m/s	0.76	50 m/s	0.36	127 m/s	0.82
CHCH 4m B	140 m/s	0.76	49 m/s	0.35	122 m/s	0.75
CHCH 5m A	150 m/s	0.74	73 m/s	0.48	127 m/s	0.72
CHCH 5m B	150 m/s	0.74	73 m/s	0.49	131 m/s	0.76
Mirabello, Italy	150 m/s	0.65	70 m/s	0.36	136 m/s	0.68
Turrell AR Blast Test 1	147 m/s	0.52	108 m/s	0.74	153 m/s	1.04
Turrell AR Blast Test 2	165 m/s	0.61	119 m/s	0.72	132 m/s	0.8

towards liquefaction. This result suggests that degradation in soil structure with increasing R_u could be decreasing the G/G_o ratio to a greater extent than would be predicted based only on the reduction in confining pressure produced by excess pore pressure. Better agreement with the measured G/G_o vs. R_u data points can be achieved using the equation

$$\frac{G}{G_o} = (1 - R_u)^{0.7} \tag{5-50}$$

to account for the effects of increasing R_u and the soil structure degradation as shown in Figure 5-44.

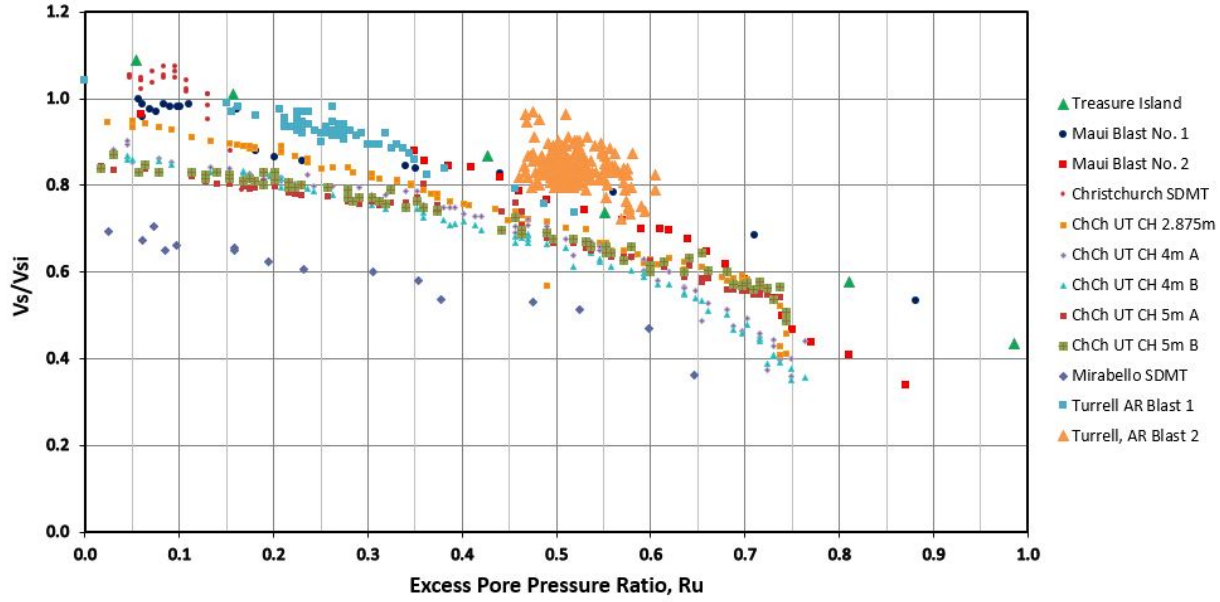

Figure 5-41: Normalized Shear Wave Velocity (Vs/Vsi) vs. Excess Pore Pressure Ratio from Blast Liquefaction Tests

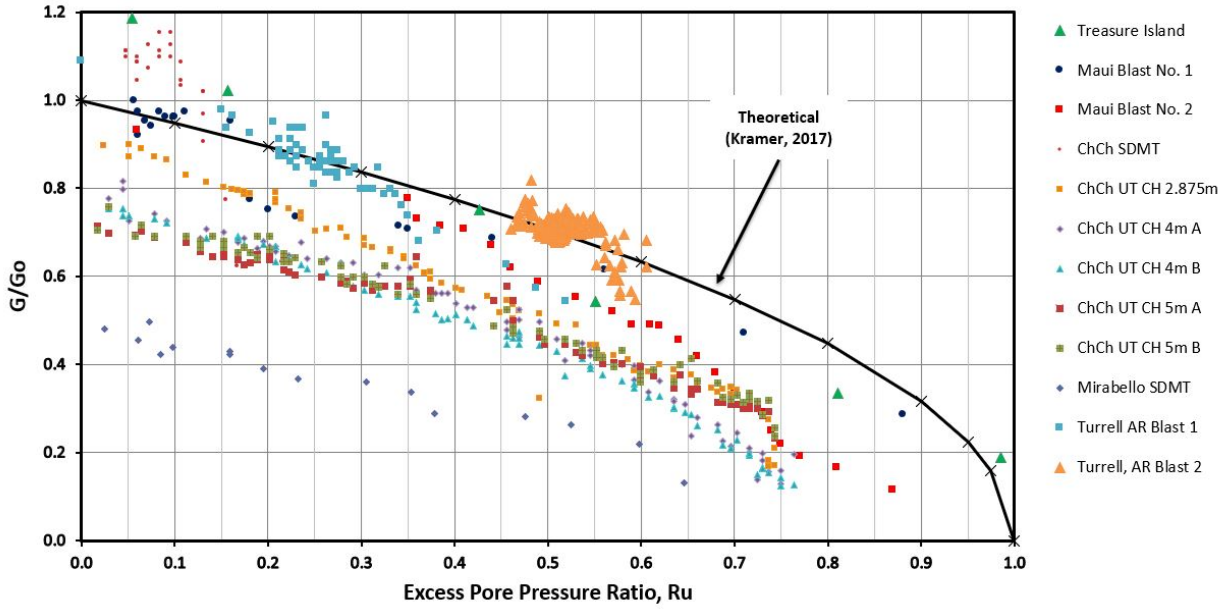

Figure 5-42: Normalized Shear Modulus (G/G0) vs. Excess Pore Pressure Ratio (Ru) Curves from Blast Liquefaction Tests along with Theoretical Curve Proposed by Kramer (Kramer & Greenfield, 2017)

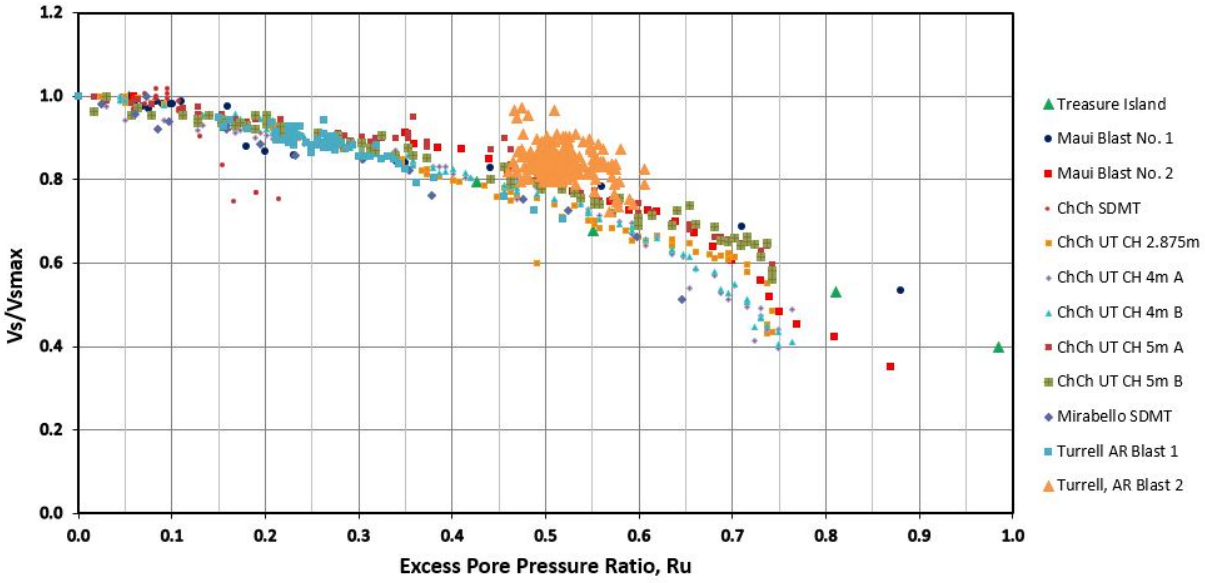

Figure 5-43: Normalized Shear Wave Velocity (Vs/Vsmax) vs. Excess Pore Pressure (Ru) for All Blast Liquefaction Tests

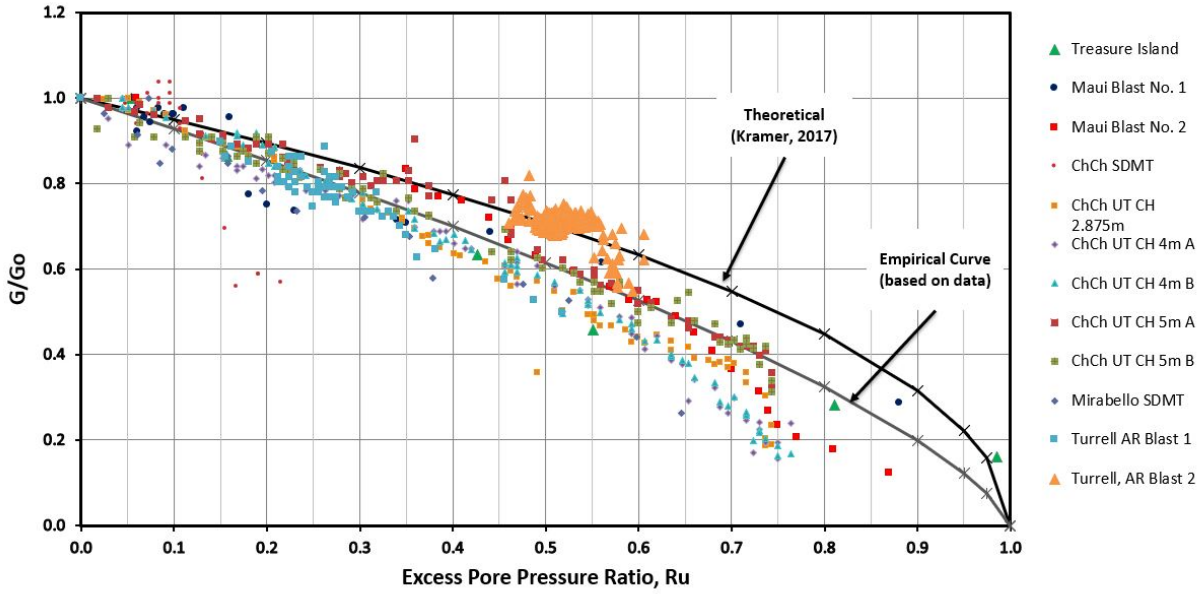

Figure 5-44: Normalized Shear Modulus (G/G0) vs. Excess Pore Pressure Ratio (Ru) from Blast Liquefaction Test in Comparison with Theoretical Curve Proposed by Kramer (Kramer & Greenfield, 2017) and Empirical Equation Based on Measured Data from This Study

5.5 G/G_o vs. Shear Strain Curves for Varying Excess Pore Pressure Ratios

The normalized shear modulus (G/G_o) and cyclic shear strain (%) data points from both the laminar shear box tests and the blast liquefaction tests have been separated into nine excess pore pressure ratio (R_u) ranges. The range limits and the associated color coding for each range are the same that were used previously, as shown in Table 5-1. Cooler colors (purples and blues) represent lower R_u values while warmer colors (orange and red) represent higher R_u values. Because the laminar shear box tests did not provide small strain data, the blast liquefaction test data are crucial in developing G/G_o vs. shear strain relationships for each R_u range from small to large strain. As indicated previously, the variation of G/G_o vs. R_u for the blast liquefaction test data was assumed to be associated with very low shear strain (10^{-4} %) because the velocity was measured before and after the blast detonation.

A plot of the G/G_o vs. shear strain data points separated into color coded excess pore pressure ratio ranges is shown in Figure 5-45. Curves showing the upper and lower range of G/G_o vs. shear strain for sands with very low R_u values proposed by Seed & Idriss (Seed & Idriss, 1970) are also provided for a frame of reference. A review of the data in Figure 5-45 indicates that the data points with lower R_u values (color coded purple to dark blue) typically fall within the range of G/G_o vs. shear strain curves originally proposed by Seed and Idriss. Of course, this result is consistent with expectations and adds credence to the procedure used to obtain the data points. However, as the R_u values increase (data points have warmer colors), the G/G_o vs. shear strain data points fall further and further below the range identified by the Seed and Idriss curves. For example, the red data points with $R_u > 0.9$ typically have G/G_o values below 0.15 at small strain and below 0.06 at large strain.

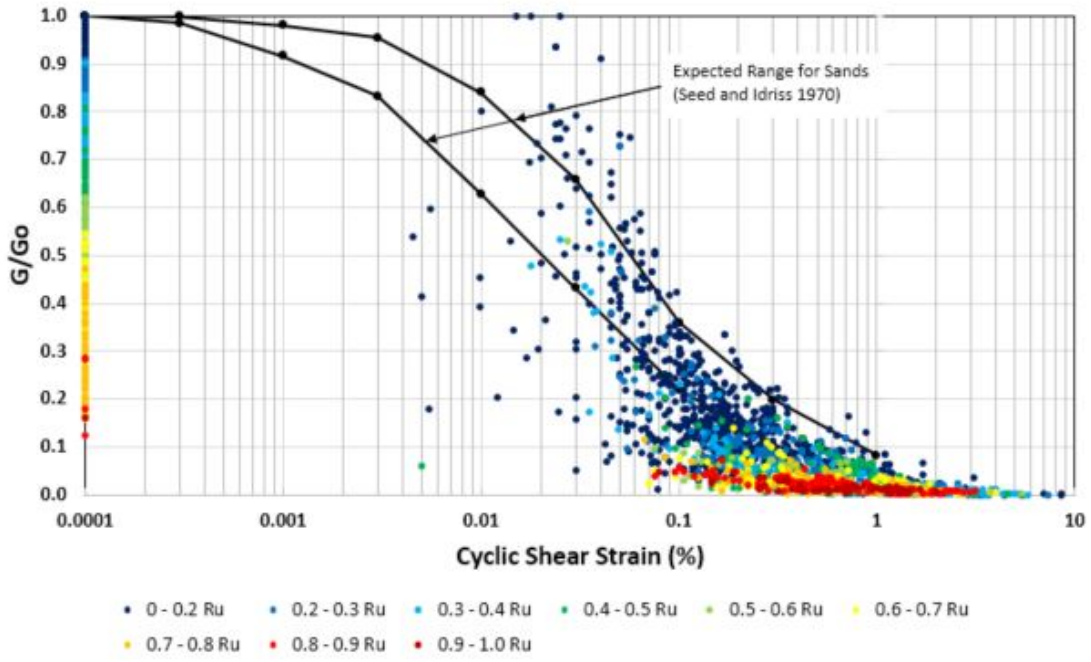

Figure 5-45: Measured normalized shear modulus (g/g0) vs. cyclic shear strain (%) values from both laminar shear box and blast liquefaction tests with color-coding to indicate pore pressure ratio (Ru), upper and lower bound curves for sands with Ru <10% as proposed by (Seed & Idriss, 1970) are shown for comparison.

5.5.1 Simplified Curve Shape for Shear Modulus and Cyclic Shear Strain for Pore Pressure Ratio Ranges

To mimic the curve developed by Seed and Idriss (Seed & Idriss, 1970), a curve fitting formula was applied. This curve fitting formula was proposed by Stokoe (Stokoe, Darendeli, Andrus, & Brown, 1999)). The curve shape is defined by the equation

$$\frac{G}{G_0} = \frac{1}{1+(\frac{\gamma}{\gamma_{ref}})^a} \quad (5\text{-}16)$$

where γ is the cyclic shear strain in percent, and γ_{ref} is the reference strain where $G/G_0 = 0.50$, and a is a curvature parameter to adjust the shape of the curve. This equation is appropriate for

conditions where excess pore pressures are low but must be adjusted for higher excess pore pressure ratios.

Equation 5-11 was adjusted independently for each pore pressure ratio range of data. The average normalized small strain shear modulus ($G/G_o = 1.0$) value for each R_u range from the blast liquefaction tests was used for the numerator in Equation 5-11 in place of 1.0. The reference strain where G/G_o was 50% of the small strain value was taken as 1.8×10^{-2} % strain and remained the same for each curve while the *a* value was adjusted slightly as needed to fit the measured data. Typically, a reasonable fit was obtained with an *a* value between 0.7 and 0.8. This process allowed the curve fit to have the familiar S-curve and be comparable to the expected range for sand, as presented by Seed and Idriss (Seed & Idriss, 1970), for small R_u values.

The G/G_o vs. γ curves for each of the nine R_u ranges shown previously in Figure 5-46, Figure 5-47, Figure 5-48 are plotted together in Figure 5-49. This figure illustrates the reduction and flattening of the G/G_o vs. γ curves as R_u increases from 0 to 1.0. The proposed curves provide a smooth transition that would be useful for capturing the effect of varying pore pressure ratios on normalized shear modulus vs. cyclic shear strain.

As a first approximation, the G/G_o curve for a given R_u and shear strain, γ could be estimated using the equation

$$\frac{G}{G_o} = \frac{(1-R_u)^{0.7}}{1+(\frac{\gamma}{0.018})^{0.8}} \qquad (5\text{-}7)$$

where R_u is the excess pore pressure ratio as a fraction, γ is the shear strain in %, 0.018 is the reference strain, γ_{ref}, and *a is* 0.8.

5.5.2 Application of Best-Fit Shear Modulus vs. Cyclic Shear Strain Curves as a Function of Pore Pressure Ratio.

By using the data from laminar shear box tests and the blast liquefaction tests as anchors, curves were fit to the data to represent potential soil response with increasing excess pore pressure ratios for clean sands. These curves could potentially be used by computer programs that employ the equivalent linear procedure such as SHAKE (Schnabel, Lysmer, & Seed, 1972), and nonlinear programs, such as DEEPSOIL (Park & Hashash, 2004). These programs use the normalized shear modulus curve with cyclic shear strain to confirm that the shear modulus for each soil layer is compatible with the average cyclic shear strain in each computed layer. The generation of excess pore pressures decreases the soil shear modulus. This effect can now be taken into consideration when using the various programs. Figure 5-46, Figure 5-47, and Figure 5-48 show the curves developed for each pore pressure range relative to the measured data points. The theoretical normalized shear modulus presented by Kramer and the empirical estimation are also plotted for small shear strains for comparison with the data presented from the blast liquefaction and laminar shear box tests.

Generally, the fit is adequate and would likely yield acceptable values for each R_u range given the available data. Nevertheless, additional data for the intermediate strain ranges would be desirable to obtain in the future and would be helpful in validating or suggesting appropriate modifications to the proposed curves.

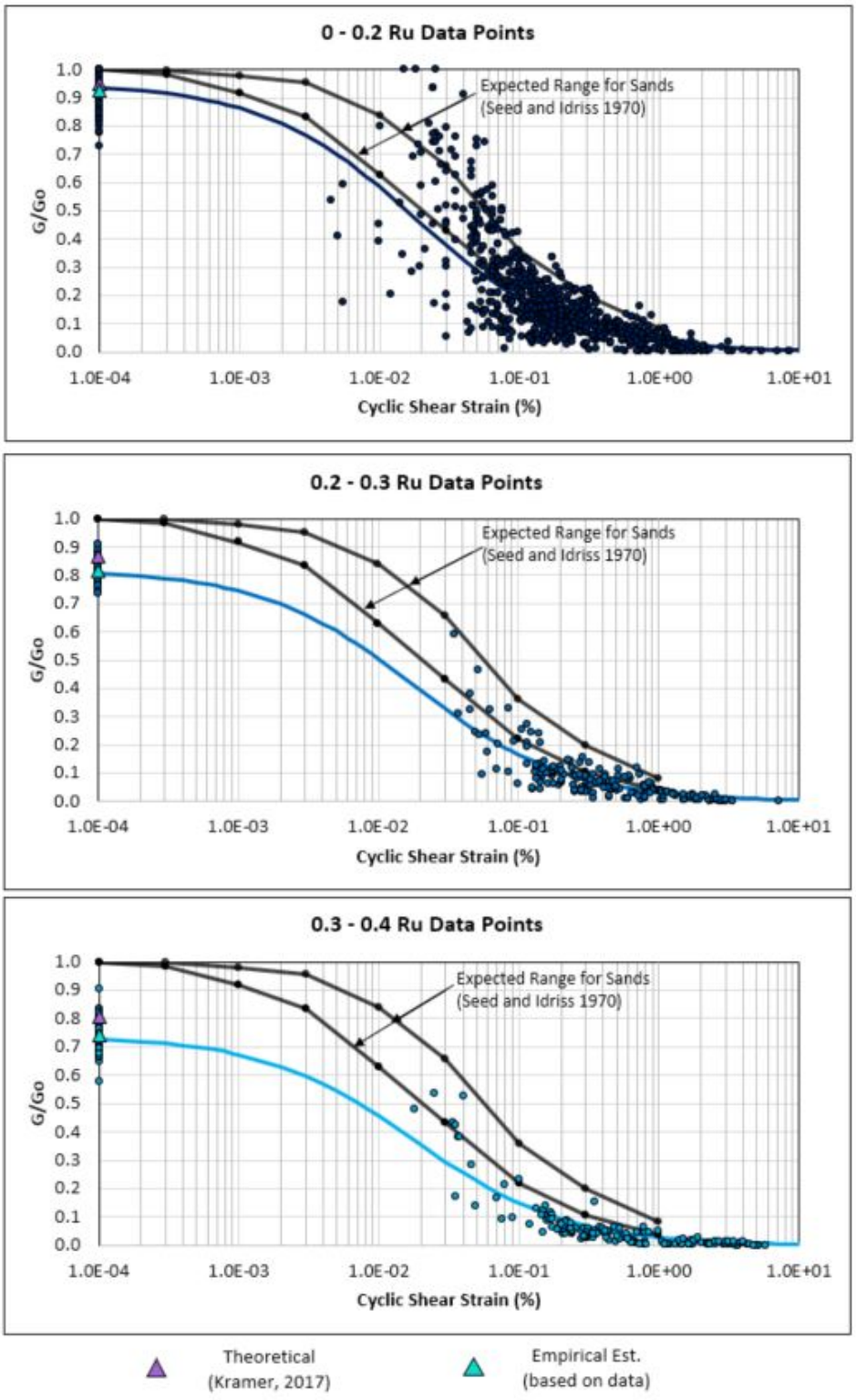

Figure 5-46: G/Go vs. Cyclic Strain for Varying Ru

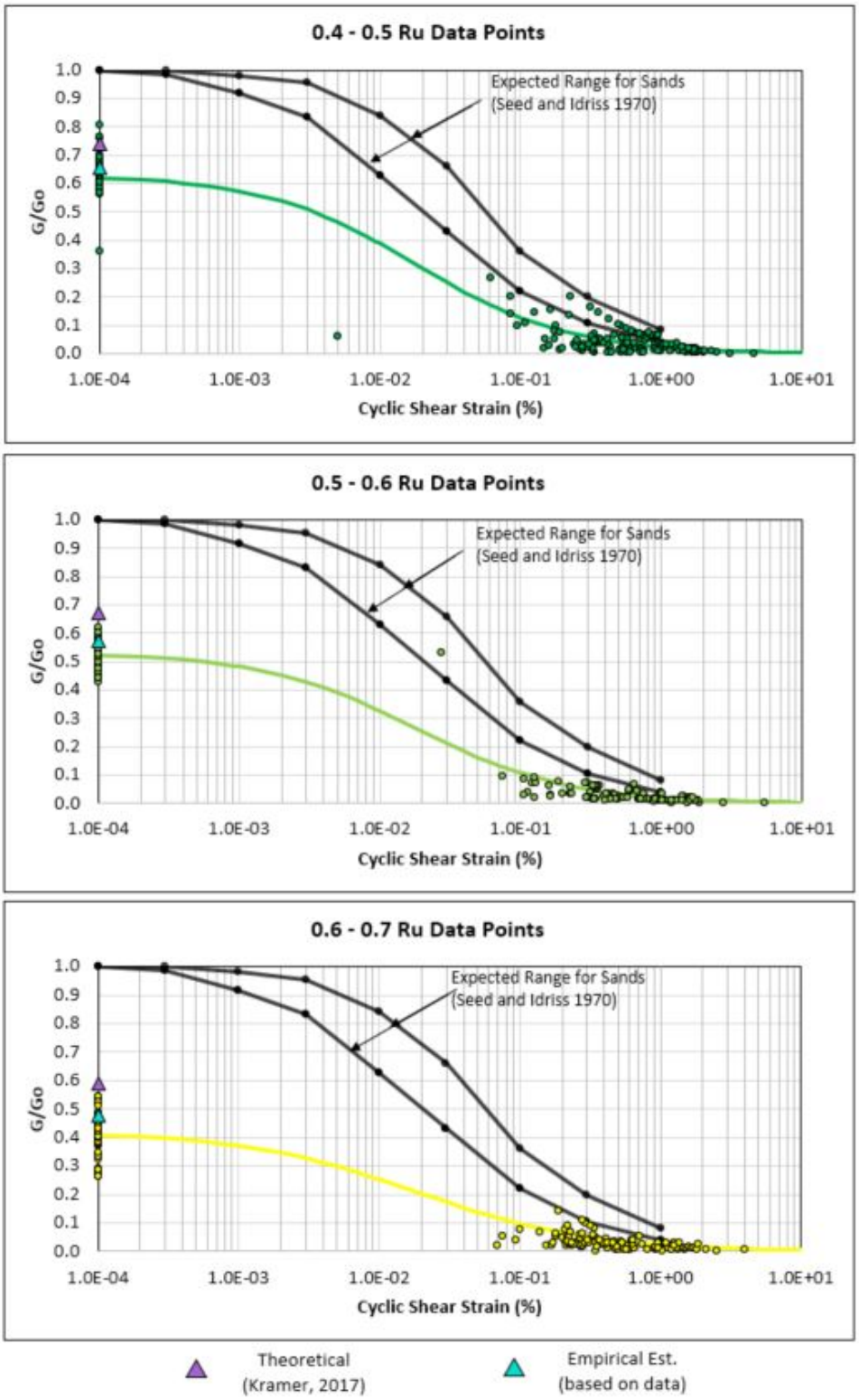

Figure 5-47: G/Go vs. Cyclic Strain for Varying Ru:

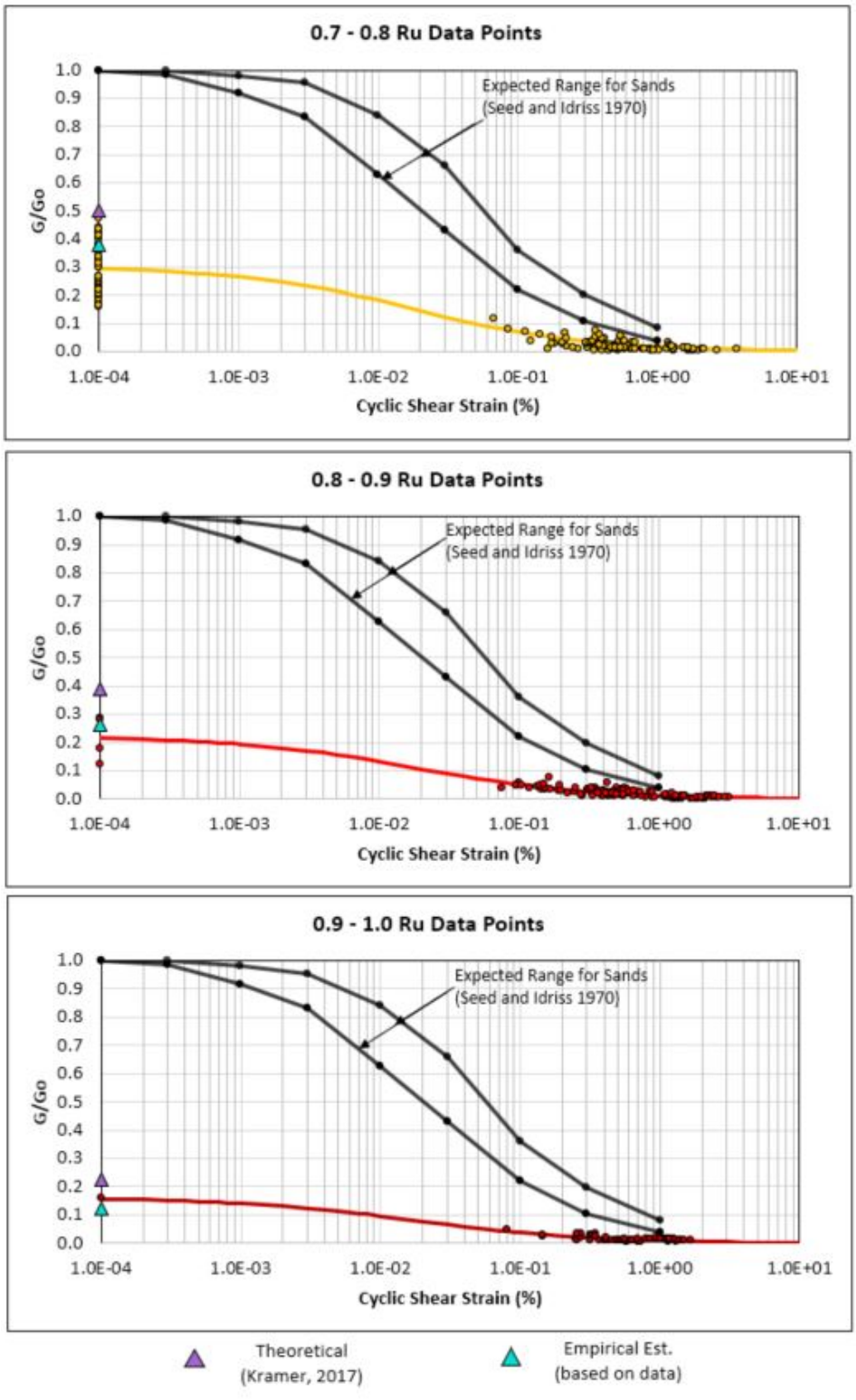

Figure 5-48: G/Go vs. Cyclic Strain for Varying Ru

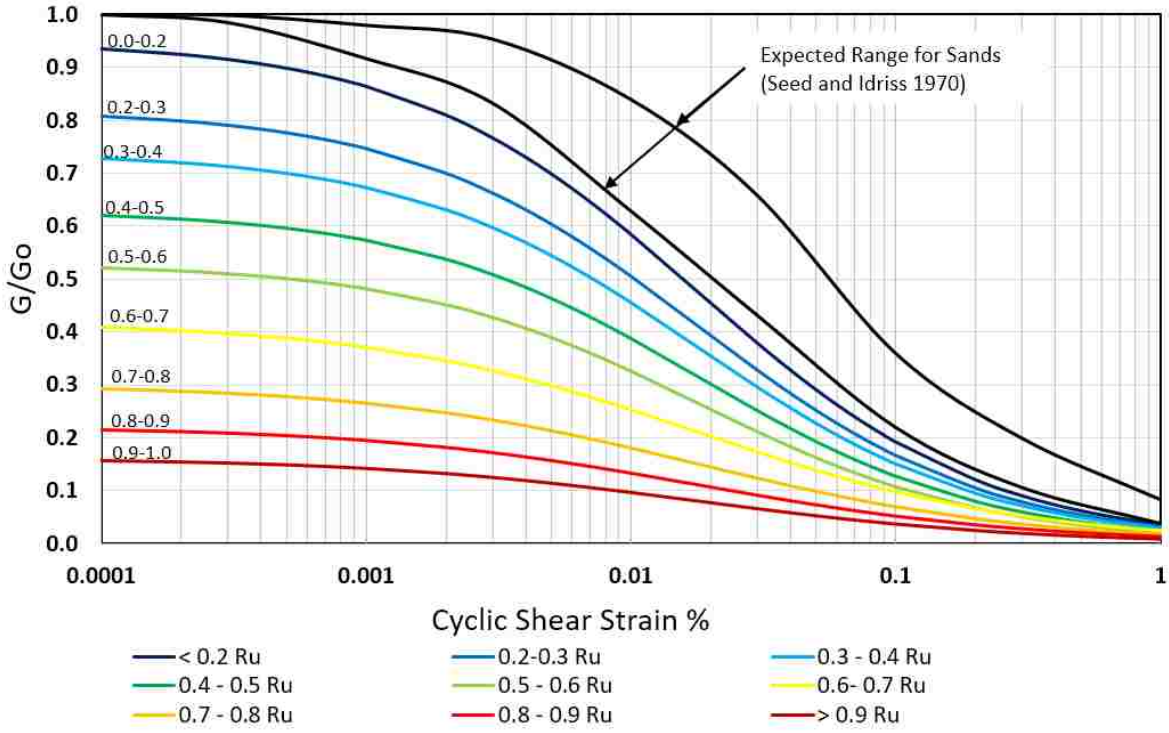

Figure 5-49: Best-fit G/G_0 vs. Cyclic Shear Strain (γ) Curves for Varying Ru values

5.6 Cyclic Shear Strain and Pore Pressure Generation

Cyclic shear strain and pore pressure generation are closely related. It is believed, generally, that cyclic strain causes pore pressure generation during earthquake shaking. Dobry and Ladd, 1980, tested a variety of sands at various relative densities using strain-controlled cyclic triaxial shear tests as show in Figure 5-50. These tests measured excess pore pressure ratio generated by ten cycles of progressively higher levels of shear strain, they determined with the testing, that a cyclic shear strain value of 10^{-2}% was necessary to generate any excess pore pressure. The 10^{-2}% cyclic shear strain became known as the threshold cyclic shear strain for sands. At strain levels higher than the threshold strain, the generated pore pressure ratios generally fell within a narrow range, as show in Figure 5-50, regardless of sand type and relative

density. This narrow range develops because dense sands require higher stresses to develop a given strain while looser sands require lower stress to develop a given strain.

The tests performed in 1985 and thereafter were all laboratory triaxial tests. Large-scale, laminar shear box tests on shake tables and centrifuge tests were later performed on clean sands and the results are presented in Abdoun in 2013. The laminar shear box tests were very similar to the box used for the study involving prefabricated vertical drains in this research study. During these tests, maximum excess pore pressure ratio and cyclic shear strain were measured at various depths. The tests also applied 10 cycles of shaking, to be directly comparable to the 1985 laboratory tests. The range of data defining excess pore pressure ratio vs. cyclic shear strain for these large scale tests is plotted in Figure 5-51 in comparison to the range obtained from laboratory tests.

The large scale or centrifuge tests experienced pore pressure generation at a lower cyclic shear strain than the sands in the triaxial tests presented by Dobry and Ladd in 1980. The threshold cyclic shear strain for the large scale and centrifuge tests is approximately $\gamma_{cl} = 0.06\%$, considerably less than $\gamma_{cl} = 0.2\%$ observed in laboratory tests by Dobry and Ladd. At higher strains, R_u was also higher for the large-scale tests than for the lab tests for a given shear strain level. Nevertheless, the large scale and laboratory tests have the same general shape and trend. Dobry and Abdoun in 2015 concluded that the large scale and centrifuge testing allowed redistribution of the excess pore pressures and that the upward movement of water lead to higher pore pressure ratios at shallow depths.

To make comparisons to excess pore pressure ratio vs. shear strain relationships for large-scale tests without drains published by Dobry and Abdoun, 2015, excess pore pressure ratio vs. shear strain data was obtained for each of the laminar shear box shake table tests in this study.

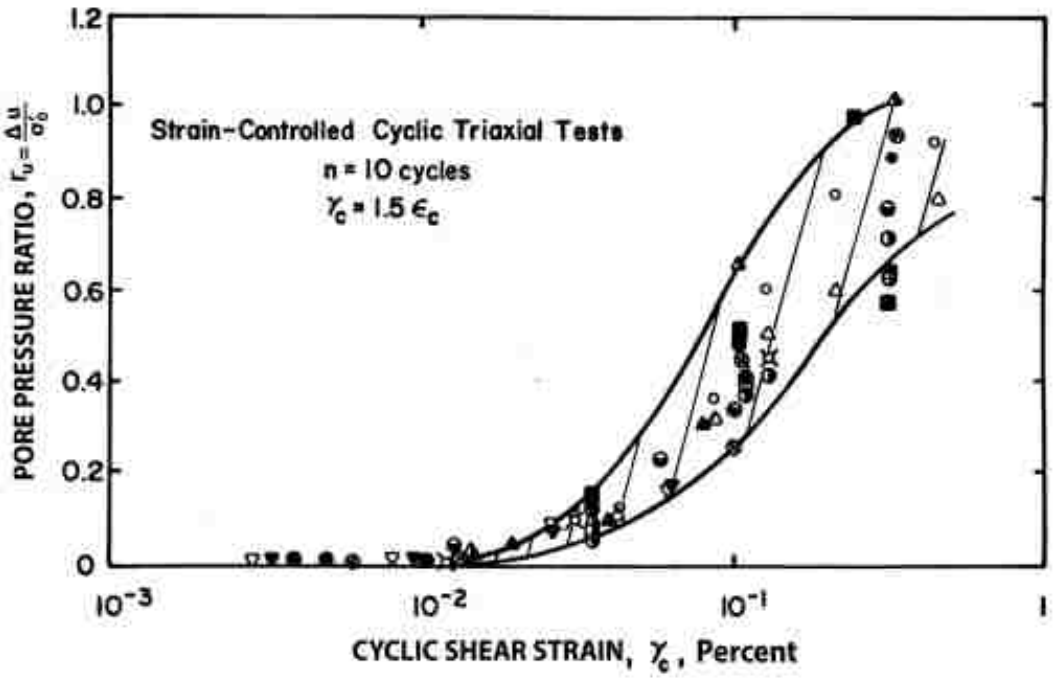

Symbol	Sand	σ'_0 (psf)	D_r (%)	Samples/ Fabric	Measured u Peak (P) or Residual (R)
○	Crystal Silica	2,000	60	Dry Vibration	P
△	" "	2,000	60	Wet Rodding	P
▲	" "	2,000	60	Dry Vibration	P
▼	Sand No. 1	2,800	60	Moist Tamping	P
▽	" "	1,400	60	" "	P
○	Monterey No. 0	2,000	60	" "	P
●	" "	2,000	80	" "	P
□	" "	2,000	45	" "	P
■	" "	2,000	45	" "	R
◨	" "	533	60	" "	P
⊕	" "	4,000	60	" "	P
●	" "	2,000	20	" "	R
•	Banding	2,000	60	" "	R
▲	"	2,000	40	" "	R
●	"	2,000	20	" "	R
●	Heber Road Point Bar	2,000	Dense	Tube Sample	R
○	Heber Road Channel Fill	2,000	Loose	" "	R
⊠	Owi Island	2,000	40	Moist Tamping	R
◯	" "	1,500	40	" "	R
⊖	" "	2,000	Medium Dense	Tube Sample	R
⊖	Mt. St. Helen Debris	2,000-4,000	50	Moist Tamping	R

Figure 5-50: Pore Pressure vs. Shear Strain (Dobry & Ladd, 1980)

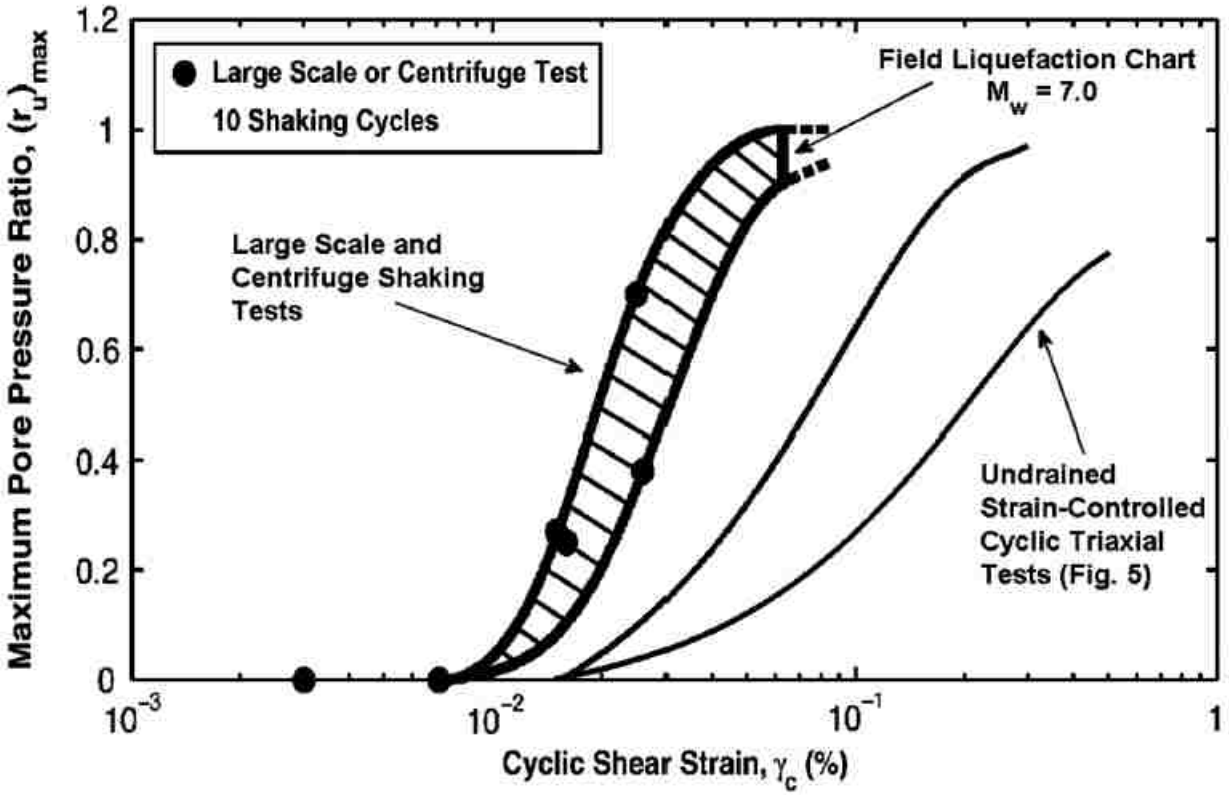

Figure 5-51: Large Scale Pore Pressure Ratio vs. Cyclic Shear Strain Compared to Triaxial Testing (Dobry & Abdoun, 2015)

The average peak shear strain was computed for 10 cycles of loading. The shear strain was the average of each peak shear strain computed at a given depth for the 10 cycles of loading after the peak input acceleration at the base was applied to be conservative and avoid outliers in the data. Maximum excess pore pressure ratios developed during the 10 cycles were obtained and paired with the respective average shear strain values. The excess pore pressure ratio and cyclic shear strain data were separated into their respective rounds of testing for each drain spacing, and then plotted against the results from the Dobry & Abdoun (2015) results, shown in Figure 5-52.

The data points from the laminar shear box tests with vertical drains plot below and to the right of the range of data identified by Abdoun and Dobry (2015). This comparison strongly suggests that the prefabricated vertical drains are effectively removing excess pore water and preventing the pore pressure ratio from increasing as much for a given strain level. Therefore, greater shear strains are required to generate a given excess pore pressure ratio because of the beneficial effect of the drains, thus moving the data points to the right.

The effects of soil densification from previous shaking events can clearly be seen in the 3-foot spacing tests. After each round of testing, the soil became denser and a higher shear strain was needed to produce the same excess pore pressure ratio. Alternatively, lower excess pore pressure ratios developed for the same shear strain. Therefore, the demand on the drains to dissipate pore water pressure decrease as the soil becomes denser. This is in comparison to Dobry and Abdoun (2015) tests, which only performed large-scale testing on newly deposited sand. Direct comparison to Dobry and Abdoun (2015) can only be made for Round 1 testing. Round 2 and 3 testing show the effects of soil densification.

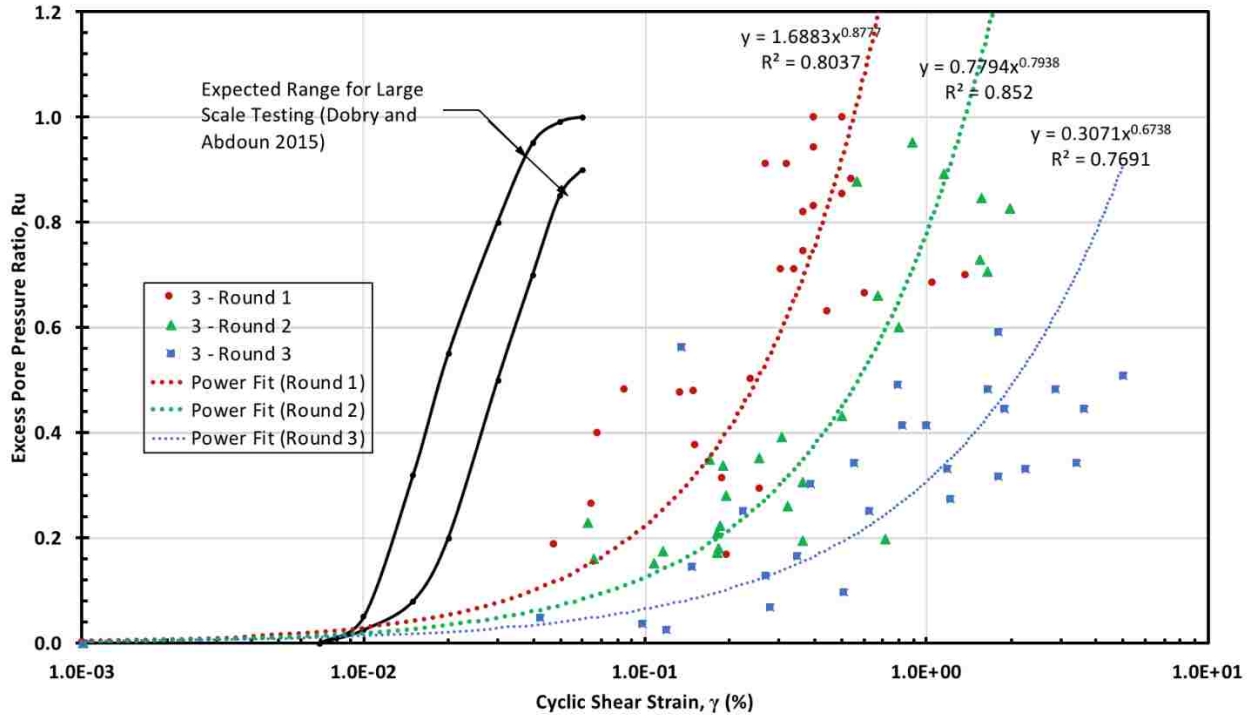

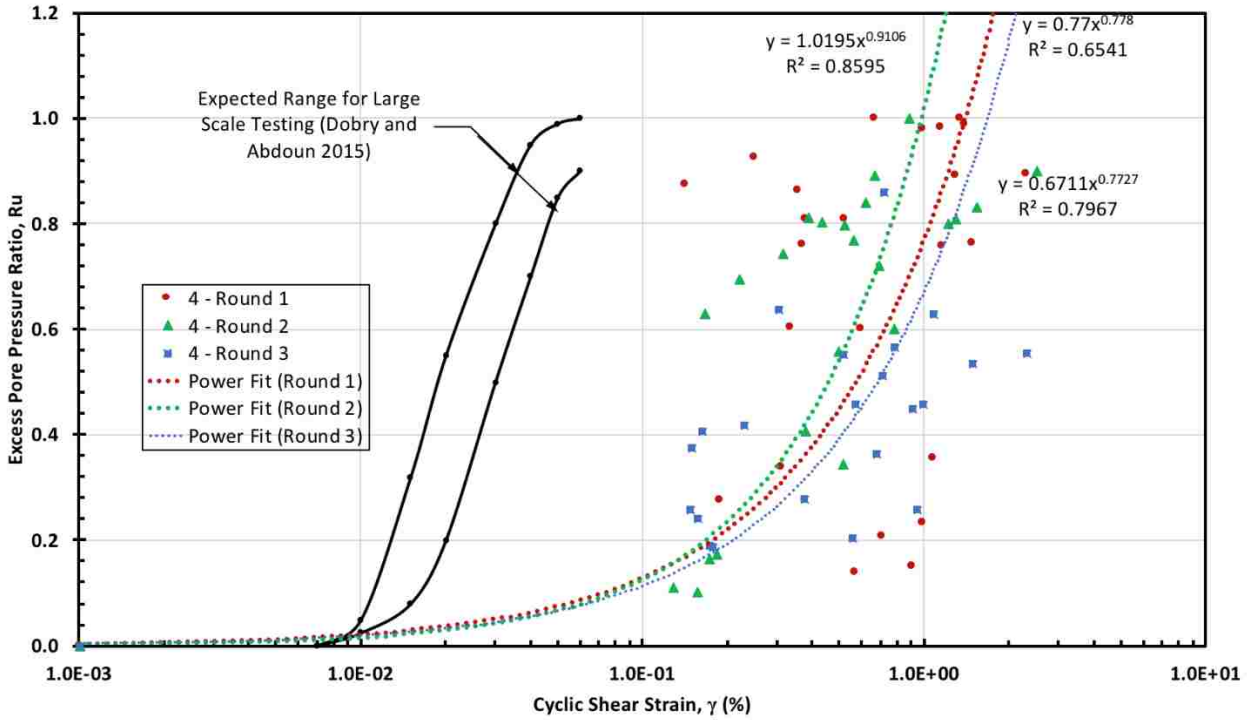

Figure 5-52: Excess Pore Pressure Ratio (Ru) vs. Cyclic Shear Strain (γ) for (a) 3 ft. and (b) 4 ft. Spacing Laminar Shear Box Tests

5.7 Volumetric Strain vs. Cyclic Shear Strain

For each depth where the average cyclic shear strain was computed, the volumetric strain was also determined. The volumetric strain is equal to the settlement between the depth increments divided by the distance between the two depths. The settlement was computed from the Sondex tube measurements. Volumetric strain is plotted as a function of cyclic shear strain in Figure 5-53 for each round of testing with drain spacings of 3 feet and 4 feet. Rough upper and lower boundaries to the data for each round are also shown in Figure 5-53.

The volumetric strain vs. shear strain boundaries for a given round of testing tends to have a positive linear slope to a concave upward slope on the semi-log plot; however, there is significant scatter within the ranges. For a given cyclic shear strain, the volumetric strain was typically highest for the first round of tests and decreased with each round of testing.

The reduction in volumetric strain is presumably a result of the increased density of the sand in each progressive round of testing. Therefore, soils that have experienced multiple shaking events tend to increase resistance to liquefaction. This correlates the results presented in Figure 5-52. Much greater scatter was observed for the 4-foot drain spacing than for the 3-foot drain spacing.

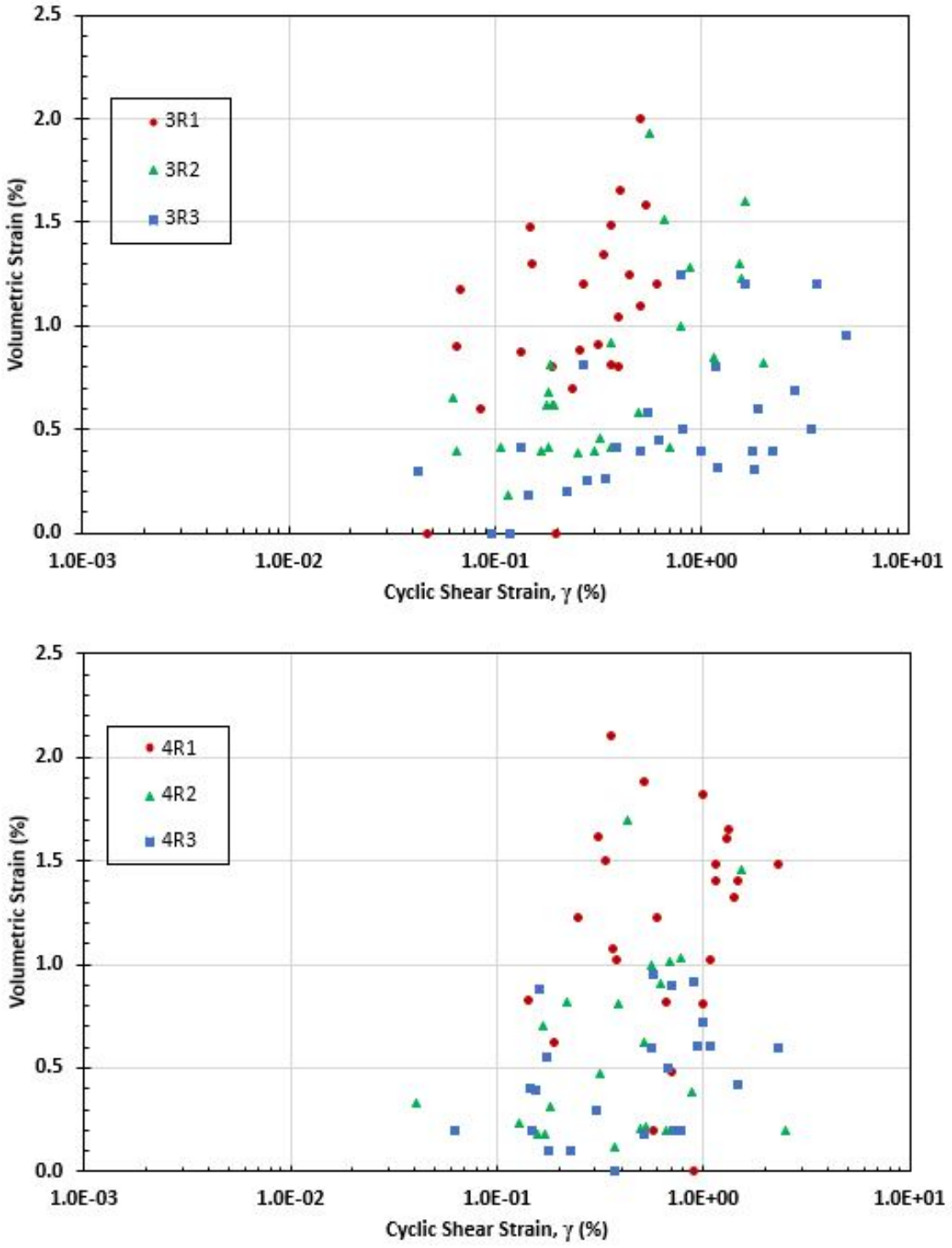

Figure 5-53: Measured Volumetric Strain vs. Cyclic Shear Strain (%) for Each Round of Testing for the 3 feet. and 4 feet. Drain Spacing Tests

5.8 Volumetric Strain vs. Excess Pore Pressure Ratio

The data points in Figure 4-8 and Figure 4-9 were also used to plot volumetric strain vs. excess pore pressure ratio for the 3 foot and 4 foot drain tests, as seen in **Error! Reference source not found.**. For both drain spacings, there is a general linear trend in volumetric strain vs. excess pore pressure, but there is also significant scatter but with no apparent trend in the relationship as a function of round of testing. As the pore pressures increased, volumetric strain increases. This could be caused by the pressure altering the given soil structure, from its original state to a much more fluid state. The results suggest that the primary factor governing the measured settlement is the excess pore pressure ratio. This indicates that if the drains can reduce the excess pore pressure ratio, then the resulting settlement can successfully be reduced during a shaking event.

The results from the laminar shear box testing correlates with data from Seed regarding peak pore pressure ratio effects on Coefficient of Volume Compressibility (Seed & et al., 1975). By reducing pore pressure ratio, the coefficient of volume compressibility remains relatively stable.

The observed scatter in the relationship between volumetric strain and excess pore pressure ratio in the laminar box tests is also consistent with post-earthquake reconnaissance studies which indicate significant scatter in liquefaction induced settlements in hydraulic fill deposits (Katsumata & Tokimatsu, 2012). Apparently, despite efforts to produce a uniformly deposited volume of soil, the hydraulic filling deposition process produces natural variations in compressibility which results in significant scatter. Likewise, others (Lee & Albaisa, 1974) observed considerable scatter in post-liquefaction settlement following cyclic triaxial shear testing despite efforts to produce consistent relative density within the test specimens.

There are more factors that contribute to settlement than simply pore pressure ratio. Wide variability in this laminar shear box test, Lee and Albaisa (1974) triaxial tests, and Katsumata and Tokimatsu (2012) reconnaissance studies appear in pore pressure and volumetric strain. Potential factors in settlement may include time for reconsolidation or time that the soil remains liquefied.

The effect of time in liquefaction can be seen in recent centrifuge testing performed by Howell et al (2012). (Howell, Rathje, Kamai, & Boulanger, 2012). The testing included soil treated with prefabricated vertical drains and untreated. The data was organized by the first and last exceedance of pore pressure ratio equal to 0.5. This was then plotted against the horizontal and vertical displacements measured at the treated and untreated areas. The results generally show larger deformations with larger time with R_u greater than 0.5. This correlates well with the conclusions from the laminar shear box testing.

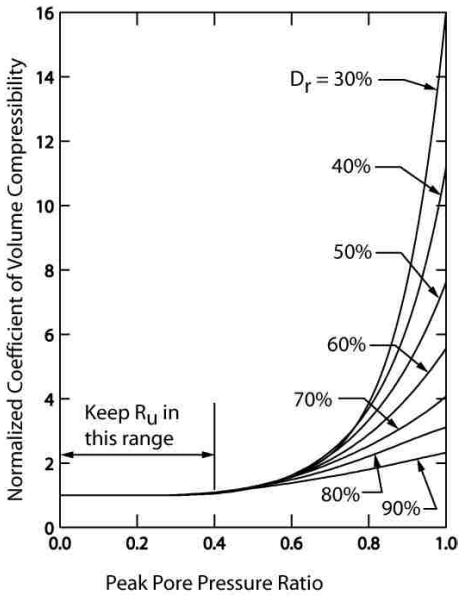

Figure 5-54: Normalized Coefficient of Volume Compressibility vs. Peak Pore Pressure Ratio for Various Relative Densities (Seed & et al., The Generation and Dissipation of Pore Water Pressures During Soil Liquefaction, 1975)

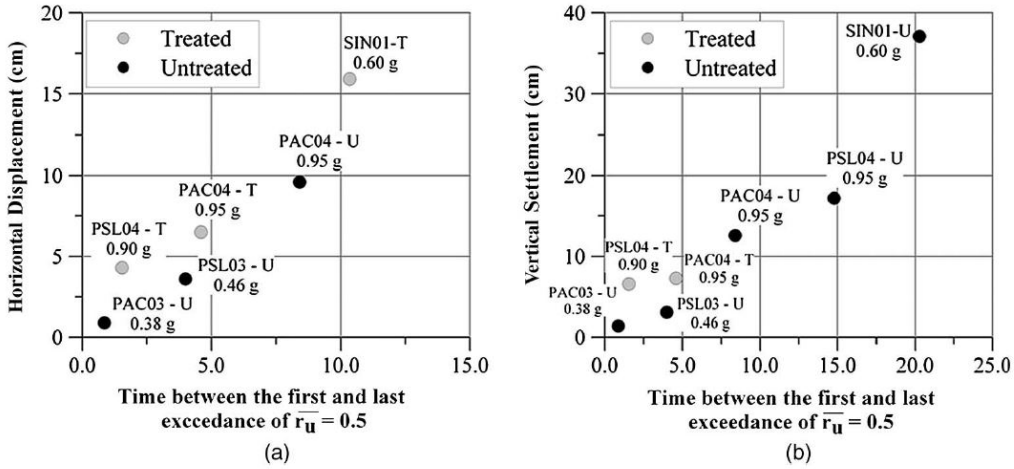

Figure 5-55: Horizontal and Vertical Deformations at Midslope in the Untreated and Treated areas: (a) Horizontal Displacement; (b) Vertical Displacement as a Function of the Time Between First and Last Exceedance of Ru = 0.5

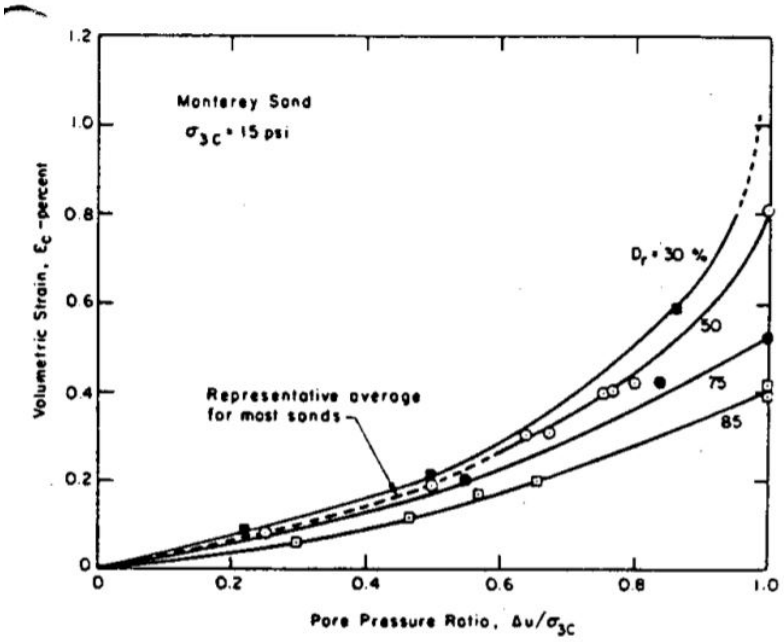

Figure 5-56: Relationship between Volumetric Strain and Pore Pressure Ratio (Lee & Albaisa, 1974)

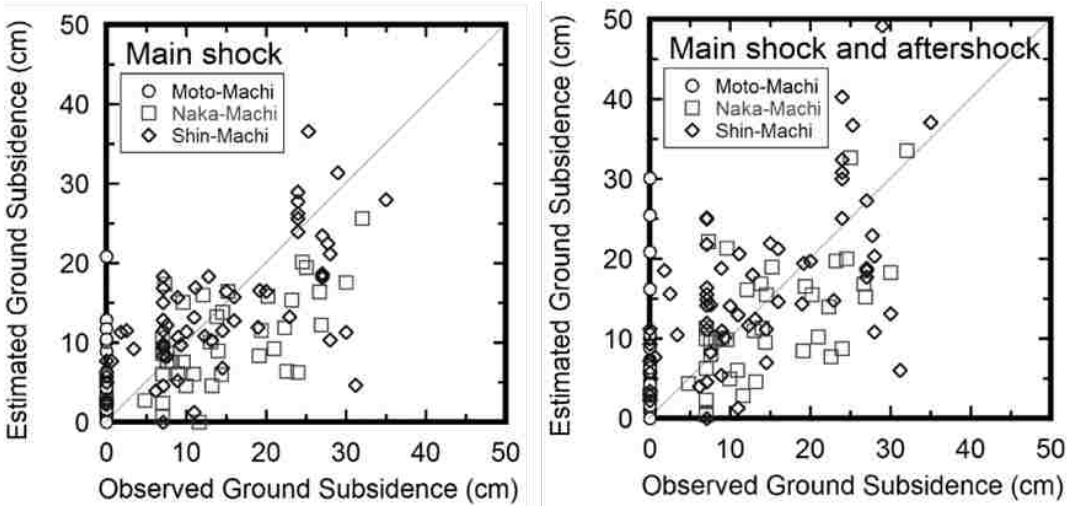

Figure 5-57: Comparison of Measured and Computed Ground Subsidence in Hydraulic Fill Sand at Sites in Japan during the 2011 Mw 9.0 Tohoku Earthquake (Katsumata & Tokimatsu, 2012)

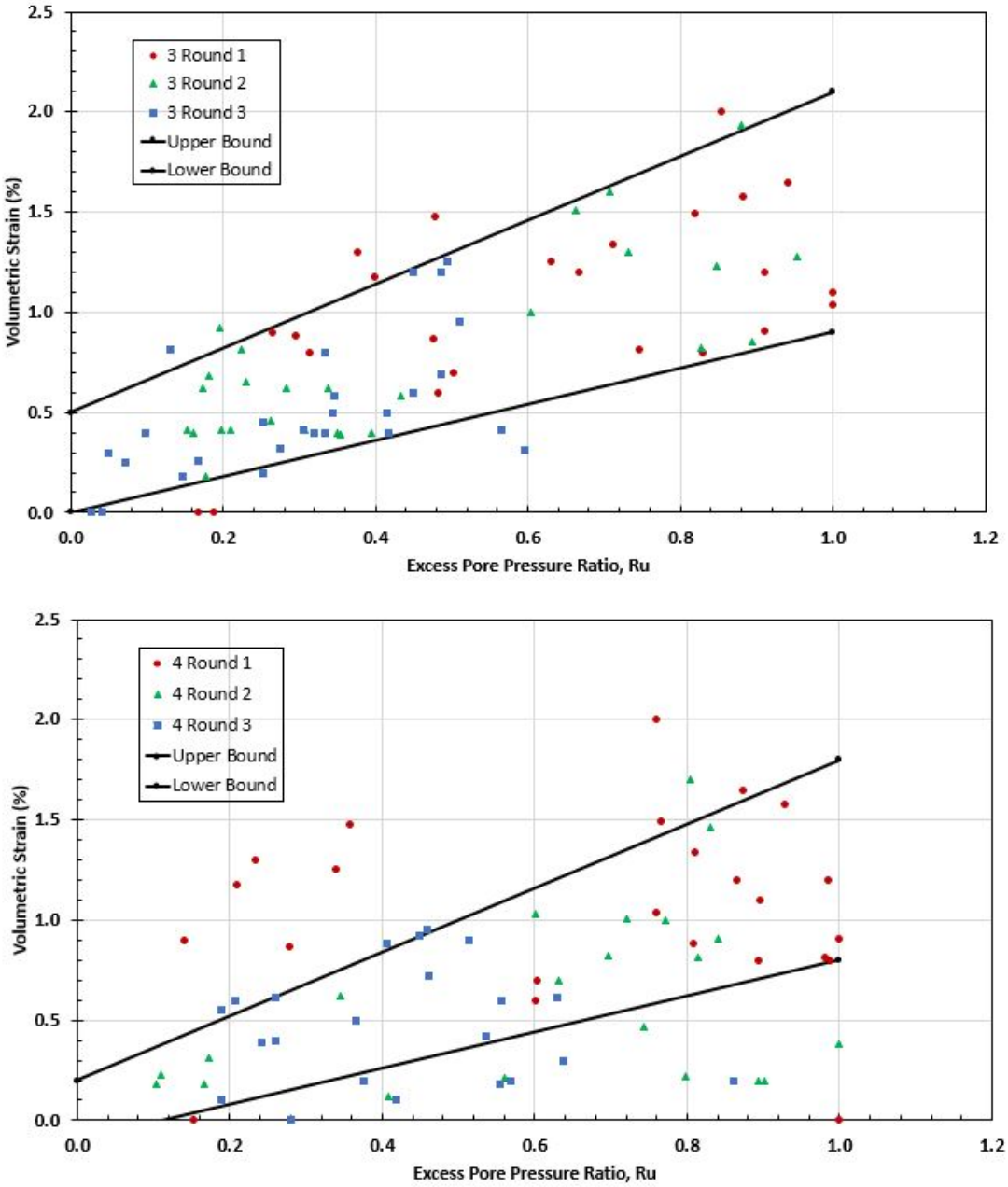

Figure 5-58: Volumetric Strain vs. Pore Pressure Ratio for 3-foot, and 4-foot Spacing

6 CONCLUSION

6.1 Introduction

The research objectives for this study, as listed in the introduction, are reviewed below:

- Define the shear modulus degradation vs. shear strain relationship as a function of excess pore pressure ratio.
- Define pore pressure generation vs. shear strain behavior in the presence of vertical drains and compare them with relationships without drains.
- Determine volumetric strain (% settlement) as a function of shear strain and excess pore pressure ratios.

The results from this thesis will be summarized by research objective and be presented in the following sections.

6.2 Shear Modulus Degradation as a Function of Excess Pore Pressure Ratio

The stiffness, shear stress vs. shear strain, of a soil can be described by the shear modulus. When the soil experiences large strains, the stiffness of the soil decreases, and the shear modulus degrades. As proposed by Seed and Idriss (Seed & Idriss, 1970), a lower and upper bound ranges of the normalized shear modulus variation with cyclic shear strain for sand can be seen in Figure 2-6.

Excess pore pressures affect the shear modulus of sand as well. As the excess pore pressure ratio increased, the shear modulus decreased. The shear modulus was directly calculated for the laminar shear box test data and paired with pore pressure information obtained by an array of sensors during the shaking event. With the accompanying pore pressure information, the effect of pore pressure generation on the normalized shear modulus vs. cyclic shear strain curve was determined. The initial resulting plot was presented in Figure 5-24.

The laminar shear box tests provided a wealth of data for the larger cyclic shear strain range of clean sands but did not have the appropriate sensors to provide similar results for small shear strains. Therefore, the variation of shear wave velocity data measured during various blast liquefaction tests was analyzed and included in this thesis study. This provided assumed small strain data (less than 10^{-4} %) defining the variation of shear modulus with excess pore pressure ratio. The normalized shear modulus vs. shear strain data obtained from blast liquefaction tests and the laminar shear box tests for various excess pore pressure ratios were plotted in Figure 5-45.

The normalized shear modulus vs. shear strain data points were then separated out for various pore pressure ratio ranges as described in Table 5-1. The resulting curves are plotted in Figure 5-46, Figure 5-47, and Figure 5-48 for excess pore pressure ratios ranging from 0 to 1.0.. With the shear modulus data separated, the effect of pore pressure generation on clean sands can be clearly observed. Higher excess pore pressure ratios resulted in a reduced normalized shear modulus, regardless of cyclic shear strain.

A summary plot showing the normalized shear modulus vs. shear strain curves for each range of excess pore pressures are plotted in Figure 5-49. Using these curves, the effect of pore pressure can be included in analysis on clean sands in computer programs that use the equivalent

linear procedure, such as SHAKE (Schnabel, Lysmer, & Seed, 1972), and nonlinear programs, such as DEEPSOIL (Park & Hashash, 2004). A generalized equation defining the curves for any shear strain and excess pore pressure ratio was also developed in this study.

6.3 The Effect of Prefabricated Vertical Drains on Pore Pressure Generation vs. Shear Strain

The generation of pore pressure has been associated with the increase of cyclic shear strain. Dobry and Ladd (Dobry & Ladd, 1980) proposed a threshold cyclic shear strain that is associated with the generation of pore pressure with various laboratory triaxial tests, as seen in Figure 2.3. This threshold strain defined the strain when pore pressure generation began. Dobry and Abdoun (Dobry & Abdoun, 2015) presented pore pressure generation vs. cyclic shear strain curves for large-scale testing and centrifuge testing without drains. They proposed that large scale testing had a lower threshold cyclic shear strain value, and produced higher excess pore pressure ratios for a given cyclic shear strain than with cyclic triaxial shear tests shown in Figure 2.5.

Excess pore pressure ratios vs. cyclic shear strain data gathered from the large-scale laminar shear box tests were compared to Dobry and Abdoun (Dobry & Abdoun, 2015) curves to judge the effect of prefabricated vertical drains on pore pressure generation. With the prefabricated vertical drains, the laminar shear box tests on clean sands experienced much smaller excess pore pressure ratios for a given shear strain, as seen in Figure 5-52. This difference in pore pressure generation can be attributed to the vertical drains effectively mitigating pore pressure build-up, thus increasing the shear strain resistance before pore

pressures were generated. This is promising evidence for the use of vertical drains to mitigate pore pressure build-up.

The process by which the drains effectively mitigate settlement is still in need of further research. One possible explanation is that pore pressure ratio is reduced and the time the sand remains liquefied decreases. As a result, the soil structure breakdown that occurs during pore pressure build-up and liquefaction also decreases. This decrease in soil structure breakdown helps the soil to resist deformation and settlement, despite the void water being drained through the vertical drains. As discussed in section 5.8, centrifuge testing performed by Howell et al (2012) indicates that settlement is related to the time that excess pore pressure remain elevated.

6.4 Volumetric Strain as Function of Shear Strain and Excess Pore Pressure Ratios

The laminar shear box testing provided data to examine volumetric strain and pore pressure generation. The volumetric strain was measured and paired with accompanying excess pore pressure ratio data for each of the three rounds of testing for both the 3-foot and 4-foot spacing of vertical drains. For both drain spacings, there is a general linear trend in volumetric strain vs. excess pore pressure, but there is also significant scatter with no apparent trend in the relationship as a function of the round of testing.

Volumetric Strain is directly related to the percentage of settlement of soil. The larger volumetric strain, the larger the settlement that will be experienced. As the pore pressures increased, volumetric strain increased. This could be caused by the pressure altering the given soil structure, from its original state to a much more fluid state. The results suggest that the primary factor governing the measured settlement is the excess pore pressure ratio. This indicates

that if the drains can reduce the excess pore pressure ratio, then the resulting settlement can successfully be reduced during a shaking event.

The volumetric strain vs. shear strain boundaries tend to have a positive linear slope to a concave upward slope on the semi-log plot; however, there is significant scatter within the ranges. For a given cyclic shear strain, the volumetric strain was typically highest for the first round of tests and decreased with each round of testing. The reduction in volumetric strain is presumably a result of the increased density of the sand in each progressive round of testing

6.5 Limitations and Future Work

The curves for shear modulus vs. cyclic shear strain as function of pore pressure ratio were developed using data with high strain (generally greater than 0.01%) and small strain (around 10^{-4}), which leaves a gap of data in the cyclic shear strain range of 0.0001 to 0.01. Further large-scale testing with appropriate sensitivity is needed to observe the effect excess pore pressure generation on intermediate levels of cyclic shear strain. The laminar shear box testing experienced extremely large shear strains. This can be attributed to very loose, newly placed sand. The large strains experienced may not be typical of real world, in-situ material.

Future studies might include more large-scale, laminar shear box testing comparing soil responses of vertical drains installed with no vertical drains. The acceleration input could be modified to a lower frequency allowing the pore pressure generation to be closely observed.

REFERENCES

Abdoun, T., & et al. (2013). Centrifuge and Large-Scale Modeling of Seismic Pore Pressures in Sands: Cyclic Strain Interpretation.". *Journal of Geotechnical and Geoenvironmental Engineering*, 1215-1234.

Amoroso, S., & et al. (2017). The First Italian Blast-Induced Liquefaction Test (Mirabello, Emilia-Romagna, Italy): Description of the Experiment and Preliminary Results. *Annals of Geophysics*.

Bennett, M. J., McLaughlin, P. V., Sarmiento, J. S., & Youd, T. L. (1984). *Geotechnical Investigation of Liquefaction Sites, Imperial Valley, California.* Washington, D.C.: Rep. 84-252, U.S. Geological Survey.

Chang, W., Rathje, E. M., Stokoe, K. H., & Cox, B. R. (2004). Direct Evaluation of Effectiveness of Prefabricated Vertical Drains in Liquefiable Sand. *Soil Dynamics and Earthquake Engineering Vol 24, Issues 9-10*, 723-731.

Cox, B. R., Stokoe, K. H., & Rathje, E. M. (2009). An In Situ Test Method for Evaluating the Coupled Pore Pressure Generation and Nonlinear Shear Modulus Behavior of Liquefiable Soils. *Geotechnical Testing Journal, Vol. 32, No. 1*, 11-21.

Cox., B. R., & et al. (2013). Liquefaction at Strong Motion Stations and in Urayasu City during the 2011 Tohoku-Oki Earthquake. *Earthquake Spectra, Vol. 29, No. S1*, S55-S80.

Davis, R. O., & Berrill, J. B. (1982). Energy Dissipation and Seismic Liquefaction in Sands. *Earthquake Engineering and Structural Dynamics, Vol. 10*, 59-68.

Dobry, R., & Abdoun, T. (2015). Cyclic Shear Strain Needed for Liquefaction Triggering and Assessment of Overburden Pressure Factor Kσ. *Journal of Geotechnical and Geoenvironmental Engineering*.

Dobry, R., & Ladd, R. (1980). Soil Liquefaction and Cyclic Mobility Evaluation for Level Ground during Earthquakes and Liquefaction Potential: Science vs. Practice. *Journal of the Geotechnical Engineering Division, Vol. 106 No.GT6*, 720-724.

Dobry, R., Ladd, R. S., Yokel, F. Y., Chung, R. M., & Powell, D. (1982). Prediction of Pore Water Pressure Buildup and Liquefaction of Sands during Earthquakes by the Cyclic

Strain Method. In *NBS Building Science Series 138.* Gaithersburg, MD: National Bureau of Standards.

EQE. (1995). *The January 17, 1995 Kobe Earthquake.* Retrieved from EQE: www.eqe.com/publications/kobe/economic.htm

Hazen, A. (1920). Hydrualic-Fill Dams. *Transactions of the ASCE*, 1713-1745.

Howell, R., & et al. (2009a). "Centrifuge Modeling of Liquefaction Sites Treated with Prefabricated Drains. *IS-Tokyo 2009 Intl. Conf. on Performance Based Design in Earthquake.* Balkema, Netherlands: Geotechnical Engineering CRC.

Howell, R., & et al. (2009b). *"Evaluation of the Effectiveness of Prefabricated Vertical Drains for Liquefaction Remediation: Centrifuge Data Report for RLH01.* Davis, CA: UCD/CGMDR-0801, Center for Geotechnical Modeling, Univ. of CA, Davis.

Howell, R., Rathje, E. M., Kamai, R., & Boulanger, R. (2012). Centrifuge Modeling of Prefabricated Vertical Drains for Liquefaction Remediation. *Journal of Geotechnical and Geoenvironmental Engineering* , 262-271.

Ishimwe, E., Coffman, R. A., & Rollins, K. M. (2016). Analysis of Post-Liquefaction Axial Capacities of Driven Pile and Drilled Shaft Foundations. *International Foundations Congress and Equipment Expo*, (pp. 272-283).

Jelinek, K., & Bay, J. (2000). *In Situ Measurements of Shear Wave Velocities After Blast-Induced Liquefaction.* Logan, UT: Utah State University.

Katsumata, K., & Tokimatsu, K. (2012). Relationships between Seismic Characteristics and Soil Liquefaction of Urayasu City Induced by the 2011 Great East Japan Earthquake. *Proc. 9th Intl. Conf. on Urban Earthquake Engineering* (pp. 601-606). Tokyo, Japan: 4th Asia Conf. on Earthquake Engineering.

Kevan, L. I. (2017). *Full-Scale Testing of Blast-Induced Liquefaction Downdrag on Driven Piles in Sand.* Provo, UT: BYU.

Kramer, S., & Greenfield, M. W. (2017). Effects of Long-Duration Motions on Soil Liquefaction Hazards. *Proceedings of the 16th World Conference on Earthquake Engineering, Santiago (CL).* Santiago, CL: WCEE.

Lee, K. L., & Albaisa, A. (1974). Earthquake Induced Settlements in Saturated Sands. *Journal of Soil Mechanics and Foundations Div. ASCE, Vol. 100, No. 4*, 387-400.

Matasovic, N., & Vucetic, M. (1993). Cyclic Characterization of Liquefiable Sands. *ASCE Journal of Geotechnical Engineering, Vol. 119, No. 11*, 1805-1822.

Nemat-Nasser, S., & Shokooh, S. (1979). A Unified Approach to Densification and Liquefaction of Cohesionless Sand in Cyclic Shearing. *Canadian Geotechnical Journal, Vol 16, No. 4*, 659-678.

NRC. (1985). *Liquefaction of Soils During Earthquakes.* National Academy Press.

Oakes, C. R. (2015). *Shaking Table Testing to Evaluate Effectiveness of Prefabricated Vertical Drains for Liquefaction Mitigation.* Provo, UT: BYU. Retrieved from http://scholarsarchive.byu.edu/etd/6152/

Park, D., & Hashash, Y. M. (2004). Soil Damping Formulation in Nonlinear Time Domain Site Response Analysis. *Journal of Earthquake Engineering, Vol. 8, No. 2*, 249-274.

Pavlenko, O., & Irikura, K. (2002). Changes in Shear Moduli of Liquefied and Nonliquefied Soils during the 1995 Kobe Earthquake and Its Aftershocks at Three Vertical-Array Sites. *Bulletin of Seismological Society of America, Vol. 92, No. 5*, 1952-1969.

Rollins, K. M., & Hollenbaugh, J. E. (2015). Liquefaction Induced Negative Skin Friction from Blast-Induced Liquefaction Tests with Auger-Cast Piles. *Procs., 6th International Conference on Earthquake Geotechnical Engineering* (p. 8). Christchurch, NZ: New Zealand Geotechnical Society.

Rollins, K. M., Evans, M., Diehl, N., & Daily, W. (1998). Shear Modulus and Damping Relationships for Gravels. *Journal of Geotechnical and Geoevironmental Engineering., ASCE, Vol. 124, No. 5*, 396-405.

Rollins, K. M., Goughnour, R. R., Anderson, J. K., & Wade, S. F. (2004). Liquefaction Hazard Mitigation by Prefabricated Vertical Drains. *Proc., Fifth Int'l Conference on Case Histories in Geotechnical Engineering*, (p. 8). New York City, NY.

Rollins, K. M., Joshua, K. S., Mccain, A. K., & Goughnour, R. R. (2003). Vertical Composite Drains for Mitigating Liquefaction Hazard. *13th Intl. Conference on Offshore and Polar Engineering* (p. 8). Intl. Society for Offshore and Polar Engineering.

Rollins, K. M., Lane, D. J., Nicholson, P. G., & Rollins, R. E. (2004). Liquefaction Hazard Assessment Using Controlled-Blasting Techniques. *Proceedings of the 11th Intl. Conf. on Soil Dynamics and Earthquake Engineering, Vol 2* (pp. 630-637). Singapore: Stallion Press.

Rollins, K. M., Lane, J. D., & Gerber, T. M. (2005). Measured and Computed Lateral Response of a Pile Group in Sand. *Journal of Geotechnical and Geoenvironmental Engineering, Vol. 131, No.1*, 103-114.

Schnabel, P. B., Lysmer, J., & Seed, H. B. (1972). *SHAKE: A Computer Program for Earthquake Response Analysis of Horizontally Layered Sites.* Berkeley, CA: Earthquake Engineering Research Center, University of California - Berkeley.

Seed, H. B., & Booker, J. R. (1977). Stabilization of Potentially Liquefiable Sand Deposits Using Gravel Drains. *Journal of Geotechnical Engineering, ASCE, 103(GT7)*, 757-768.

Seed, H. B., & et al. (1975). *The Generation and Dissipation of Pore Water Pressures During Soil Liquefaction.* Earthquake Engineering Research Center, Report No. CB/EERC 75-26.

Seed, H. B., & Idriss, I. M. (1970). *Soil Moduli and Damping Factors for Dynamic Response Analyses.* Univ. Of CA - Berkeley: Earthquake Engineering Research Center.

Seed, H. B., Wong, R. T., Idriss, I. M., & Tokimatsu, K. (1986). Moduli and damping factors for dynamic analyses of cohesionless soils. *Journal of Geotechnical Engineering, Vol. 112, No. 11*, 1016-1032.

Silver, M. L., & Seed, H. B. (1971). Volume Changes in Sands during Cyclic Loading. *Journal of Soil Mechanics*, 1171-1182.

Stokoe, K. H., Darendeli, M. B., Andrus, R. D., & Brown, L. T. (1999). Dynamic Soil Properties: Laboratory, Field and Correlation Studies. *2nd Intl. Conf. on Earthquake Geotechnical Engineering Vol. 3* (pp. 811-845). Balkema, Rotterdam: Seco e Pinto.

Thevanayagam, S., Yeigan, M., Stokoe, K., & Youd, T. L. (2015). *Induced Partial Saturation Method for Soil Liquefaction Mitigation - Large Scale Shake Testing.* Buffalo, NY: The University at Buffalo, State University of New York.

Wentz, F. J., van Ballegooy, S., Rollins, K. M., Ashford, S. A., & Olsen, M. J. (2015). Large-Scale Testing of Shallow Ground Improvements using Blast Induced Liquefaction. *6th Inter. Conference on Earthquake Geotechnical Engineering.* Christchurch, NZ.

Zeghal, M., & Elgamal, A. W. (1994). Analysis of Site Liquefaction using Earthquake Records. *Journal of Geotechnical Engineering, ASCE Vol. 120 No. 6*, 996-1017.